Fisheries New Zealand
Tini a Tangaroa

The influence of warming and acidification on coastal plankton in New Zealand and potential effects on green-lipped mussels

New Zealand Aquatic Environment and Biodiversity Report No. 277

C.S. Law, M. Gall, N. Barr, L. Northcote, A. Sabadel, A. Gutiérrez-Rodríguez, M. Meyers, M. Miller, M. Decima, K. Robinson, K. McComb, N. Ragg, E. Frost, J. Ren, E. Armstrong, K. Safi

ISSN 1179-6480 (online)
ISBN 978-1-99-101998-1 (online)

November 2021

New Zealand Government

Requests for further copies should be directed to:

Publications Logistics Officer
Ministry for Primary Industries
PO Box 2526
WELLINGTON 6140

Email: brand@mpi.govt.nz
Telephone: 0800 00 83 33
Facsimile: 04-894 0300

This publication is also available on the Ministry for Primary Industries websites at:
http://www.mpi.govt.nz/news-and-resources/publications
http://fs.fish.govt.nz go to Document library/Research reports

TABLE OF CONTENTS

EXECUTIVE SUMMARY

Law, C.S.[1,2]; Gall.; M.[1]; Barr, N.[1]; Northcote, L.[1]; Sabadel, A.[3]; Gutiérrez-Rodríguez, A.[1]; Meyers, M.[2]; Miller, M.[4]; Decima, M.[1]; Robinson, K.[1]; McComb, K.[3]; Ragg, N.[4]; Frost, E.[5]; Ren, J.[1]; Armstrong, E.[3]; Safi, K.[1] **(2021). The influence of warming and acidification on coastal plankton in New Zealand and potential effects on green-lipped mussels.**

New Zealand Aquatic Environment and Biodiversity Report No. 277. **82 p.**

Climate change is impacting marine ecosystems by altering biodiversity, productivity, and biogeochemical cycling. This study assesses whether future changes in water temperature and pH projected for the New Zealand region will influence coastal phytoplankton biomass and speciation, and so the nutritional value of plankton in coastal food webs. Four different climate perturbation experiments were carried out on coastal seawater containing mixed plankton communities within 4000-Litre containers in a mesocosm facility in autumn, and then in spring, over three consecutive years. The experiments ran for 18–22 days, with the response in ambient controls compared with that of two treatments – one with lower pH (-0.33 to -0.5), and the other with lower pH in combination with higher temperature (+2.7 to +4.5 °C), to simulate conditions projected for the years 2100 and 2150. A range of biological and biogeochemical parameters were sampled to determine how projected changes in pH and temperature may impact coastal plankton.

Phytoplankton biomass, as measured by chlorophyll-*a*, was unaffected by lower pH, indicating resilience to future acidification. Conversely, there was a significant biomass increase of 20–64% in the combined treatment in three experiments, indicating that future warmer temperature may increase food availability for the lower food web. However, this response was dependent upon nutrient availability, which also influenced the phytoplankton size spectrum with a marked decrease in size when nutrients were depleted and an increase when nutrient supply was maintained. Changes in the dominant phytoplankton group also occurred, with diatoms increasing in abundance at both lower pH, and also low pH with warming when nutrients were maintained. Despite the increase in phytoplankton biomass, there were indications of a decrease in food quality, with higher carbon: nitrogen (C:N) ratios in two of the four experiments; however, particulate amino acid content and N isotopic signature were not affected. Particulate fatty acid content was insensitive to lower pH, although there were increases in saturated and total fatty acids with low pH combined with warming. The proportion of particulate polyunsaturated fatty acids (PUFA), and the essential n-3 PUFA group decreased under future conditions in one experiment, but there was no corresponding decline in zooplankton fatty acid content. Future conditions had no effect on zooplankton community composition and abundance, possibly due to the short duration of the experiments. Contradictory responses in zooplankton grazing were observed, with short-term single copepod species incubations showing lower grazing under future conditions, whereas amino acid isotopes indicated accelerated zooplankton grazing and metabolism under warmer temperatures. Overall, the combination of warmer temperature and lower pH had a greater impact than low pH alone, and so temperature change is expected to be the dominant climate-related driver of future phytoplankton biomass and composition in Aotearoa/New Zealand coastal waters. As the phytoplankton responses to future conditions were not reflected in the zooplankton, the lower food web in coastal waters appears relatively robust to projected future changes.

Green-lipped mussel (*Perna canaliculus)* larvae were maintained in the mesocosms during one experiment over 11 days to determine impacts on growth and survival. There were no significant differences in survival, abnormality, or shell length between control and future conditions, although

[1] National Institute of Water and Atmospheric research (NIWA), New Zealand.
[2] Department of Marine Sciences, University of Otago, New Zealand.
[3] Department of Chemistry, University of Otago, New Zealand.
[4] Cawthron Institute, Nelson, New Zealand.
[5] University of Auckland, Auckland, New Zealand.

maximum final shell size was smaller in both treatments, potentially due to lower carbonate availability associated with low pH. The observed responses in phytoplankton biomass and carbon in the mesocosm experiments were incorporated into a Dynamic Energy Budget model for green-lipped mussels to examine how future changes in coastal phytoplankton may influence their growth and survival. Warmer temperature influences mussels directly via physiological processes and indirectly via increased food availability under future conditions. The model outputs predict future increases in food uptake rate, energy allocation, shell length, and flesh weight for green-lipped mussels although this was based upon the maximum significant responses only and is only representative of conditions in the mesocosm experiments.

1. INTRODUCTION

Aotearoa/New Zealand's marine realm is already experiencing the effects of climate change, as demonstrated by documented increases in sea surface temperature and ocean acidification. Ocean acidity has increased by ~7% over 20 years, with warming exceeding 0.3 °C per decade (Sutton & Bowen 2019, Ministry for the Environment & Stats NZ 2019). These trends are also evident in coastal waters which have warmed by 0.2 °C per decade and are influenced by additional sources of acidity that result in lower average pH than the open ocean (Vance et al. 2019). Model projections suggest the pH of open ocean waters around Aotearoa/New Zealand will further decrease by 0.3 to 0.4 pH units, with warming of +2.5 °C by the end of this century (Law et al. 2018b).

These climate driven changes have implications for coastal marine ecosystems, but impacts are currently unclear. A major uncertainty is the response of the plankton which occupy the base of the marine food web, with the phytoplankton providing a critical source of energy and carbon for higher trophic levels. Recent trends in New Zealand offshore waters indicate decreases in surface chlorophyll-*a*, and hence phytoplankton biomass, in warmer subtropical waters, reflected in declines in coastal water chlorophyll-*a* around Te Ika a Māui/North Island and the west coast of Te Waipounamu/South Island (Ministry for the Environment & Stats NZ 2019). Temperature is an important determinant of phytoplankton growth but warming may also indirectly affect phytoplankton production by reducing nutrient availability due to stratification. The influence of ocean acidification on phytoplankton can also vary; increases in dissolved CO_2 may potentially enhance primary production (Riebesell 2004), whereas calcifying phytoplankton may be negatively impacted due to decreased availability of dissolved carbonate. Responses to lower pH vary between phytoplankton groups and species, reflecting different physiological mechanisms for accessing dissolved carbon. Small picoeukaryotes appear to benefit under lower pH when nutrients are in short supply and diatoms, which are an important phytoplankton group in Aotearoa/New Zealand coastal waters, also show responses to lower pH that are modulated by both nutrient availability and temperature (Alvarez-Fernandez et al. 2018).

Changes in phytoplankton biomass and community composition in response to warming and ocean acidification may have ramifications for coastal water biogeochemistry and also food webs via changes in the availability and quality of planktonic food. For example, although phytoplankton carbon content may increase under elevated CO_2 (low pH) food quality may be reduced with negative impacts on grazers (Schoo et al. 2013). Lower pH may also alter the fatty acid content of phytoplankton, including the essential polyunsaturated fatty acids (PUFA), which grazers cannot synthesise and so are dependent upon phytoplankton for. Phytoplankton PUFA content decreases at higher temperatures (Hixson & Arts 2016) and changes in phytoplankton community composition can also alter PUFA availability (Galloway & Winder 2015). Fatty acids, and particularly PUFA, are important for zooplankton reproduction and immune responses, and consequently any future change in phytoplankton fatty acids induced by warming and acidification may indirectly impact zooplankton and higher trophic levels (Bermudez et al. 2016). Furthermore, declines in nauplii recruitment and elevated mortality may occur in certain zooplankton species under lower pH (Cripps et al. 2014), whereas other species are unaffected. The observed variation in response and sensitivity of plankton to climate stressors presents a challenge to predicting the future status of coastal food webs under global environmental change.

Molluscs are susceptible to ocean acidification with several studies identifying negative impacts on survival, calcification, growth, and development. Molluscan larvae are particularly sensitive, because this life stage involves rapid shell development that may be impaired by the lower saturation of carbonate in water as a result of acidification (Kroeker et al. 2013). High larval mortalities in oyster hatcheries have been attributed to ocean acidification (Barton et al. 2012), and so ocean acidification represents a potential threat to other molluscs such as the green-lipped mussel (*Perna canaliculus*), an important aquaculture species in New Zealand. Green-lipped mussel larvae show decreased shell growth and calcification (Ericson 2010), and embryos are particularly vulnerable during the initial 48 hours before their shells form (N. Ragg, pers. comm). Growth and survival of other life stages of *P. canaliculus* appear relatively unaffected by lower pH projected for the year 2100 (N. Ragg, pers. comm), although diversion of energy from other metabolic processes for maintenance of their carbonate shell may result in a decline in flesh condition and productivity. Warming may also affect feeding and metabolic

processes in mussels (Clements et al. 2018), and the mussel aquaculture sector has recently experienced major spat failures and die-offs that were tentatively attributed to warming.

This study assesses whether future changes in water temperature and pH arising from climate change will influence coastal phytoplankton biomass and speciation, and specifically the nutritional value of plankton to Aotearoa/New Zealand coastal food webs. It builds upon a series of manipulation experiments in which natural coastal plankton communities were exposed to future conditions in a large volume mesocosm facility, carried out during the MBIE-funded CARIM (*Coastal Acidification: Rates, Impacts and Management)* project. Although single species laboratory and culture studies provide valuable information on climate sensitivities in individual species there is evidence that community interactions may mitigate the impacts of ocean acidification (Rossoll et al. 2013). The study of natural communities in large volume mesocosms facilitates more realistic interaction between organisms, from species to trophic levels and also exposure to natural environmental conditions and processes, thereby generating more robust information for future projections.

In each of the four experiments natural coastal plankton communities were maintained for 18–22 days under lower pH alone, and also lower pH in combination with elevated temperature, as projected for New Zealand waters for the year 2100 (and in one experiment, 2150). This approach enabled the effect of low pH, and the combined and potentially synergistic effect of warming and ocean acidification, to be examined. The responses in the treatments were compared with that of ambient controls for a range of parameters, including chlorophyll-*a*, particulate carbon and nitrogen, phytoplankton and zooplankton species composition, particulate fatty acid and amino acid concentrations, and zooplankton grazing rates. In addition, green-lipped mussel larvae were maintained under future conditions for 11 days to determine the impacts of lower pH and elevated temperature on their growth and survival. Significant responses in some parameters (phytoplankton biomass and carbon) in the mesocosm experiments were also incorporated in a Dynamic Energy Budget model for green-lipped mussels to examine how future changes in coastal plankton may influence their growth and survival.

Overall Research Objective

To assess the effects of warming and ocean acidification on plankton and biogeochemistry in New Zealand coastal waters.

Specific Research Objectives

- Collect and analyse samples for amino acid (AAs) and fatty acid (FAs) content from three mesocosm manipulation experiments, in which the effects of pH and elevated temperature are assessed relative to controls for coastal seawater from Ākautangi/Evans Bay, Wellington.
  Results from four mesocosm experiments are discussed with additional ancillary variables presented for context and interpretation. Further parameters, such as zooplankton grazing, are included to determine the impact of future conditions on food webs, and a phytoplankton culture experiment was added to further examine the impact on Fatty Acids.
- Examine how coastal acidification influences the total content of fatty acids in green-lipped mussels.
  Replaced by an experiment examining the effect of low pH and low pH/warmer temperature on mussel larvae growth and survival. (Variation 31/7/18: "The final CARIM mesocosm experiment scheduled for September will incorporate shellfish larvae to determine both direct & indirect effects of OA & warming".)
- Combine results on change in food quality and transfer with observed direct effects of acidification (obtained in the CARIM project) on green-lipped mussels, to develop projections of future population success and the potential implications for the New Zealand mussel aquaculture industry.
  Future changes in food quality identified in the mesocosm experiments were incorporated into a Dynamic Energy Budget model with implications determined for green-lipped mussels, although this did not incorporate the direct effects of acidification on mussel physiology and growth, which were part of the broader CARIM project (published by Ren et al. 2020).

2. METHODS

2.1 Specific Research Objective 1: Effect of future changes on coastal plankton

Collect and analyse samples for amino acid (AA) and fatty acid (FA) content from three mesocosm manipulation experiments, in which the effect of pH and elevated temperature are assessed relative to controls for coastal seawater from Ākautangi/Evans Bay, Wellington.

Mesocosm experimental framework

The mesocosm experiments were carried out as part of the CARIM (*Coastal Acidification: Rate, Impacts and Management*) project. Four mesocosm experiments (ME1-4) were carried out between 2016 and 2019 in a 4-m deep seawater pond at NIWA Wellington, with each experiment incorporating nine 3.7-m long mesocosm bags (see Figure 1) filled with ~4 m^3 of seawater pumped from a depth of ~15 m in Ākautangi/Evans Bay. Each bag had a solid plastic base (lower former), a transparent perspex lid attached to an upper plastic former that accommodated a headspace, and an integrated mixing system to ensure vertical uniformity in water properties and control of pH and temperature (see Figure 1). In each experiment two different treatments were compared with present-day ambient conditions (Control), with triplicate bags for each treatment and the Control randomly positioned in the seawater pond (see Figure 2).

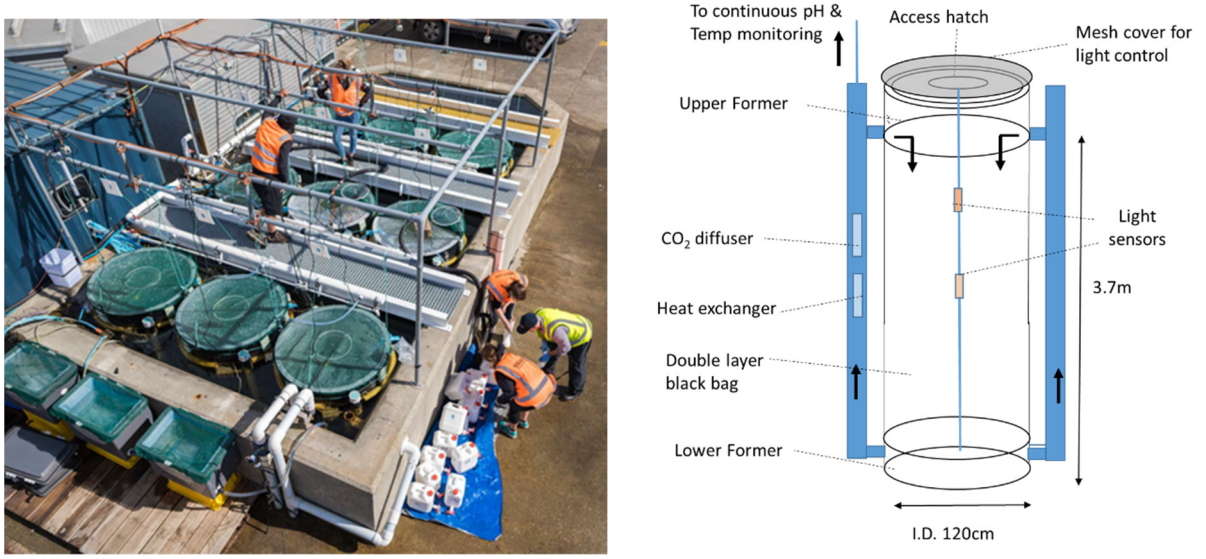

Figure 1: a) Overhead view of the mesocosm pond showing the layout of the nine bags and b) mesocosm bag design.

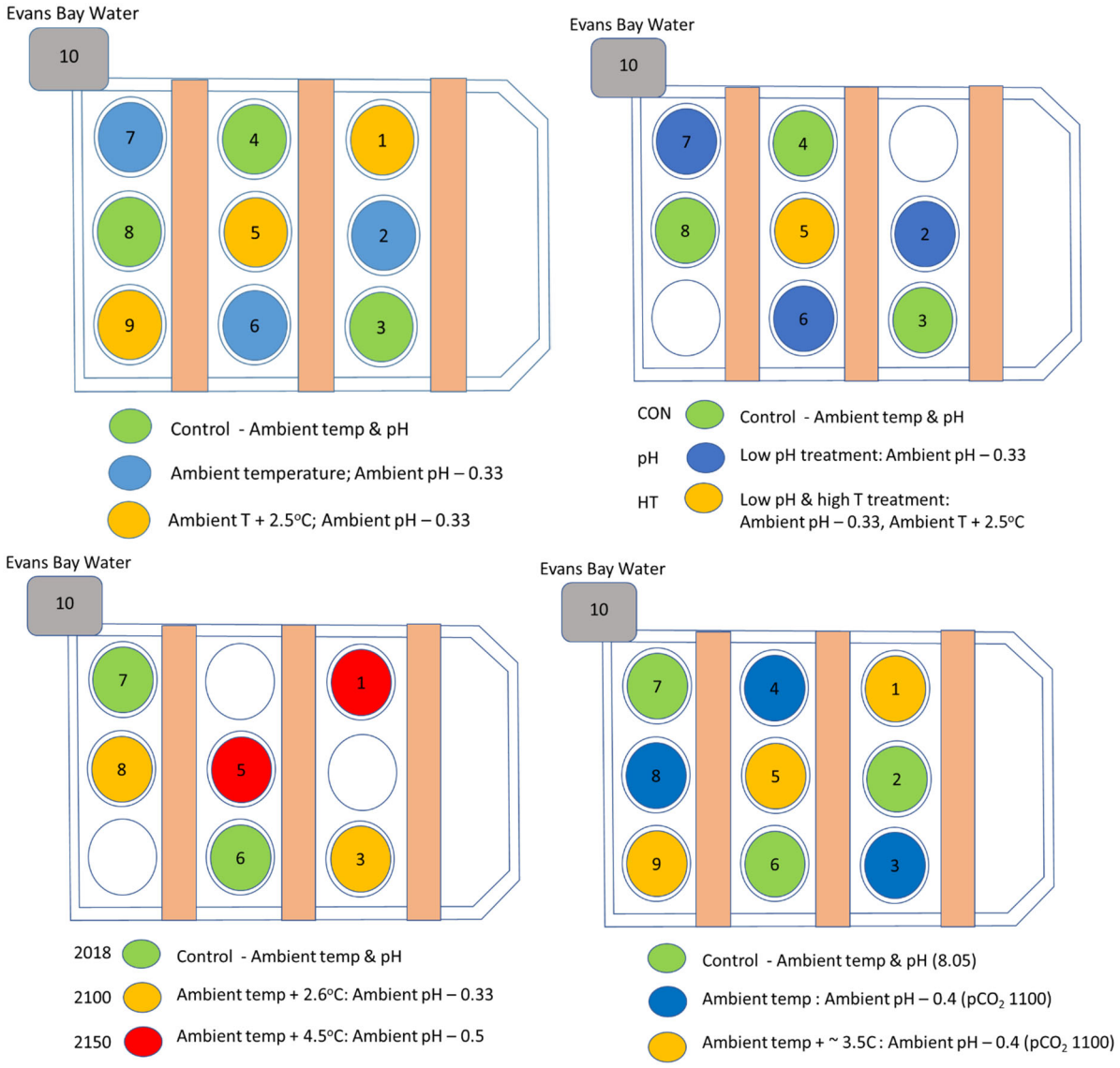

Figure 2: Experimental layout of ME1, ME2 (left to right, upper row) and ME3, ME4 (left to right, lower row), showing the nine mesocosm bags, with treatments indicated by colour and white indicating where bag results were omitted from data analysis due to technical difficulties. Water samples were also collected from Ākautangi//Evans Bay water (10) for comparison. ME1, ME2, and ME4 have similar treatments of three bags under low pH only (*pH*), and three bags under combined low pH and elevated temperature (*pH/T*). ME3 had a different experimental question and incorporated *pH/T* treatments for two future time points, the Years 2100 (*2100*) and 2150 (*2150)*, with no pH only treatment. Although ME1 took place prior to the start of this research project the results are incorporated for context and to assist interpretation. Further experimental details are in Table 1.

The bags were initially overflowed for a minimum of 24 hours to ensure thorough flushing, and the pH and temperature then adjusted to target values in the treatment bags over the following 24–36 hours. The target pH and temperature values were based upon future projections for the New Zealand region, derived using an Earth System Model and the RCP8.5 emission scenario (see Law et al. 2018b for further details), and achieved by adjusting the ambient pH and temperature at the start of the experiment by the incremental change projected (see Table 1). ME1, 2, and 4 used a consistent framework that compared ambient conditions in the Control with a treatment where only pH was adjusted (identified hereon as *pH*) and a second treatment in which both pH and temperature were adjusted (hereon identified as *pH/T*). This approach was used to distinguish the separate influences of temperature and pH, and also to assess the response to the actual future scenario of combined warming and lower pH (as opposed to pH alone, which will not occur without associated warming). The ME3 experiment used a different approach to the other

experiments by comparing two future combinations of pH and temperature, projected for *2100* and *2150*, with the Control.

Table 1: Mesocosm experiment details of initial conditions (left hand columns), experimental treatments (central columns) and sample parameters discussed in this report (right hand columns). The colour coding and nomenclature for the treatments is used throughout the Results section and Figures. Acronyms: NO_3^-: Nitrate-Nitrogen, P: Phosphate, Si: Silicate, NH_4^+: ammonium-Nitrogen, PC/PN: Particulate Carbon and Nitrogen, FAs: Fatty Acids, AAs: Amino Acids, CSIA-AA: Compound Specific Isotope Analysis Amino Acids, Chl-*a*: chlorophyll-*a*.

Exp.	Month	Initial Temp (°C)	Initial pH	Initial Chl-*a* (µg/l)	Test Scenario	Treatments (*pH, pH/T*)	Days	Nutrient addition	Parameters - Phytoplankton and Particulate	Parameters - Zooplankton and larvae
ME1	April 2016	17.1	8.03	0.8	2100 pH 2100 pH/T	-0.33 -0.33/+2.5°C	18	None	Biomass, Composition, PC/PN	Composition, abundance, grazing rate
ME2	Oct 2016	13.4	8.03	0.35	2100 pH 2100 *pH/T*	-0.33 -0.33/+2.5°C	18	NO_3^-, P, Si 2-6 days	Biomass, Composition, PC/PN, FAs	Grazing rate
ME3	Nov. 2017	15.6	8.02	1.2	2100 *pH/T* 2150 *pH/T*	-0.33/+2.6°C -0.5/+4.5°C	22	NO_3^-, P, Si, NH_4^+ Daily	Biomass, Composition, PC/PN, FAs, AAs/CSIA-AA	Composition, abundance, grazing, FAs, CSIA-AA
ME4	Sept-Oct 2018	12.1	8.20	7.0	*pH* *pH/T*	-0.5 -0.5/+3.5°C	20	NO_3^-, P, Si, NH_4^+ Daily	Biomass, Composition, PC/PN, FAs, CSIA-AA	Composition, abundance grazing, FAs, CSIA-AA, mussel larvae growth & survival

Temperature and pH were monitored continuously, and also controlled in the treatment bags by a Labview software system that responded to changes detected by pH and temperature sensors by adjusting pH via CO_2 injection through a permeable diffusion tubing coil, and temperature using a heating element (see Figure 3). As the temperature of the Control and *pH* treatments were maintained by surface seawater supply it tracked Ākautangi/Evans Bay water temperature and also showed some diurnal oscillation. The Control pH also showed some diurnal oscillation (see Figure 3) but was higher than that of Ākautangi/Evans Bay water due to the elevated productivity (see Results).

A variety of parameters were sampled for over the following 18–22 days. Selected parameters were monitored in real time using an in-line system that pumped water from each bag once every hour through an Exosonde system incorporating sensors for temperature, pH, dissolved oxygen, salinity, and fluorescence. This enabled environmental conditions to be monitored continuously and any issues, such as power or sensor failures, to be rapidly identified. Core parameters, including nutrients, chlorophyll-*a*, bacteria, and phytoplankton abundance were sampled every day in the first three experiments (ME1–3), and on every second day during ME4, with all other parameters sampled at 2–4 day intervals.

Due to technical difficulties during ME2, only one *pH/T* bag was maintained to the end of the experiment and, although these data are presented, they are not interpreted due to the lack of replication. In ME3, only two bags were maintained to the end of the experiment for the Control and treatments, and so statistics and interpretations are based upon duplicate samples.

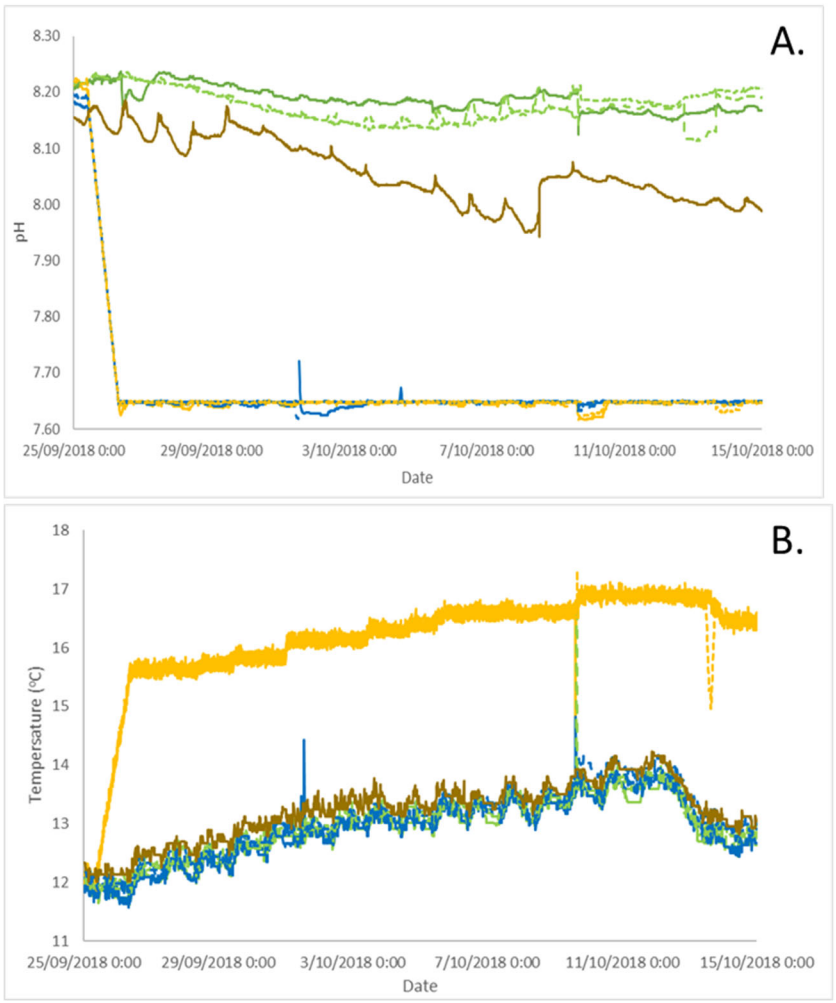

Figure 3: A. Temperature (°C) and B. pH during ME4 showing Control (green), *pH (*blue), *pH/T (*orange) and ambient Ākautangi/Evans Bay water (brown). The 24-hour adjustment period is apparent at the start of the experiment on 25–26/9/20218. Occasional spikes in the dataset correspond to cleaning or removal of sensors. The initial pH of 8.2 is relatively high compared with the other experiments due to ME4 starting during a major phytoplankton bloom.

Different nutrient regimes were applied in the four experiments (see Table 2). No nutrients were added in ME1 so that the results reflected the response in a nutrient-limited system. In ME2 the major nutrients nitrate, phosphate and silicate were added intermittently; as nitrogen is the primary limiting nutrient in coastal waters the concentration was replenished at six timepoints during the experiment, whereas phosphate and silicate were added on two and three occasions, respectively. In ME3 and ME4 nutrient supply was more regular with a lower dose of these three macronutrients and also ammonium on each day. Nutrient addition was required to sustain the phytoplankton as the experimental water in the bags was isolated from the main sources of nutrients in Ākautangi/Evans Bay, such as the sediments and freshwater input. ME2, ME3, and ME4 received similar total additions of dissolved inorganic nitrogen (nitrate and ammonium), whereas silicate addition was relatively larger in ME2 and phosphate relatively lower in ME3.

Table 2: Nutrient additions in relation to concentrations in Ākautangi/Evans Bay. There were no nutrient additions during ME1.

Concentration/addition (µmol/l)	Nitrate	Ammonium	Phosphate	Silicate	N:P	Si:N
ME1 *Evans Bay mean*	*1.18*	*1.57*	*0.46*	*3.09*	*6.0*	*1.1*
ME2						
Evans Bay mean	*0.53*	*0.89*	*0.34*	*9.00*	4.2	6.3
Addition to each bag	0.5-0.67	0	0.66-0.92	1.22-2.9		
Total addition in ME2	3.83	0	1.58	6.28	2.4	1.6
Addition as % of Evans Bay mean	*100-126*	*0*	*194-270*	*12.5-32*		
ME3						
Evans Bay mean	*0.46*	*0.39*	*0.30*	*2.87*	2.8	3.4
Daily Addition to each bag	0.15	0.12	0.02	0.13		
Total addition in ME3	2.66	2.16	0.29	2.60	16.4	0.5
Addition as % of Evans Bay mean	*32.3*	*33.7*	*5.4*	*4.5*		
ME4						
Evans Bay mean	*0.27*	*0.53*	*0.30*	*1.50*	2.7	1.9
Daily Addition to each bag	0.13	0.13	0.06	0.14		
Total addition in ME4	1.78	1.77	0.91	1.97	3.9	0.6
Addition as % of Evans Bay mean	*47.0*	*23.8*	*21.6*	*9.4*		

Phytoplankton culture experiment

Water was subsampled at the end of ME3 from which the dominant diatom species (*Cylindrotheca closterium)* was isolated and cultured. The diatom was grown in f/20, a medium consisting of 1/10th of the recommended addition of Guillards f/2 (Sigma G0154) to natural seawater. The seawater was collected at Portobello Marine Laboratory (Otago) with nominal concentrations of 0.3–0.4 µmol/l phosphate, 3–6 µmol/l nitrate, and 4–6 µmol/l silicate. The f/2 addition raised the phosphate concentration by an additional 3.67 µmol/l and nitrate concentration by an additional 0.88 µmol/l. As there was no silicate in the Sigma f/2 preparation, an additional 5 µmol/l silicate was added. Prior to the experiment, the diatom was cultured for a week in 250-ml acid-cleaned, sterile, polycarbonate bottles (Nalgene), with lids modified with two openings. Special air mixes (380 ppm CO_2, 21% oxygen in nitrogen for the Control, and 750 ppm CO_2 for *pH/T*) were transferred through one opening into the bottle headspace via a 0.22 µm syringe filter to maintain target pH, with an exhaust 0.22-µm filter attached to the second opening to relieve pressure. The bottles were incubated in two incubators at 15.5 °C and 18 °C, respectively for the Control and *pH/T* treatment, with irradiance set at 60 µE m^2/s on a 12 hour:12 hour light:dark cycle.

At the start of the experiment, cells were inoculated into two batches of 3 x *Now* medium, representing the Control situation. Three of these were used as the 1st batch of Future *pH/T* cultures and were bubbled with 750 ppm CO_2 for the following 48 hours to gradually reduce the seawater pH. The temperature was increased by 0.5 ºC every 12 hours from 16 to 18 ºC over the same period. Following this treatment, the diatom species was inoculated into fresh *Now* and *Future* medium, as described above, for the remainder of the incubation. The diatoms were maintained in a semi-batch style to keep the cells in exponential growth. Cell concentration was also kept low to keep the pH at the target value. The total incubation time was 19 days. At the end of the experiment, samples for fatty acid analysis were collected on ashed GF/F (Whatman) filters, which were rinsed with sterile seawater after filtration and sent to the Cawthron Institute for analysis (see Fatty Acid methodology below).

Ancillary parameters

Total **Chlorophyll-*a*** (Chl-*a*) was determined every day (and every second day in ME4) by filtering a 250-ml sample onto a GF/F filter, which was folded and then snap-frozen in Liquid Nitrogen and then subsequently stored at -80 ºC prior to extraction in 90% acetone and analysis using a Turner Design fluorometer. The Chl-*a* content of different size fractions (0.2–2µm, 2–5µm, 5–20µm, > 20µm) was

also determined on every second day by filtering 500 ml through sequential filters to provide information on changes in the size spectrum of the phytoplankton.

Phytoplankton community composition and cell numbers for species > 5 µm were determined using optical microscopy. One litre of water was preserved every 2–4 days during the experiments, using Lugol's solution, and subsequently examined using optical microscopy, as described by Safi et al. (2007) and references therein. Briefly, 150-ml subsamples were settled for 24 hours before being examined in Utermohl chambers on a Leitz inverted microscope. Where possible, all abundant organisms were identified to genus or species level before being counted. Biovolume was calculated for each species, using formulae representing the geometrical solids that approximated cell shape and adjusted for cell shrinkage, following Verity et al. (1992). Phytoplankton carbon (µg C/l) was then calculated using the conversion equations of Montagnes & Franklin (2001) for diatoms; Eppley et al. (1970) for dinoflagellates and Menden-Deuer & Lessard (2000) applied to other low biomass groups including small flagellates, raphidophyceae, prymnesiophyceae, cryptophyceae, chrysophyceae, euglenoids, and monads.

The abundance of different phytoplankton size classes was also determined with counts obtained for picoeukaryotes (0.2–2 µm) and nanoeukaryotes (2–20 µm). Samples were obtained each day with 1.8 ml of seawater fixed with 36 µl 25% glutaraldehyde to a final concentration of 0.5% glutaraldehyde in cryovials. Samples were flash frozen in liquid nitrogen and stored at -80 °C until analysis. Total numbers were determined by flow cytometry using a BD Accuri™ C6 Plus instrument (BD Biosciences). A 250-µL aliquot sample was analysed and the eukaryotic plankton populations were identified using a SSC vs. FL3 plot and the prokaryotic picoplankton (*Synechococcu*s sp.) population was identified using a FL1 vs. FL2 plot.

Particulate Carbon and **Nitrogen** were determined by filtering 500 ml of sample water through a pre-combusted 25-mm GF/F filter and stored at -20 °C. Samples were collected every 2 days (and every 4 days in ME4) with analyses carried out on a DELTA V Plus continuous flow isotope ratio mass spectrometer linked to a Flash 2000 elemental analyser (EA-IRMS) via a ConFlo IV, and using a MAS 200 R autosampler (Thermo-Fisher Scientific, Bremen, Germany) at the NIWA Environmental & Ecological Stable Isotope Facility in Wellington, New Zealand. Carbon and nitrogen content (%C and %N) were calculated from thermal conductivity detector values during EA-IRMS analysis.

Zooplankton identification and abundance

Mesozooplankton were collected between 10AM and midday, using a 23-mm diameter ring net fitted with a 64-µm mesh net. Each mesocosm bag was sampled with one vertical haul for zooplankton identification and one haul for zooplankton grazing experiments (see below), by lowering the net to a depth of 3 m (close to the bottom of the mesocosm bag) and raising it to the surface, filtering a volume of ca. 125 L. Once the cod-end was out of the experimental bag, the contents were poured into 400-ml jars and fixed with 5% buffered formalin for taxonomic identification. Samples were rinsed in tap water through a 50-µm sieve, placed on a sorting tray, and counted and identified to species level if possible. Zooplankton identifications were done on samples from the last day to investigate the effect of ocean acidification on the acclimated community. Mesozooplankton identifications were not processed for ME2 due to low numbers and high variability from grazing estimates. As the sampling for zooplankton species and abundance took place at one time point only within each experiment, differences between Controls and treatments were tested for using one-way Analysis of Variance (ANOVA), with analyses carried out using MATLAB 2017.

Seeding. Due to low zooplankton abundances in ME1 and ME2, the bags were seeded with a pre-concentrated zooplankton community from Ākautangi/Evans Bay and Lyall Bay in ME3 and ME4. For ME3, plankton tows were conducted at Lyall Bay (2 tows) and Ākautangi/Evans Bay (7 tows), using a 200-µm 'Heron net' and filtering cod-end. Approximate filtered volumes (estimated using length of tow, metres, and mouth of net, square metres) were 3400 L per tow. Tow contents were diluted into ambient seawater and then pre-filtered through 2-mm Nitex mesh to screen out gelatinous organisms. In the laboratory, tow contents were settled, and debris (sand, macroalgal detritus, marine snow) was gently suctioned from the bottom of the sample jar to minimise the contribution of non-living zooplankton.

Visual inspections showed negligible detritus. 'Clean' aliquots were transferred slowly into two holding tanks to homogenise the seed population, for a total of 100 L of concentrated zooplankton. Each mesocosm bag was seeded with a combination of 5 L from each holding tank (total = 10 L seed zooplankton). One litre aliquot was preserved in buffered 5% formalin for later enumeration, with two aliquots of 2 L each filtered onto pre-combusted 47-mm diameter GF/F filters with the filters frozen at -20 ºC for subsequent fatty acid and amino acid analysis (see below). The seeding for ME3 did not result in a significant addition of zooplankton due to the naturally lower zooplankton concentrations at that time of the year.

For ME4, zooplankton tows were collected at the entrance of Ākautangi/Evans Bay on September 24th, 2018, between 10AM and 1:30PM. A 0.5-m diameter plankton net, equipped with > 500-µm mesh net, was deployed from the stern of the boat, and towed for a distance of ~255 m, at a speed of ~1.2 knots, equating to about 6 minutes of tow time. Transects were run between two set points, and the contents of the two tows concentrated in each 20-L bucket. These transects were repeated nine times (for a total of 18 plankton tows), and distributed into 9 x 20-L buckets, to seed each mesocosm bag. The approximate volume filtered per tow was 50.1 m^3, and so each mesocosm was seeded with the > 500-µm plankton filtered from 100 m^3 of sea water. Visual inspections of plankton contents indicated a high number of crab megalopa and decapod larvae, with copepods, ctenophores, and jellyfish. Although the ME4 tow volume was about 15 times that of ME3, comparison of zooplankton numbers (all taxon) for ME1, ME3, and ME4 showed no significant change in initial vs. final concentrations, suggesting the elevated zooplankton concentrations, particularly in ME4 were not unsustainable. Comparison of zooplankton abundances showed that the initial stocks in ME1 (not seeded, but with naturally higher zooplankton abundance) had similar abundances to the seeded ME4 (average initial abundance 13 700 individuals/m^3 in ME4, 11 500 in ME1; equivalent to 13 individuals/ L in ME4 vs. 11.5 individuals/ L in ME1). These numbers are comparable with other New Zealand neritic regions (e.g.; 8 individuals/ L, summer coastal Otago, M. Meyers and M. Decima, pers. comm.).

Fatty acids

Fatty acid (FA) concentration was determined in bulk particulates, obtained from the filtration of 3 or 4 l of seawater onto a 0.7-µm GF/F filter during ME2, ME3, and ME4, and also in the dominant zooplankton species during ME3 and ME4. FA analyses were carried out by the Cawthron Institute (Nelson), using methodology consisting of direct methylation and extraction in acidic conditions in methanol, with the resulting FA methyl esters (FAME) extracted in hexane and analysed by Flame Ionisation Detector (Iatron Laboratories, Tokyo, Japan), as described by method AOAC 963.22 OMA and Miller & Tain (2018). This is an IANZ accredited test, as used by Miller et al. (2014a). Minor FAME were further identified via GC-Mass spectroscopy.

A full list of the FA species measure is provided in Appendix 1 and the results are discussed in terms of the FA groups:

- Monounsaturated Fatty Acids (MUFA)
- Saturated Fatty Acids (SFA)
- Polyunsaturated Fatty Acids (PUFA)
- n-3 Polyunsaturated Fatty Acids (n3PUFA)
- Total Fatty Acids (TFA)

Amino acids

Amino acids (AAs) are structural components of proteins and are an important nitrogen source for most organisms. Measurement of AA concentration provides an indication of nutritional value that can be complemented by the additional measurement of AA stable isotopes (Compound Specific Isotope Analysis of Amino Acids (CSIA-AA)). These measurements provide a means to identify the sources and pathways of essential organic compounds and energy through a food web, and thus information on both trophic interaction and transfer (Eglite et al. 2018, Yamaguchi & McCarthy 2018).

Seawater (10 L per mesocosm bag) was collected in 10-L HDPE containers. For each bag, a 3-L subsample was immediately filtered on pre-combusted (450 ºC, 2 h) GF/F glass-fibre filters (nominal 0.7-µm pore size GF/F). Samples collected represented between 400 and1000 µg of C and 75–200 µg of N on each

filter. Filters containing particulate organic matter (POM) were rinsed with Milli-Q water and immediately dried in an oven at 50 ºC for 24 h. An internal standard, norleucine (50 µl of 1 mg/ml solution), was added to monitor the wet chemistry and AA stable isotope values. Amino acids were then extracted by hydrolysing whole dried filters with 7 ml of 6-M HCl at 110 ºC for 24 h in a N_2 atmosphere. Solutes were then dried under a gentle flow of N_2 at 60 ºC and subsequently converted into N-acetyl isopropyl (*N*AIP) ester derivatives following the protocol described by Sabadel et al. (2016), modified from Styring et al. (2012). Both concentrations and isotopes values can be measured from the same prepared samples. Eleven amino acids from each sample were measured with no peak co-elutions, as listed here. In order of elution: alanine (Ala), glycine (Gly), valine (Val), leucine (Leu), isoleucine (Ile), threonine (Thr), serine (Ser), proline (Pro), aspargine + aspartic acid (Asx), glutamate + glutamic acid (Glx), and phenylalanine (Phe). Note that during the hydrolysis step, aspargine is converted to aspartic acid (hence the notation Asx) and glutamate is converted to glutamic acid (hence the notation Glx).

Amino acid concentrations measurements. Concentrations of AAs were measured using a GC-FID. The instrument used for these measurements was a Hewlett Packard (HP 6890 Series), combined with a Hewlett Packard autosampler (HP 7683 Series Injector). The column used for the separation of AAs was a VF-35 ms column (0.32 mm ID and a 1.0 µm film thickness). The samples were injected with a 1:3 split ratio and carried to the detector with helium at a flow rate of 1.4 mL/min. Both injector and detector were maintained at 250 ºC, and the GC initial temperature was set at 40 ºC and held for 5 min, then increased to 120 ºC at 15 ºC/min, then to 180 ºC at 3 ºC/min, then to 210 ºC at 1.5 ºC/min, and finally to 270 ºC at 5 ºC/min and held for 7 min.

CSIA-AA measurements. Stable isotope ratios of nitrogen in AAs ($\delta^{15}N_{AA}$) were measured by gas chromatography/combustion/isotope ratio mass spectrometer (GC-IRMS), using a Thermo Trace gas chromatograph, the GC combustion III interface, and a Delta^{plus} XP isotope ratio mass spectrometer (Thermo Fisher Scientific). Two hundred nL aliquots of derivatised AA were injected, with the inlet at 270 °C in splitless mode, carried by helium at 1.4 ml min^{-1} and separated on the same VF-35 ms column used for AA concentrations. The GC sample treatment programme was also identical to the one used for AA concentrations. The oxidation rector was set at 980 °C and the reduction reactor at 650 °C and a liquid nitrogen cold trap employed after the reduction reactor. Samples were analysed in triplicate along with amino acid standards of known isotopic composition (measured by define-IRMS) and bracketing of each triplicate measurement. Each run contained no more than six samples. The δ values were reported following the conventional method of expressing δ at natural abundance, in per mil (‰), of the ratio of ^{15}N to ^{14}N, relative to an international standard: atmospheric N_2 for $\delta^{15}N_{AA}$. Precision (1 standard deviation, SD) for $\delta^{15}N_{AA}$ ranged from 0.1 to 1.0‰ with an average SD of 0.5‰.

Statistical analysis

Two types of statistical analysis were carried out on the above parameters to examine a) temporal variation in response and (b) magnitude of response.

a) GAMMs (Generalised Additive Mixed Models) were used to identify if there were significant temporal variations in the treatments relative to the Control over the duration of each experiment. A GAMM is an extension of a generalised linear model in which the response is dependent upon non-linear smoothing functions of associated predictors. Datasets were provisionally tested for normality using a Shapiro-Wilks test to confirm $p > 0.01$ and then assessed using a Normal Q-Q plot to ensure that each dataset was normally distributed. Three models were then generated, with each accounting for repeated measures with inclusion of an auto-correlation term for each treatment replicate (two or three bags per treatment):

Model 1 provided a global smooth across the experiment, with no breakdown into different treatments, and so predictors were Day Number and the auto-correlation term. As this model represents one underlying process over time with no effect from treatments, this was the Null model.

Model 2 provided independent smooths across each experiment for each treatment, with predictors of Day Number subset by Treatment ID and the auto-correlation term, and so represented individual processes occurring over time in each treatment.

Model 3 provided a global smooth across Days and independent smooths across Days for each treatment using predictors Day Number, Day Number subset by Treatment ID, and the auto-correlation term. This model represents one underlying process affected by individual treatment effects.

The relative information loss between models was assessed using the Akaike information criteria (AIC). The lower the AIC value the less information is estimated to have been lost; therefore, if Model 1 results in the lowest AIC then differences between Control and treatment are negligible whereas if Models 2 or 3 have the lowest AIC, there is evidence for differences based on the treatments. In the latter case, additional assessment was carried out by determining smoothing functions that best represented the difference between each of the treatments and the Control by testing the deviation from zero (Rose et al. 2012; "itsadug" package, R Core Team 2019). If the AIC indicated a treatment effect, the difference between the Control and treatment GAMMs was calculated and tested for deviation from zero using a Wald's test, with an indicated difference shown by a $p < 0.1$ and a significant difference by a p of < 0.01.

b) The GAMMs approach facilitated comparison of temporal trends across each experiment but was less suitable for identifying treatment effects that become dominant with time, and in generating comparative means for different experimental phases. Consequently, differences between the Control and treatments were also assessed for the final phase of each experiment (see definition of phases in Chlorophyll-*a* results below) by comparison of the mean values for this period. This was carried out using *t*-test and Wilcoxon rank sum approaches, with the latter applied due to non-normal behaviour in some cases, and adjusted for family-wise error using the Holm-Bonferroni correction to reduce the number of Type I errors (false positives). As these mean estimates accommodate the temporal variation of replicates over a 6–8 day period in addition to natural population variance, significant differences are identified at $p < 0.1$, with indicative but non-significant differences at $p < 0.15$ also noted.

As the majority of the GAMMs and Phase 3 analyses yielded no significant difference between treatment and Control, the discussion focuses primarily on the significant differences only. Different statistical approaches were used for other parameters where appropriate, as noted in the following sections.

2.2 Specific Research Objective 2: Influence of future changes on rates

Examine how coastal acidification influences the total content of Fatty Acids in green-lipped Mussels

Microzooplankton grazing

An experimental approach was used to investigate the effects of ocean acidification and warming on:
(a) phytoplankton intrinsic growth rate (μ_0) and its relation to maximum growth rate (μ_{nut}),
(b) microzooplankton grazing,
(c) net growth rate, and
(d) the dynamic coupling between phytoplankton growth and microzooplankton grazing.

Dilution grazing experiments were coupled with Chl-*a* concentration and flow cytometry analysis (see above) to assess growth and grazing rates of the phytoplankton community and picophytoplankton groups in three experiments (ME1, ME2, and ME3). The 2-point dilution approach (Landry et al. 1984, Gutiérrez-Rodríguez et al. 2015) was adopted, which reduces the number of bottles substantially relative to the standard experimental design (11 bottles), allowing replicated experiments to be run for each of the nine mesocosm bags. Seawater from each mesocosm was collected into a 10-L carboy from which 3 x 2.2-L polycarbonate bottles were prepared with a mixture of whole and filtered seawater. One 2.2-L bottle was filled with 30% of seawater filtered by gravity through a 0.2-µm pore size, and a second bottle was filled with whole seawater. Dissolved inorganic nutrients, including $NaNO_3$ (9.18 µM), NaH_2PO4 (1 µM), NH_4Cl (1 µM), and $NaSiO_3$ (11 µM), as well as vitamins and trace metals (in f/20 concentration), were added to these two bottles to ensure sufficient nutrients during the 24-h incubation. A third bottle filled with whole seawater was prepared as a control without nutrient addition. The 10 experiments (i.e.; 30 bottles in total) were incubated under the respective treatment temperature and light in three temperature-controlled, flow-through incubators located next to the experiment pool. Chl-

a and flow cytometry samples were taken in triplicate from each of the 10-L carboys used to set up the dilution grazing experiments.

After 24 h, the ten experiments were sequentially terminated and final samples for Chl-*a* and flow cytometry were taken. Analyses were conducted following standard fluorometric and flow cytometry analytical methods (see above). The Chl-*a* and cell abundance estimates were used to calculate the net rates of change (k) of phytoplankton community and picophytoplankton populations (*Synechococcus*, Picoeukaryotes, and Nanoeukaryotes), respectively, assuming that grazing mortality declined linearly with dilution. Accordingly, the net rate of change is $k = \alpha - x_m$ in the undiluted (whole seawater) bottles and $k_d = \alpha - x_m$, where x is the fraction of natural grazer density in the diluted treatment (0.20 in ME1 and 0.3 in ME2 and ME3) and m = instantaneous microzooplankton grazing coefficient (/day). The two equations:

$$m = \frac{kd-k}{1-Xm} \text{ and } \mu = k + m$$

were then solved for the two unknowns in the nutrient amended bottles (μ_{nut} and m). Intrinsic growth rate (μ_0) at in situ nutrient conditions was calculated as the net rate of change estimated in the unamended incubation plus grazing ($\mu_0 = k + m$). Linear regression analysis between phytoplankton growth and microzooplankton grazing was used to investigate the coupling between these processes, with analysis of covariance (ANCOVA) used to compare between treatments

Copepod grazing rate from gut content analysis

Sampling on day 2 was carried out using 47-mm GFFs on the whole > 64-µm plankton community. However, because of the presence of large phytoplankton, an extra haul was conducted to obtain a grazing estimate of a second size fraction > 80 µm, with the aim of excluding large phytoplankton aggregates. For these hauls, cod-end contents were filtered onto pre-cut 80-µm nitex-mesh filters. Samples for grazing rate determination were immediately flash frozen in liquid nitrogen and subsequently stored at -80 ºC. During ME3, grazing estimates were carried out only on the > 80-µm zooplankton community to decrease the potential of phytoplankton contamination. Filters with zooplankton were added to a test tube with 6 mL of 90% acetone and sonicated with an ultrasonic tissue homogeniser. Samples were settled in the dark at -20 °C for 4–24 h for Chl-*a* extraction. Samples were then centrifuged at 3000 g for 5 min to remove zooplankton particles and poured into 8-mL borosilicate glass tubes for fluorometric analysis. Chl-*a* and phaeopigments were analysed using a 10AU Turner fluorometer with a Chl-*a* filter set (excitation band-pass filter 340–500 nm (Turner Designs 10-050R), and a long-pass emission filter from 665 nm (Turner Designs 10-051R), before and after acidification with 2 drops of 10% HCl. Phaeopigments were used in estimates of grazing to ensure phytoplankton contamination was not contributing to these estimates. Pigment contents were multiplied by a temperature-dependent gut passage rate (Dam & Peterson 1988), and a 12-hour feeding period was assumed to obtain daily grazing rates.

Copepod grazing rate incubations

Incubations were carried out to assess the effects of future climate conditions on zooplankton grazing rates, prey selectivity, and trophic network interactions. Copepods typically dominate mesozooplankton (200–2000 µm) communities in coastal areas and, via grazing, can have significant top-down effects on phytoplankton and microzooplankton (20–200 µm) communities and trophic pathways (Armengol et al. 2017). Trophic relationships among phytoplankton, microzooplankton, and copepods are crucial for maintaining coastal ecosystem health and function, but their natural dynamics may shift with changing ocean conditions.

Wild-caught copepods were acclimated for 24 h in ambient conditions before each 24-h grazing incubation. Grazing incubations were set up to incorporate the dilution method following Landry & Hassett (1982) and to correct for the grazing impact of microzooplankton, following Nejstgaard et al. (2001). Subsamples of Ākautangi/Evans Bay water used to fill each of the incubation jars were analysed to characterise the initial prey community and, after 24 hours, the water in the jars was analysed to characterise final prey community and determine grazing rates. All prey particle concentration and

compositional characteristics were analysed using a FlowCam, with image files analysed using Visual Spreadsheet software. The final estimates of copepod grazing result from a stepwise series of calculations that were based upon differences in phytoplankton growth among the three jars of the incubation set-up: Control, Dilution, and Copepod. Calculations followed the methods and formulas presented by Frost (1972), Landry & Hassett (1982), and Nejstgaard et al. (2001). During ME3, three 24-h zooplankton grazing incubations were conducted on days 10, 17, and 21 of the mesocosm experiment, as detailed in Table 3. During ME4, two 24-h grazing incubations using the calanoid copepod *Temora turbinata* were conducted on days 10 and 16 of the mesocosm experiment, with details of the experimental design summarised in Table 4.

Table 3: Summary of three zooplankton grazing incubations carried out during ME3.

Timing during mesocosm experiment		Mesocosm bags used for incubation			Copepod species	Copepod source	Pre-condition period (d)	Incubation period (d)
		Control	*2100*	*2150*				
Inc. 1	Day 10–11	2, 6, 7	3, 4, 8	N/A	*Temora turbinata*	Evans Bay	1	1
Inc. 2	Day 17–18	6	3	N/A	*Paracalanus* sp.	Evans Bay	1	1
Inc. 3	Day 21–22	6	3	N/A	Natural mixed community	Mesocosm bags	N/A	1

Table 4: Summary of the two zooplankton grazing incubations carried out during ME4.

Timing during mesocosm experiment		Mesocosm bags used for incubation			Copepod species	Copepod source	Pre-condition period (d)	Incubation period (d)
		Control	pH	*pH/T*				
Inc. 1	Day 10–11	2, 6, 7	3, 4, 8	1, 5, 9	*Temora turbinata*	Evans Bay	1	1
Inc. 2	Day 17–18	2, 6, 7	3, 4 ,8	1, 5, 9	*Temora turbinata*	Evans Bay	1	1

Green-lipped mussel veliger larvae growth and survival

Experiments on mussel larvae were carried out during one mesocosm experiment (ME4) only. Farmed green-lipped mussels (*Perna canaliculus*) were harvested from Pelorus Sound in late 2017 and held in broodstock conditioning systems at the Cawthron Aquaculture Park, Nelson. Mussels were induced to spawn on 1/10/18 by thermal cycling, and fertilised eggs allowed to incubate for 48 h until early D-veliger larvae had formed under ambient pCO_2 conditions. Larvae were retained on a mesh screen and transported to NIWA Wellington in air at 6 °C, where they were suspended in a known volume of water with volumetric counts carried out using a stereomicroscope. Known suspension density was used to transfer approximately 700 individuals into PVC cages (Figure 4a). The cages were arranged in clusters of 5 and lowered into each of the nine mesocosm bags, which were randomly assigned to the Control, *pH*, and *pH/T* bags, with a total of 15 cages added to each bag (Figure 4b). An additional 10 cages were immersed in a Control bag to provide a baseline reference.

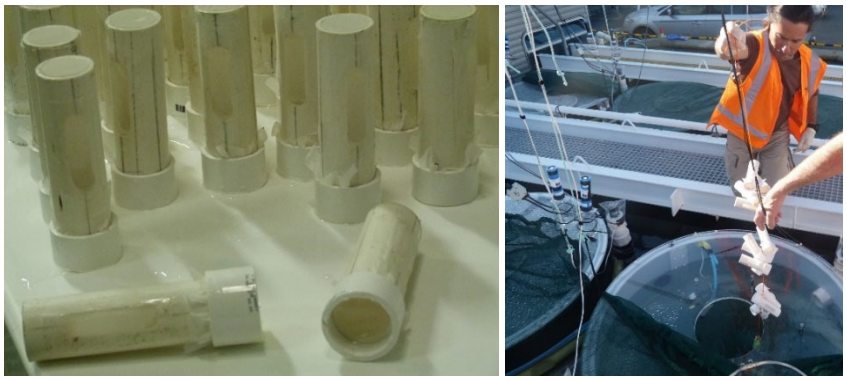

Figure 4: a (left) 50-mL PVC cages used to retain larvae. 45-µm mesh was used in the side and end windows to facilitate water exchange. b (right) Clusters of 5 larval cages, each allocated to a specific sample day.

Larval census (survival and retention) and shell length measurement

The 10 reference cages suspended in bag 2 were removed after 1–2 h, and the contents of each tube rinsed into a 4-mL tissue culture dish well and fixed with 200 µL of 4% formalin. The larvae were then counted under a low power inverted microscope. The mean cage population was taken to be the theoretical starting population for all subsequent assessments. Clusters of 5 cages were removed from each bag after 2, 5, and 9 days (i.e.; 4-, 7-, and 11-days post-fertilisation). The larvae were fixed and counted, with the number of malformed individuals (distorted shell or velum) and dead shells counted separately. The shell length of a minimum of 25 individual larvae from each cage was determined using calibrated Nikon cellSense software applied to low power microscope images.

Statistical analysis

The proportion of two-day old larvae surviving at the end of the trial (i.e.; 11 days old) were compared by analysis of variance (ANOVA) of arcsine-square root transformed data, followed by Tukey's honestly significant difference (HSD) comparison of means. Sample time was considered a fixed effect in a two-way analysis of variance applied to the data.

2.3 Specific Research Objective 3: Projecting future impacts on green-lipped mussels

Growing and maintaining green-lipped mussels in the mesocosm experiments would have been challenging due to the long-time frame (on the order of months), and large food volume required to sustain the mussels. Instead, results from the ME experiments were applied in a dynamic energy budget (DEB) model that was previously developed to simulate the energetics of this species (Ren et al. 2020). DEB models utilise relationships between an organism's physiology and the environment to examine the metabolic dynamics of an individual organism through its life cycle, and so provide a framework to investigate the influence of stressors, such as ocean acidification. The DEB model includes food uptake, assimilation, energy allocation, maintenance, reproduction, and growth (shell and flesh) under dynamic environmental conditions, and a detailed description and parameterisation of the model is given by Ren et al. (2020). The DEB model requires time-series environmental data and mussel growth data including length, flesh weight, food availability, and temperature. The DEB model was calibrated and validated with data collected in the coastal Marlborough Sounds and so is readily applicable to the Ākautangi/Evans Bay inner harbour ecosystem; however, the current form of the model was not calibrated with data from the mesocosms in which experimental conditions differed from natural ecosystems. Although the model cannot simulate the absolute energetics of mussels without calibration of environmental and mussel growth data, it can be used to simulate the relative performance of mussels under the different environmental conditions. Consequently, rather than simulate absolute energetic or growth, the aim was to simulate the potential performance of mussels in response to different environmental scenarios, i.e.; between Controls and the *pH* or *pH/T* treatments.

The model simulations were based on the assumption that mussels were grown in the Control and treatment conditions for a period equivalent to the 18–24-month lifespan of mussels in longline aquaculture in New Zealand. The model outputs were analysed and compared between treatments and included food uptake rate, energy allocation for reproduction, and growth of shell length and flesh weight. For each Control and treatment, the model was run for a period of five years with constant input data values of 'food' and temperature obtained from Phase 3 of the mesocosm experiments. Although constant food and temperature do not reflect natural environmental conditions, it is considered appropriate for understanding potential growth performance of mussels between the Control and different treatment conditions.

For application in the DEB model, two 'food' variables were utilised as energy input (e.g.; joule or carbon), and independently assessed to determine their effect on mussel energetics:

- Chlorophyll-*a* was used as an indicator of phytoplankton biomass, using conversion ratios of 50:1 for carbon to chlorophyll, and 49 joule/mg C (Mackenzie et al.1986, van der Meer 2006).
- Particulate carbon consists of living phytoplankton cells and detritus, of which the former is the primary food contribution, and the latter contribute little to mussel energetics and growth (e.g.; Ren & Ross 2005, Ren & Schiel 2008). This is because detritus contains both labile and refractory components, and the latter contributes a large proportion to total detrital biomass. Ideally, separation of phytoplankton and detrital carbon would accurately reflect 'food' availability to mussels, but the ME particulate carbon data consist of a mixture of phytoplankton and detrital carbon. Furthermore, the DEB model uses total particulate carbon as an indicator of mussel 'food' for model simulations and includes a blended digestion efficiency that reflects different particle sources and quality (Ren & Ross 2005). The use of total particulate carbon may compromise the model simulation results for absolute energetics and growth of mussels and so total cellular carbon was determined using the carbon content of phytoplankton >5 µm, estimated by optical microscopy as described above, combined with particulate Carbon in the 2–5-µm fraction, as estimated by applying the carbon to chlorophyll conversion ratio of 50:1 in the 2–5-µm size fraction for chlorophyll (see above).

2.4 Presentation of Results

To assist interpretation and continuity the results of Research Objective 1 are followed by the DEB model results (Research Objective 3), as the model uses results from Objective 1.

The results, figures, and discussion primarily focus on significant treatment effects (those that differ between treatment and control). Data for some ancillary parameters and those that showed negligible treatment effects are presented in the Appendices.

Responses to the experimental treatments are described using the following notation:

- Ambient conditions (Control)
- low pH (*pH*)
- low pH combined with elevated temperature (*pH/T)*.

In ME1 and ME2, incremental changes based upon projections for 2100 for the open ocean (Law et al. 2018b) were made relative to the ambient temperature and pH at the start of the experiments. In ME3, two future scenarios, incorporating both pH and temperature changes, were used for the years *2100* and *2150.* In ME4, a lower absolute pH value of 7.65 was used in both *pH* and *pH/T* treatments, as this was the minimum pH value projected for another New Zealand coastal site (the Firth of Thames) for 2100 (K. Currie and S. Mikaloff-Fletcher, pers. comm.).

For most parameters, data are presented in two graphical forms:

a) individual datapoints for each treatment replicate are plotted against time over the course of the experiment, and overlain by GAMMs (General Additive Mixed Model, see above), and
b) the mean for the control and treatments are plotted against time over the course of the experiment and overlain by the phase mean and standard deviations for each temporal phase of each experiment. These phases are based on Total Chl-*a* biomass and are described below in Section 3.

3. RESULTS AND DISCUSSION

3.1 Specific Objective 1: Effect of future changes on coastal plankton

Ancillary variables

Total Chlorophyll- *a*

Initial total Chlorophyll- *a* (Chl-*a*) differed between experiments with relatively low values of 0.5–1.0 mg/m^3 in autumn in ME1 and spring ME2 and ME3, but elevated concentrations in ME4 (7.0 mg/m^3) as the latter began during a major bloom in Ākautangi/Evans Bay. These differences in initial conditions reflect inter-annual variation in the onset of stable conditions for phytoplankton growth conditions in spring (Pinkerton et al. 2018). The temporal trends in total Chl-*a* also differed between experiments, with the nutrient-deplete ME1, and ME2 exhibiting a mid-experiment maximum, whereas Chl-*a* increased throughout ME3 and declined throughout ME4 (see Figure 5; ME2 not shown). These trends within experiments likely reflect nutrient availability and the status of the phytoplankton community at the start of each experiment, with the mesocosm bag environment providing more stable conditions for growth in ME1–ME3; conversely biomass declined from the peak of a natural bloom at the start of ME4.

Temporal phases of experiments derived from Chl-a

The observed temporal trends in total Chl-*a* (and particulate carbon) were used to divide each ME into temporal phases. All experiments exhibited an initial adjustment over Days 1–6 in Phase 1 during which the planktonic community altered in response to conditions in the mesocosm bags. Although the experiments were run under largely natural conditions it was not possible to completely simulate the natural mixing and ambient light climate in Ākautangi/Evans Bay, hence the initial adjustment in the phytoplankton community. During Phase 2, ME1 and ME2 exhibited a phytoplankton biomass maximum between Days 6 and 12, whereas ME3 and ME4 biomass remained relatively constant but subsequently increased in Phase 3 (the final 6–8 days, see Figure 5). This trend may reflect nutrient availability as the nutrients were added on a daily basis in ME3 and ME4. Propagation of treatment effects may be expected to increase with time and so the response in the final week of each experiment is considered more representative of the long-term response; indeed treatment and control responses were generally most divergent in this final phase (see Figure 5). Consequently, the following discussion focuses primarily on differences in treatment and Control responses in Phase 3.

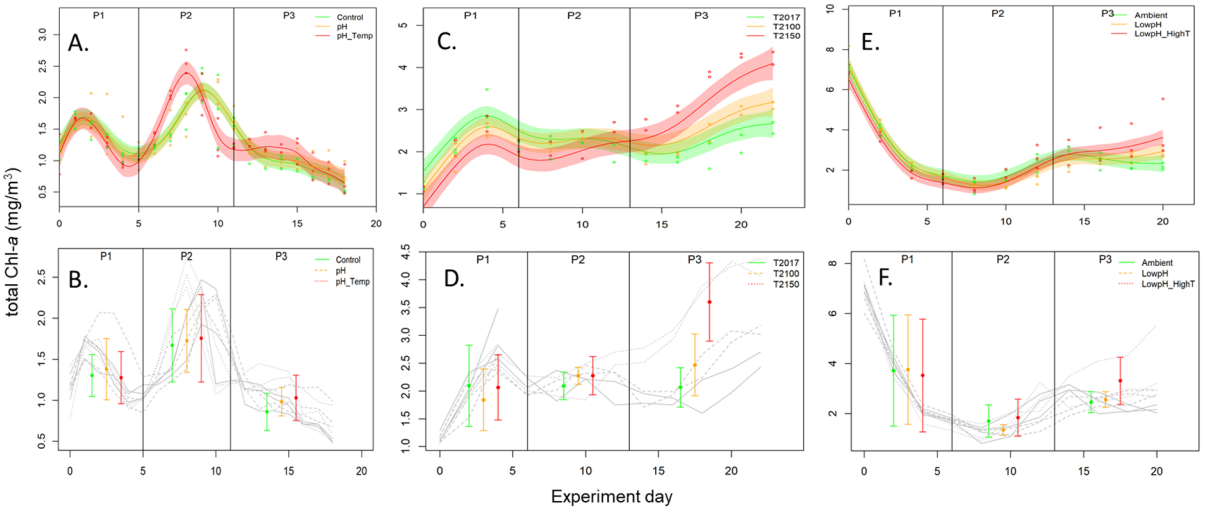

Figure 5: Response of total Chl-*a* (mg/m^3) for ME1 (A, B), ME3 (C, D), and ME4 (E, F) against time in days (x-axis). The upper row (A, C, E) shows the individual datapoints from each replicate bag overlain by the GAMM fits (mean and error) for the Control (green) and treatments (*pH,* orange, and *pH/T* pink, in ME1 and ME4; *2100* orange and *2150* pink, in ME3) for each experiment. The lower row (B, D, E) shows the mean of the replicates for the Control and treatments, overlain by the mean and standard deviation for each phase (using same colour scheme). The different phases, P1, P2, and P3 are delineated by the vertical lines. ME2 data not shown.

Total Chl-*a* did not differ significantly between the Control and *pH* in ME1, ME2, and ME4 (Figure 5), which indicates that projected future changes in the carbonate system alone will not alter Chl-*a* biomass. However, total Chl-*a* exhibited a significant response when low pH was combined with elevated temperature in the *pH/T* treatments in ME1, ME3 and ME4 (ME2 was discounted as there was only one replicate for this treatment). The GAMM fits for *pH/T* and the control showed a significant ($p < 0.01$) difference in ME1, with the biomass maximum occurring 1–2 days earlier in the treatment, potentially due to the warmer temperature. An earlier occurrence of phytoplankton blooms, on timescales of days, under warmer temperatures has been reported previously in mesocosm studies (Sommer & Lengfellner 2008, Sommer & Lewandowska 2011). The significance of this temporal shift in phytoplankton biomass in coastal waters is unclear, as variation on the order of days is within the interannual variability in coastal chlorophyll for the Wellington region (Pinkerton et al. 2018). However, an earlier biomass maximum is consistent with reports of shifts in oceanic plankton phenology associated with climate change (Chivers et al. 2020) and may potentially propagate to phenological shifts in the higher food web. Chl-*a* was also significantly higher in Phase 3 in *pH/T* relative to the Control (+20%; 1.03 ± 0.28 vs. 0.86 ± 0.23 mg/m^3, p = 0.13) in ME1.

The GAMM fits for *2100* and *2150* in ME3 showed a significant difference (p < 0.01) to the Control, primarily as a result of the earlier biomass maximum in the treatments (see Figure 5C); however, the Phase 3 mean was only significantly greater in *2150* (+64%; 3.4 vs. 2.4 mg/m^3; p = 0.0006; see Figure 5D). Total Chl-*a* biomass in ME4 showed a similar response with the *pH/T* GAMM fit being significantly different from the Control (<0.01, Figure 5E), with a significantly higher *pH/T* Phase 3 mean (+34%; 3.31 vs. 2.46 mg/m^3, p = 0.01; Figure 5F).

The absence of sensitivity to changes in CO_2/pH in phytoplankton biomass has been reported for coastal waters in other studies (Rossoll et al. 2012, Paul et al. 2015, Gazeau et al. 2017). This is perhaps not surprising as coastal waters and their extant planktonic communities may experience significant shifts in pH over short timescales (Hofmann et al. 2011) and so may be relative insensitive to the rate and magnitude of pH change applied in the mesocosm experiments. However, in time-series measurements of pH in Ākautangi/Evans Bay, a minimum of 7.85 was observed (Vance et al. 2020), which is higher than the pH in the treatments (7.65–7.8). In addition, pH is generally > 8.0 during the spring period

when months the experiments were carried out, and so the extant phytoplankton community at this time would not experience such low pH values. Consequently, the lack of response does not appear to be due to previous exposure to low and variable pH and instead may reflect physiological flexibility to cope with low pH.

The enhancement of total Chl-*a* biomass in *pH/T* relative to the Control in three of the four experiments is consistent with observed trends in open ocean phytoplankton, with laboratory and culture studies showing enhanced total Chl-*a* at elevated temperatures (Feng et al. 2010, Hare et al. 2007). However, some mesocosm studies of natural community responses have reported the reverse trend, with a significant decrease in total phytoplankton biomass (Sommer & Lengfellner 2008, Lewandowska & Sommer 2010, Sommer & Lewandowska 2011). The latter responses were attributed to an increase in grazing under warmer conditions (Lewandowska & Sommer 2010) and are consistent with observations that warmer temperature enhances heterotrophy relative to autotrophy (Brown et al. 2004, O'Connor et al. 2009). However, as with experiments in the Baltic Sea (Taucher et al. 2012), biomass accumulation occurred under elevated temperatures in the current study indicating that, on the timescale of these experiments, phytoplankton growth exceeded grazing. This is further examined below in the microzooplankton grazing experiments in Objective 3 in section 3.3.

The observed increase in chlorophyll-*a* biomass under future conditions suggests increased food availability at the base of the coastal food web, and so potential for increased carbon and energy flow in coastal food webs. However, a future increase in phytoplankton biomass in response to warming may also increase eutrophication and deoxygenation in regions that are subject to high nutrient loading (Zeldis et al. 2015, Zeldis & Swaney 2018).

Size-fractionated plankton

The observed responses in total Chl-*a* may reflect a change in overall biomass across the spectrum of phytoplankton sizes and taxa, or alternatively species or group-specific responses. Division of Chl-*a* into different size fractions (0.2–2, 2–5, 5–20, and >20 µm) was used to provide information on the relative changes in different phytoplankton size classes in response to the various treatments. Results are presented and discussed for each experiment separately.

ME1 - As with total Chl-*a*, the *pH/T* treatment had more effect on the different size fractions than *pH* (see Figure 6), with only the 2–5-µm fraction showing a significant difference in the GAMM fits ($p < 0.01$) with lower *pH* biomass in Phase 2 (Figure 6B and C). Although the smallest size fraction, 0.2–2 µm, did not show a difference in the GAMMs between *pH/T* and Control, the Phase 3 *pH/T* mean was significantly higher (0.28 vs. 0.21 mg/m^3, $p = 0.07$; Figure 6A). The earlier peak in biomass during Phase 2 in the dominant 5–20-µm fraction (Figure 6C) resulted in a significantly different GAMM for *pH/T* relative to the Control ($p < 0.01$, Figure 6E), but no significant difference in phase means (Figure 6F). The >20-µm size fraction was significantly lower in both *pH* ($p = 0.04$) and *pH/T* ($p = 0.0005$) relative to the Control (0.04 vs. 0.02 mg/m^3 in both treatments) (Figure 6G and H).

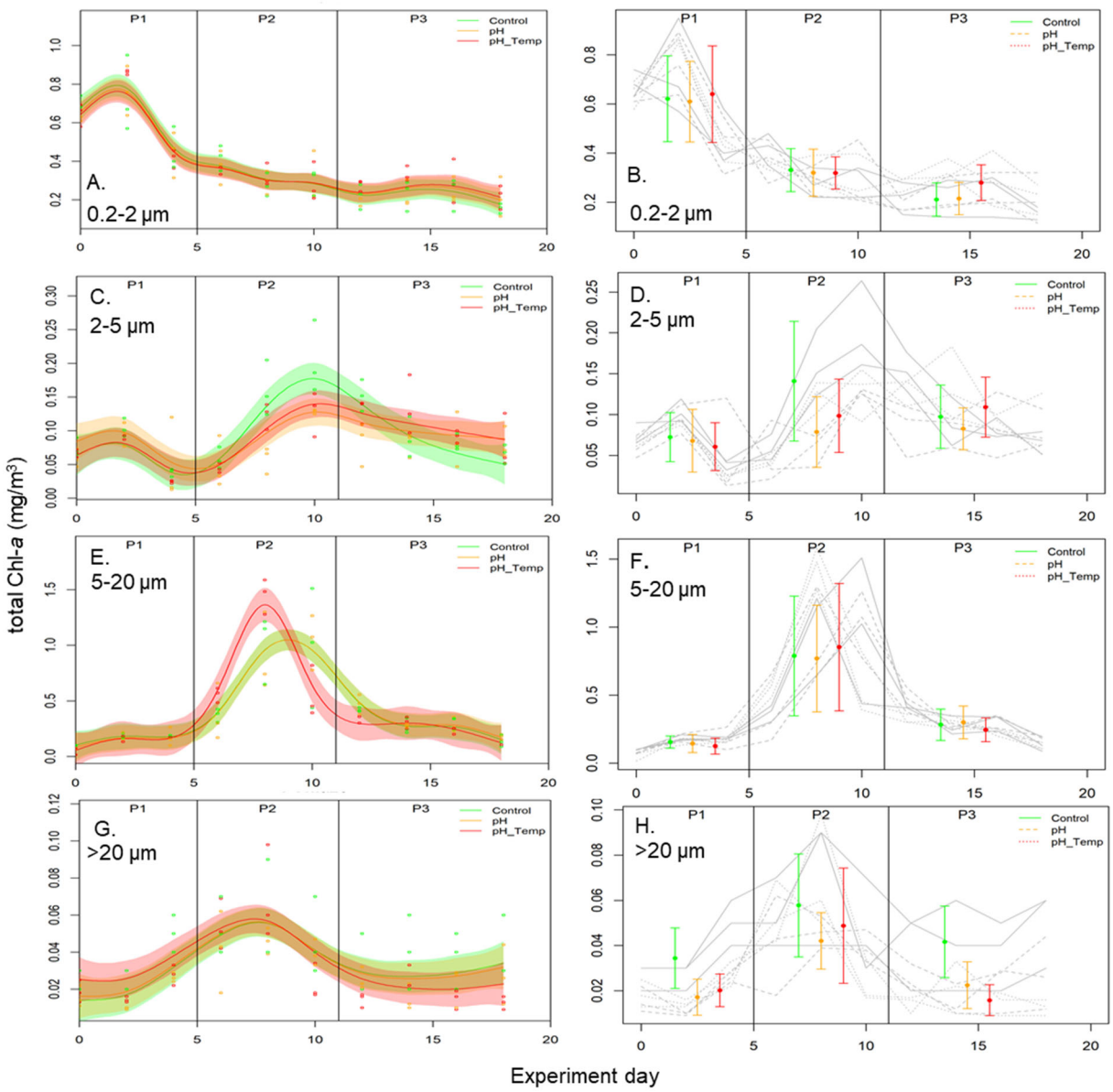

Figure 6: Response of different Chl-*a* size fractions (mg/m^3) for ME1, showing 0.2–2 µm (A, B), 2–5 µm (C, D), 5–20 µm (E, F), and >20 µm (G, H) fractions against time in days (x-axis). A, C, E, and G show the individual data points from each replicate bag overlain by the GAMM fits (mean and error) for the Control (green) and treatments (*pH,* orange and *pH/T,* pink) for each size fraction. B, D, E, and H show the mean of the replicates for the Control and treatments, overlain by the mean and standard deviation for each phase (using same colour scheme) for each size fraction. The different phases, P1, P2, and P3 are delineated by the vertical lines.

The ME1 size-fractioned Chl-*a* results were confirmed by the flow cytometry data, with cell counts for the different size fractions showing similar trends. The GAMMs for the picoeukaryotes (0.2–2 µm) in ME1 showed significant differences for *pH* ($p < 0.1$) and *pH/T* ($p < 0.01$), relative to the Control (see Figure 7A), with lower cell counts in Phase 3 in the Control (mean ± standard deviation, 16215 ± 7470), relative to *pH* (22576 ± 7244, $p = 0.03$) and *pH/T* (29083 ± 11372, $p = 0.0003$). In addition, the GAMMs were significantly different between the Control and *pH/T* ($p < 0.01$) for the nanoeukaryotes (2–20 µm, Figure 6E), although there were no significant differences in Phase 3 means (see Figure 6F) as with total Chlorophyll-*a*. Both size-fractionated Chl-*a* and cell counts for different fractions indicated an overall decrease in phytoplankton size spectrum under future conditions when nutrients are limited.

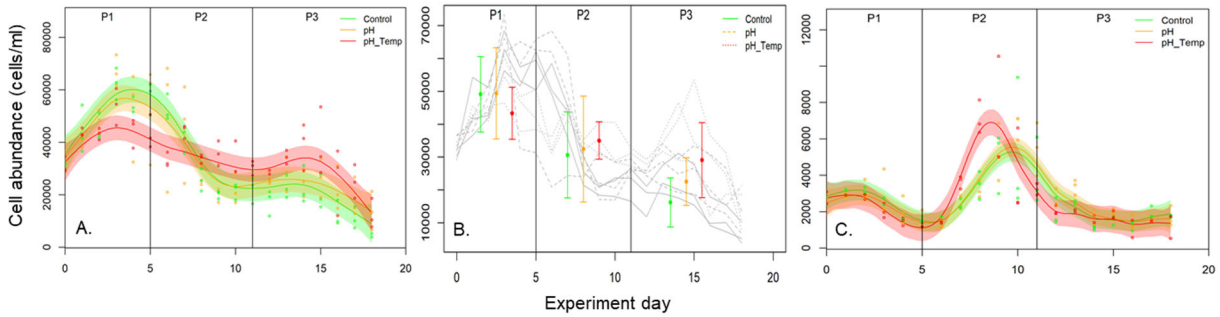

Figure 7: Cell abundance in ME1 for the picoeukaryotes (0.2–2 µm): A. individual datapoints from each replicate bag overlain by the GAMM fits (mean and error) for the Control (green) and treatments (*pH,* orange and *pH/T,* pink); B. the mean of the replicates for the Control and treatments, overlain by the mean and standard deviation for each phase (using same colour scheme). C. shows the nanoeukaryote (2–20 µm) cell abundance, with individual datapoints from each replicate bag overlain by the GAMM fits (mean and error) using same colour scheme.

ME2. As with Total Chl-*a*, none of the chlorophyll size fractions showed significant differences between *pH* and the Control in GAMM fits or between Phase 3 means (data not shown).

ME3. Significant treatment effects were apparent (Figure 8), some of which were the inverse of results in ME1 (Figure 6). For the smallest 0.2–2-µm fraction the GAMMs were significantly different between the Control and the two treatments, *2100* ($p < 0.1$) and *2150* ($p < 0.01$). Biomass peaked earlier than in the Control, with a maximum during Phase 2 but was significantly lower than the Control in Phase 3 (*2100* 0.56 ± 0.2; *2150* 0.46 ± 0.23; Control 0.83 ± 0.14; $p = 0.03$; Figure 8A). This was confirmed by picoeukaryote cell abundance which showed corresponding significant differences in Phase 3 between the Control and *2100* ($p = 0.02$), and *2150* ($p = 0.04$) (data not shown).

The GAMMs for 2–5 µm and 5–20 µm were significantly different between the Control and both treatments ($p = 0.01$), with a Phase 2 maximum in the 2–5-µm fraction in *2100* (Figure 8C). Both treatments also showed higher Phase 3 biomass for the 5–20-µm fraction, but this was only significantly greater for *2150* ($p = 0.05$; 1.61 ± 0.57 mg/m^3 vs. 0.94 ± 0.15 mg/m^3 in the Control; Figure 8F). The > 20-µm GAMM was also significantly different for *2150* ($p < 0.01$) relative to the Control, with a significantly higher Phase 3 mean (1.28 ± 0.59 vs. 0.35 ± 0.17 mg/m^3, $p = 0.0019$; Figure 8H). Overall, the future conditions resulted in a temporal shift in size spectrum response, with the smaller groups responding positively at an earlier stage but then declining, and the larger groups also responding positively but maintaining elevated biomass to the end of the experiment. The contrasting response to ME1, particularly in Phase 3, suggests contrasting responses in phytoplankton size spectrum under future conditions dependent upon nutrient concentrations, with a decrease in size under nutrient limited conditions (ME1), and an increase when nutrients are available (ME3).

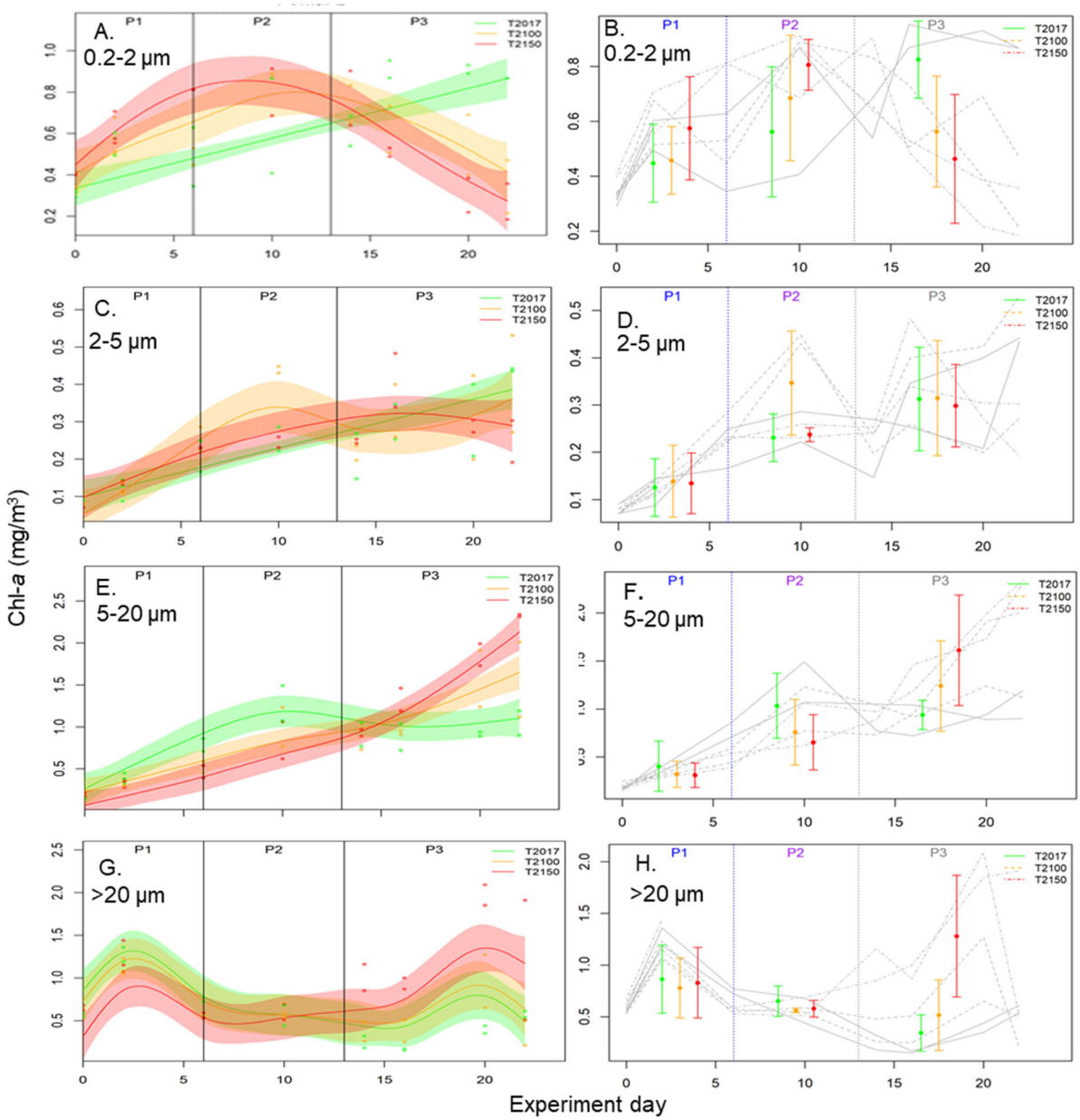

Figure 8: Response of different Chl-*a* size fractions (mg/m^3) for ME3, showing fractions of 0.2–2 µm (A, B), 2–5 µm (C, D), 5–20 µm (E, F), and > 20 µm (G, H) against time in days (x-axis). A, C, E, and G show the individual data points from each replicate bag overlain by the GAMM fits (mean and error) for the Control (green) and treatments (*2100,* orange and *2150*, pink) for each size fraction. B, D, F, and H show the mean of the replicates for the Control and treatments, overlain by the mean and standard deviation for each phase (using same colour scheme) for each size fraction. The different phases, P1, P2, and P3 are delineated by the vertical lines.

ME4. Treatment effects were less apparent in ME4, although *pH* exhibited more significant responses than in the preceding experiments (Figure 9). For example, in Phase 3 the 0.2–2-µm fraction was significantly larger in *pH* relative to the Control in Phase 3 (0.93 vs. 0.71 mg/m^3; $p = 0.08$; Figure 9B), and the 5–20-µm fraction had a significantly different GAMM ($p < 0.01$) relative to the Control for *pH* (Figure 9E), with lower Phase 3 biomass (not significant). GAMM fits for the treatments and Control differed for both the 2–5-µm (p <0.1) and > 20-um fractions ($p < 0.1$), with both treatments showing significantly higher biomass in the > 20-µm fraction in Phase 3 (*pH* 0.43 ± 0.41, *pH/T* 1.1 ± 0.84 vs. Control 0.15 ± 0.04; Figure 9H).

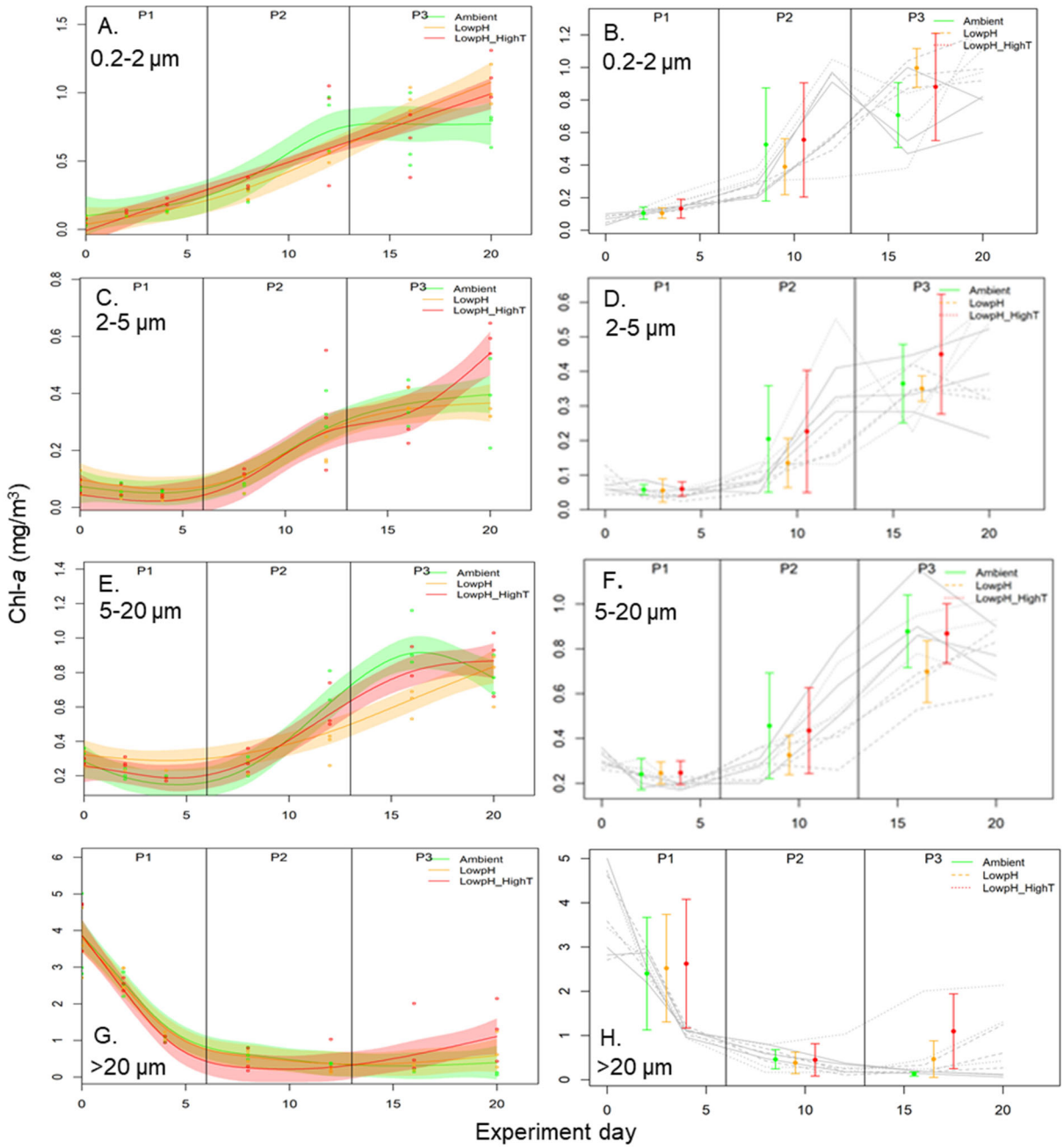

Figure 9: Response of different Chl-*a* size fractions (mg/m^3) for ME4, showing 0.2–2 µm (A, B), 2–5 µm (C, D) 5–20 µm (E, F) and > 20 µm (G, H) fractions against time in days (x-axis). A, C, E, and G show the individual data points from each replicate bag overlain by the GAMM fits (mean and error) for the Control (green) and treatments (*pH*, orange and *pH/T*, pink) for each size fraction. B, D, F, and H show the mean of the replicates for the Control and treatments, overlain by the mean and standard deviation for each phase (using same colour scheme) for each size fraction. The different phases, P1, P2, and P3 are delineated by the vertical lines.

Although trends differed between experiments, the size-fractionated biomass generally reflected the overall response of total Chl-*a* (Figure 5). Few significant changes were apparent in *pH,* although this did induce shifts between size groups in ME4, with an increase in the 0.2–2- and > 20-µm fractions and a decrease in the dominant 5–20-µm fraction (Figure 9). Overall *pH/T* was generally favourable to larger phytoplankton groups (particularly in *2150* in ME3) when nutrients were added, but favoured the smaller groups when nutrients were limited (as in ME1, Figure 6B). This is consistent with previous observations that mean cell size of phytoplankton communities tends to decrease with temperature but is dependent upon nutrient availability (Peter & Sommer 2013). Nutrient requirements are generally proportional to size and, as small cells have higher surface-to-volume ratio, higher growth, and nutrient uptake affinities (Hein et al. 1995, Litchman et al. 2007), they are able to prosper in nutrient-limited

environments and so may be more tolerant of temperature change. Conversely, larger cells are more diffusion-limited than small cells and may benefit from an increase in dissolved CO_2 if nutrients are also available (Wu et al. 2014). Overall, the results suggest that nutrient availability is an important factor in determining the response of phytoplankton community composition to future warming and acidification, which should be considered in modelling and future management of coastal waters.

Phytoplankton community composition

Phytoplankton taxa (> 5 µm) were identified and counted in all experiments, with cell abundance converted to volumetric carbon (mg C/m^3), for eleven different phytoplankton groups which were summed to give total phytoplankton carbon. This generally showed a similar trend to the 5–20-µm and > 20-µm chlorophyll size fractions, as expected, except for ME1 in which total phytoplankton carbon lagged the chlorophyll maximum. Significant responses in total phytoplankton carbon occurred in two experiments (see Appendix 2) with *2100* and Control GAMMs differing ($p < 0.1$) in ME3, corresponding to a significantly higher Phase 3 mean in *2100* ($p = 0.01$). Conversely in ME4, *pH* and Control GAMMS differed ($p < 0.01$), with a higher *pH* Phase 3 Mean ($p = 0.12$).

Changes in total carbon content for specific phytoplankton groups were also assessed, with three of the major groups (diatoms, dinoflagellates, and small flagellates) showing significant treatment effects.

Diatoms

Diatoms represented a significant component of the initial phytoplankton biomass in ME1 and increased from 1 to 2 mg C/m^3 to a maximum of 19 mg C/m^3 after 18 days (see Figure 10A). Diatom biomass was dominated by the pennate diatom *Cylindrotheca closterium* (see Figure 12A), with *Thalassionema nitzschioides* and *Thalassiosira minima* contributing most of the remaining biomass. However, diatom biomass showed no significant treatment effect in ME1. Diatom biomass was considerably greater in ME2 (Figure 10B), reaching a maximum of 100–200 mg C/m^3 on Day 6, with *Skeletonema* spp. dominating and with contributions from *T. minima* (maximum 40 mg C/m^3) and *C. closterium* (maximum 7–19 mg C/m^3, Figure 12B). The GAMM for *pH* differed to that for the Control (data not shown) in ME2, primarily due to the short-lived peak in diatom numbers on Day 7 (see Figure 10B).

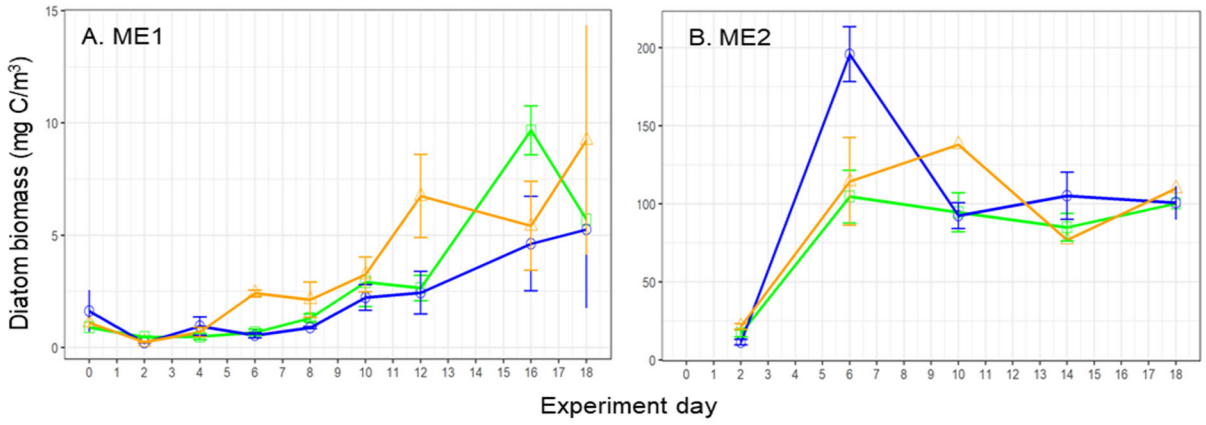

Figure 10: Diatom biomass (mg C/m^3) during A. ME1 and B. ME2, showing the mean and standard deviation of all replicates for treatments and Control (Control – green, *pH* – blue, *pH/T* – Orange) every 2 or 4 days. Note the absence of error bars for *pH/T* from Day 10 onwards in ME2 as there was only one replicate.

Diatoms also dominated phytoplankton biomass in ME3, with initial concentrations of 15–35 mg C/m^3 increasing to 17–250 mg C/m^3 by Day 22 (Figure 11A, B). This was dominated by the pennate diatom *C. closterium*, which accounted for 50% of final diatom biomass, although *T. nitzschiodes* dominated in one of the *2150* replicates with a biomass > 200 mg C/m^3. Other diatom species dominated at earlier stages, with *Pseudonitzschia* spp. reaching a maximum of ~67 mg C/m^3 before declining to the end of the experiment. Unlike the first two experiments, the diatoms exhibited significant treatment effects in ME3. The GAMM for both future treatments differed from the Control ($p < 0.01$; see Figure 11A), with significantly higher biomass in Phase 3 for both *2100* (58.7 mg C/m^3, $p = 0.0009$) and *2150*

(54.1 mg C/m^3, p = 0.0014) relative to the Control (15.1, Figure 11B). This is reflected in the response of the pennate diatom *C. closterium* (see Figure 12C, and below).

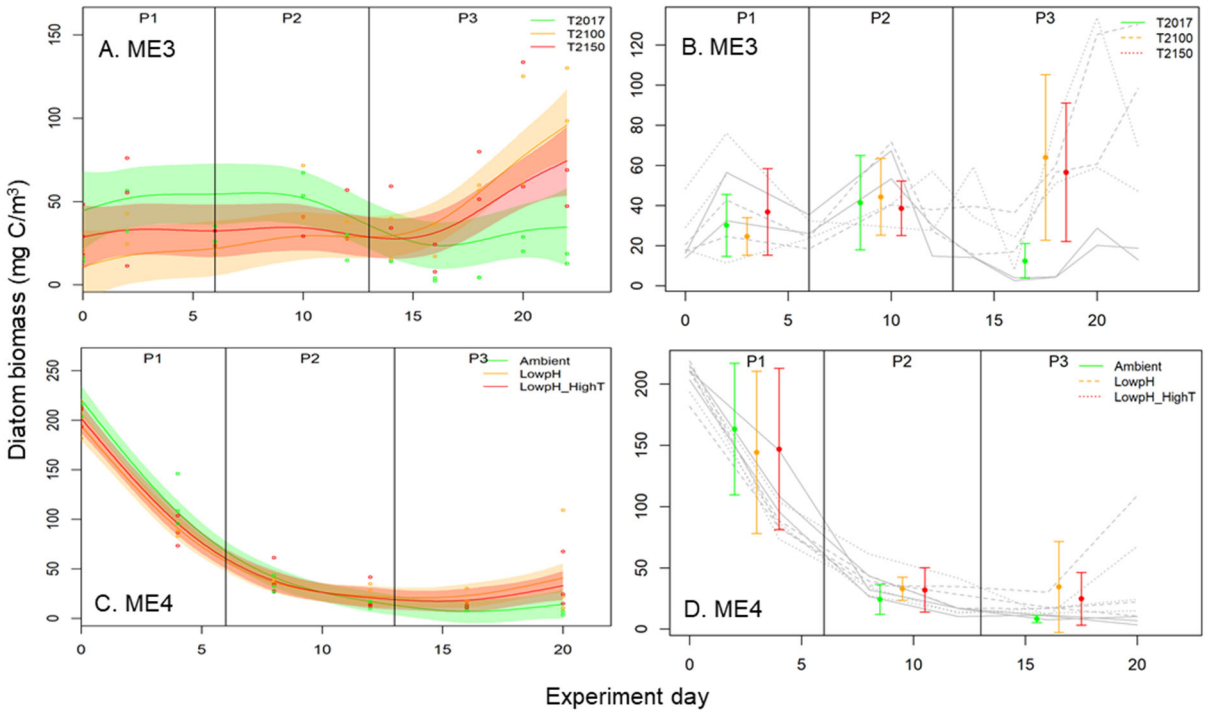

Figure 11: Response of diatom biomass in ME3 (A, B; Control, green, *2100,* orange, *2150* pink) and ME4 (C, D; Control green, *pH* orange, *pH/T* pink), showing the individual data points from each replicate bag overlain by the GAMM fits (mean and error) for each size fraction in A and C. The mean of replicates for the Control and treatments, overlain by the mean and standard deviation for each phase (using same colour scheme) for each size fraction are shown in B and D. The different phases, P1, P2, and P3 are delineated by the vertical lines.

ME4 started during a phytoplankton bloom dominated by diatoms (> 200 mg C/m^3) which declined over 7 days to < 20% of the initial biomass (see Figure 11C, D). This was reflected in the decline of a number of diatom species, including *Chaetoceros* spp. (initially 50 mg C/m^3), and *Lauderia* spp. (initially > 80 mg C/m^3), but was followed by an increase in the biomass of *Cylindrotheca closterium,* which exceeded 40 mg C/m^3 by Day 20 (see Figure 12D). The GAMMs for diatom biomass differed between treatments and Control (pH < 0.01, pH/T < 0.1, Figure 11C), with significantly higher Phase 3 means for both pH (33.5 mg C/m^3, p = 0.03) and pH/T (24.7 mg C/m^3, p = 0.01) relative to the Control (8.36 mg C/m^3, Figure 11D).

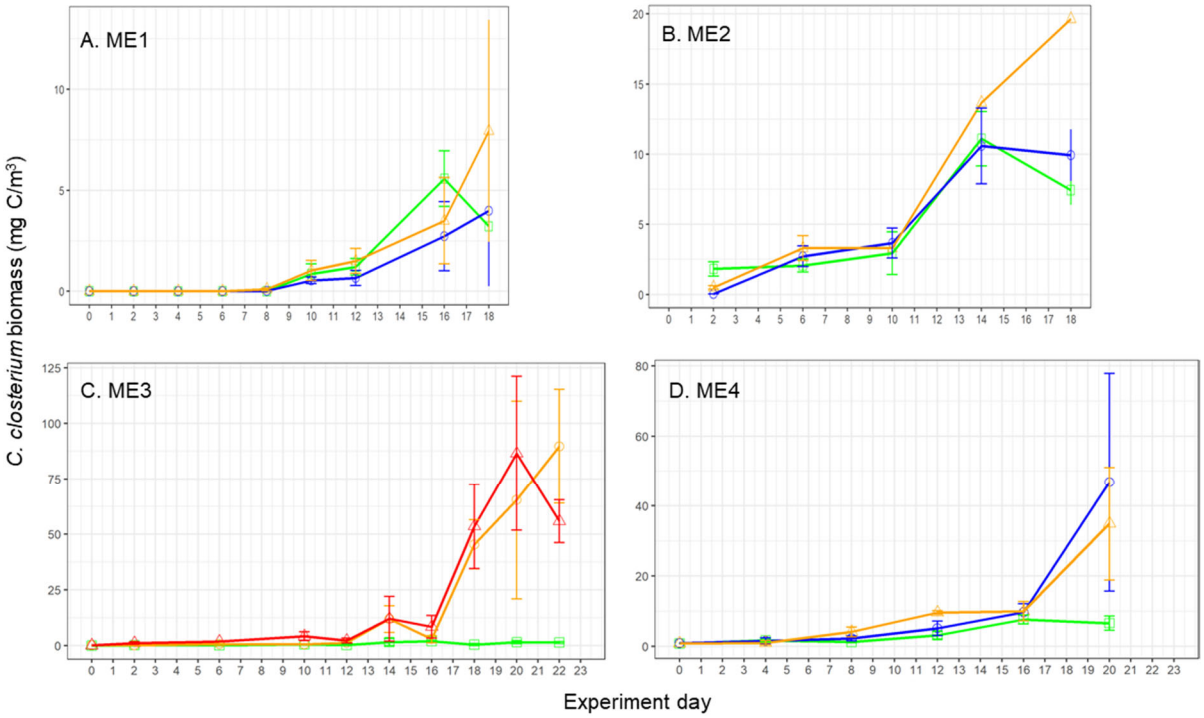

Figure 12: Biomass (mg C/m^3, mean ± standard deviation) of the pennate diatom *C. closterium* in A. ME1, B. ME2, C. ME3 and D. ME4, with treatments colour-coded (*2100* – orange, *2150* – red in C. ME3; Control – green, *pH* – blue, *pH/T* – orange in experiments A B and D). The x-axes are aligned to enable comparison of temporal trends. Note the different vertical axis scales and the absence of error bars for *pH/T* from Day 10 onwards in ME2 as there was only one replicate.

Diatoms are considered the most important taxonomic group of primary producers on Earth (Bach & Taucher 2019), with a significant contribution to carbon sequestration and food webs in coastal waters (Ambrust 2009). Syntheses of published experiments indicate that diatoms generally respond positively to lower pH/elevated CO_2 although this response is moderated by light and nutrient availability. However, there is lower sensitivity in coastal waters relative to the open ocean, with only 32% of coastal experiments reporting increases in diatom biomass under lower pH (Bach & Taucher 2019).

The positive response of the diatoms in the treatments in ME2, ME3, and ME4 (Figures 10A and 11C, D) indicates that pH may be an important influence in the future. An increase under low pH is consistent with suggestions that larger diatoms may benefit from future acidification (Tortell et al. 2008, Bach & Taucher 2019). This has been attributed in part to the increase in dissolved CO_2 that compensates for the lower surface area to volume ratio of diatoms, and the corresponding lower diffusive CO_2 supply relative to carbon demand in larger diatoms (Wu et al. 2014). This increase in diatoms, and the corresponding 5–20-µm and > 20-µm size fractions, may benefit coastal food webs, as a greater proportion of larger phytoplankton reduces food web transfers and increases trophic transfer efficiency (Sommer et al. 2002). However, nutrient availability influenced the response to lower pH as diatom, and also *C. closterium*, biomass (see Figure 12) increased in both treatments in the nutrient-amended ME3 and ME4 experiments, but not in the nutrient-limited ME1 (Figures 10 and 11).

Cylindrotheca closterium was the phytoplankton species that exhibited the most significant biomass response to treatments across all experiments (Figure 12). Previous studies have not observed stimulation of this species under elevated CO_2 in culture studies (Wu et al. 2012), and higher CO_2 was reported to favour a larger centric diatom (*Chaetoceros* spp.) over *C. closterium* in experiments on Ross Sea phytoplankton (Feng et al. 2010). Regardless, conditions in Ākautangi/Evans Bay water are clearly favourable to *C. closterium* and were further enhanced by elevated CO_2. *C. closterium* is globally ubiquitous in neritic waters and is meroplanktonic with a niche that is part planktonic and part benthic (Kingston 2009). It is possible that *C. closterium* may benefit from elevated pCO_2 as it may be adapted to the higher CO_2/lower pH environment of surficial sediment. Furthermore, *C. closterium* has a higher

growth rate than other diatom species (Tanaka 1984, from Kingston, 2009) and so the potential to respond more rapidly to elevated pCO_2 when other environmental conditions are favorable.

Dinoflagellates

The dinoflagellates accounted for a minor proportion of phytoplankton biomass in most experiments but showed significant responses in treatments in certain experiments. They were in relatively low abundance in ME1 (Figure 13A), accounting for < 0.4 mg C/m^3, with their biomass dominated by *Tripos* spp. and *Protoperidinium bipes* (0.1–0.3 mg C/m^3). Despite significant variability between triplicates in each treatment during Phase 1 and 2 in ME1, the Phase 3 mean was significantly lower for both *pH* (0.07 ± 0.06 mg C/m^3, p =0.02) and *pH/T* (0.06 ± 0.07 mg C/m^3, p = 0.003) relative to the Control (0.22 ± 0.1 mg C/m^3), with *Tripos spp.; P. bipes*, and *Prorocentrum triestinum* all at higher abundances in the Control than the treatments. Conversely dinoflagellate biomass declined throughout ME2, with no treatment effect (data not shown).

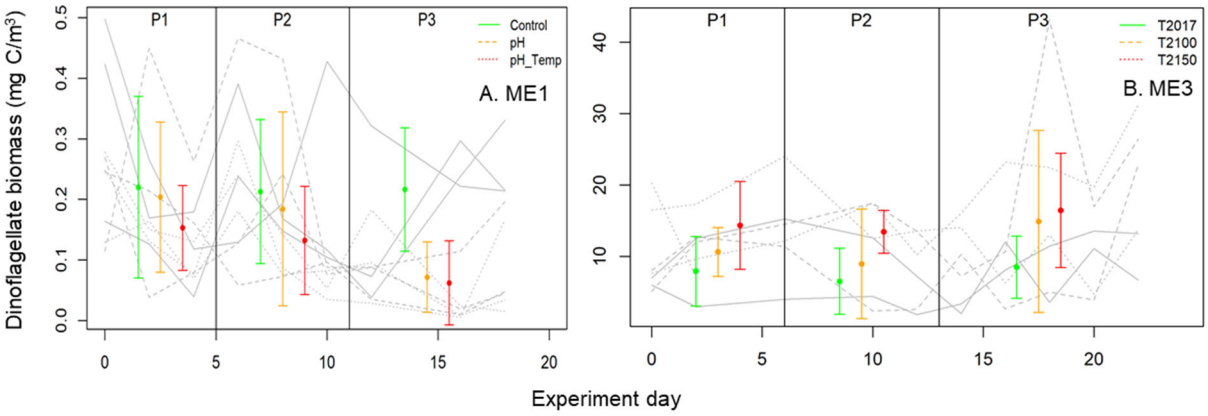

Figure 13: Dinoflagellate biomass (mg C/m^3, mean ± standard deviation) in A. ME1 (Control – green; *pH* – blue, *pH/T* – orange), and B. ME3 (Control – green, *2100* – orange, *2150* – red), showing the mean of replicates for the Control and treatments, overlain by the mean and standard deviation for each phase. The different phases, P1, P2, and P3 are delineated by the vertical lines. Note the different vertical axis scales.

Dinoflagellate biomass was considerably higher in ME3, increasing from initial values of 5–15 mg C/m^3 to > 40 mg C/m^3 towards the end of the experiment. This was largely dominated by *Gymnodinium* spp. and *P. bipes*. The Phase 3 mean for dinoflagellate biomass was significantly higher in *2150* (15.7 mg C/m^3, p = 0.03) relative to the control (8.4 mg C/m^3), reflecting the response of *P. bipes* (data not shown). ME4 also started with relatively higher dinoflagellate biomass (12–15 mg C/m^3) that increased to > 30 mg C/m^3 and was dominated by *Gymnodinium* spp. and *Prorocentrum minimum* (reaches > 20 mg C/m^3), but there was no treatment response in the dinoflagellates.

The zooplankton net hauls also sampled the large heterotrophic dinoflagellate *Noctiluca scintillans,* which showed significantly lower ($p < 0.05$) abundances in *pH/T* (5 ± 5 individuals/m^3; mean ± standard deviation) relative to both *pH* (19 ± 26 individuals/m^3) and the Control (75 ± 17 individuals/m^3) in ME4 (see Appendix 3). This was surprising, as increases in *N. scintillans* have been linked to warmer temperature in relation to warm core eddies (McLeod et al. 2012). As with other aspects of the phytoplankton the response of the dinoflagellates to the treatments may be influenced by nutrient availability, but the contrasting, and limited, treatment effects observed (negative in ME1, positive in ME3) limit conclusions as to how dinoflagellates will respond to future conditions in coastal waters.

Small flagellates

Phytoplankton carbon biomass > 5 µm was dominated by small flagellates in ME1, which increased from initial levels of 5 mg C/m^3 to > 30 mg C/m^3 by Day 10 in *pH/T* (Figure 14A). This resulted in a significant treatment effect, as evident in the different GAMM fits ($p < 0.01$), but no Phase 3 mean difference (Figure 14B). Although small flagellates also dominated phytoplankton biomass during ME2 (initially 30–40 mg C/m^3), they did not show any significant treatment effect (data not shown). In ME3 the small flagellate biomass was again high, initially 10–35 mg C/m^3 increasing to 60–130 mg C/m^3 by

Day 22 with a maximum of 180 mg C/m^3 in the Control on Day 18 (Figure 14C). Despite no significant difference in the GAMMs in ME3, Phase 3 biomass declined in *2150* relative to the Control (p = 0.06, Figure 14D). In ME4, small flagellate biomass exceeded 170 mg C/m^3 by the end of the experiment, with the *pH/T* GAMM significantly different to the Control ($p < 0.1$, Figure 14E), and a corresponding lower Phase 3 mean (99.6 ± 11.33 vs. Control 135.8 ± 37.1 mg C/m^3, p = 0.08, Figure 14F). Although responses varied between experiments, small flagellate biomass generally declined under lower pH and elevated temperature particularly when nutrient supply was maintained, which suggests they were outcompeted by the diatoms which benefitted under these conditions (see Figure 11). As small flagellates represent an important sink for bacteria via grazing, future decreases in their abundance may influence bacterial abundance and processes in coastal waters; however, there were no corresponding responses in bacterial abundance in ME3 or ME4 (data not shown). A separate study identified a link between this phytoplankton group and DMSP (Dimethylsulphoniopropionate) concentrations in the mesocosm experiments, inferring that future declines in small flagellates may impact coastal emissions of the trace gas DMS (Dimethylsulphide), which influences aerosol formation in the air (Saint-Macary et al. 2021).

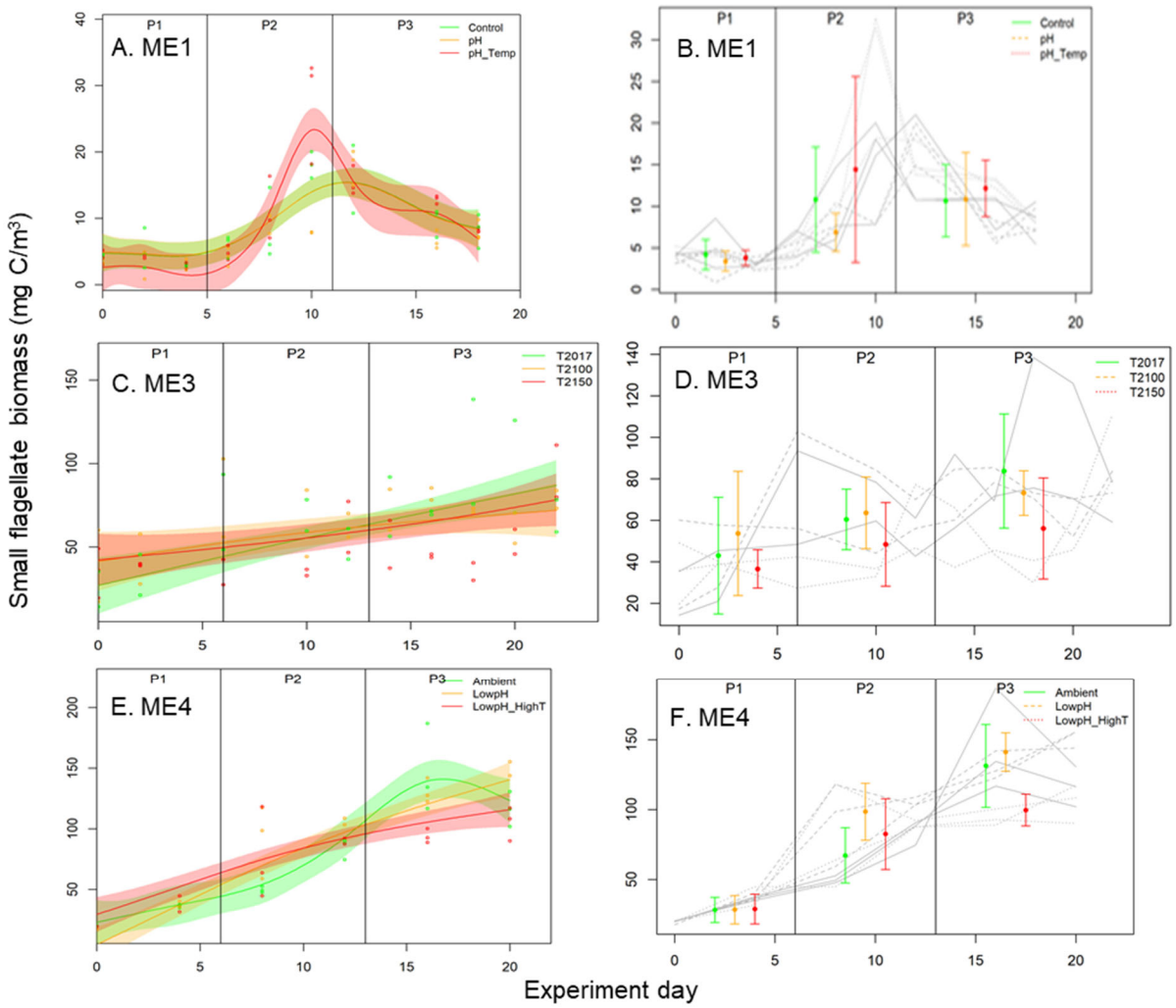

Figure 14: Small flagellate biomass (mg C/m^3, mean ± standard deviation) in A, B. ME1, C, D. ME3, and E, F. ME4, with treatments colour-coded (ME3: Control – green, *2100* – orange, *2150* – red; ME1 and ME4: Control – green, *pH* – blue, *pH/T* – orange). Individual data points from each replicate bag are overlain by the GAMM fits (mean and error) in A and C, and B and D show the mean of the replicates for the Control and treatments, overlain by the mean and standard deviation for each phase. The different phases, P1, P2, and P3 are delineated by the vertical lines, and the x-axis are aligned to enable comparison of temporal trends. Note the different vertical axis scales.

Other phytoplankton groups

Coccolithophores were only present at relatively low biomass in ME2 (maximum 6 mg C/m^3), during which significant decreases occurred in both treatments relative to the Control. This is not surprising as low pH is associated with lower carbonate availability and a decline in coccolithophore abundance under low pH is consistent with other reports (Meyer & Riebesell 2015). Elevated biomass of other phytoplankton groups, including the raphidophytes, silicoflagellates, and other flagellates (dominated by *Cryptomonas* spp.) occurred during ME4, relative to the other experiments, but none of these groups exhibited significant treatment effects.

Zooplankton community composition

Taxonomic identification of the zooplankton community was carried out on samples collected on the final day of ME1, ME3, and ME4 to test for differences between treatments and controls. Sixteen classes of zooplankton were detected in ME1, with total counts of 995 ± 622 (mean ± standard deviation) in the Control, 1032 ± 750 in *pH*, and 2180 ± 1945 in *pH/T*; however, the large variability in replicates obscured any evidence of significant differences between treatments in abundance of total zooplankton or zooplankton classes (one-way ANOVA, $p = 0.1$ or $p = 0.05$; see Appendix 3). Thirteen zooplankton classes were detected in ME3 (see Appendix 3) with total counts of 866 ± 113 in the Control, 1091 ± 1475 in *2100*, and 866 ± 113 in *2150*. Again, the variability between replicates precluded identification of significant differences, except for *Oithona* abundance which was significantly greater (ANOVA, $p < 0.1$) in *2150* (48 ± 11), relative to the Control (12 ± 17), and absent from *2100*. Following the bloom at the start of ME4 zooplankton diversity and abundance were considerably higher with 30 different groups identified (see Appendix 3) and counts of 15 615–17 749 individuals. Although there was no difference in total abundance in ME4 there was a significant difference in the abundance of small medusa (ANOVA $p<0.1$), which were present in *pH/T* (11 ± 9) but absent from *pH* and the Control.

Most previous studies of zooplankton response to ocean acidification have focused on copepods and shown that responses are generally related to bottom-up controls such as alteration of primary production or phytoplankton community composition (Alvarez-Fernandez et al. 2018, Meunier et al.; 2017). In two studies on two *Calanus* species, low pH did not directly alter grazing or body mass, suggesting no change in metabolic energy use (Hildebrandt et al. 2015, and references within), although Rossoll et al. (2012) suggest that low pH may affect copepod growth and reproduction indirectly via changes in phytoplankton food quality. In a mesocosm study incorporating both warming and low pH, Garzke et al. (2016) report that warmer temperatures decreased nauplii, copepodite, and adult copepod abundances. In general, the generation time of copepods is in the order of one month (egg to adult at 15 °C), and so the duration of the ME experiments was possibly too short to detect significant treatment effects. In addition, because there was a succession of phytoplankton groups and taxa responding to the treatments (see Figures 6–16) the community composition was not in steady-state, and so the zooplankton community response to a varying microplankton community would also require a longer timescale. In terms of the significant responses observed it is unclear why *Oithona* increased in *2150* in ME3, as there were no corresponding increases in its microzooplankton prey (see below). Medusa are reported to be positively affected by increases in both temperature and food supply (Han & Uye 2010), consistent with the observed treatment response in *pH/T* in ME3.

Particulate Carbon and Nitrogen

Particulate Carbon (PC) and Nitrogen (PN) concentrations were measured every 2–4 days in all ME experiments, and results for Phase 3 are summarised in Table 5. Initial and final Phase 3 PC concentrations generally reflected nutrient status, being lowest in ME1 and highest in ME3.

Table 5: **Particulate Carbon and Nitrogen concentrations (mean and standard deviation, mg/m^3) and molar C:N ratios in Phase 3 for all ME experiments. Treatments are colour-coded (ME3: Control – green, *2100* – orange, *2150* – red; ME1, ME2, and ME4: Control – green, *pH* – blue, *pH/T* – orange); note ME2 *pH/T* results are excluded. *S*ignificant (p < 0.1) and indicative (p < 0.15*)* differences in Phase 3 means are shown by ## and # respectively, and significant differences (p <0.01) in GAMM fits between treatments and Control by ^.**

	ME1	ME2	ME3	ME4
Particulate Carbon (mg/m^3)	142.6 ± 26.7 147.4 ± 31.0 159.3 ± 35.2	158.3 ± 21.1 181.9 ± 19.5^##	328.7 ± 19.1 341.4 ± 39.6^ 326.40 ± 43.1^	276.7 ± 27.4 262.0 ± 27.1 272.5 ± 46.9
Particulate Nitrogen (mg/m^3)	16.3 ± 4.9 16.0 ± 4.9 18.4 ± 5.7	16.3 ± 1.7 17.2 ± 1.5	52.0 ± 2.0 50.2 ± 4.3 44.7 ± 2.6^#	50.5 ± 2.5 50.0 ± 2.4 45.9 ± 4.7
C:N (mol)	10.7 ± 2.3 11.37 ± 3.3 10.4 ± 1.9	11.4 ± 1.3 12.3 ± 1.0#	7.4 ± 0.3 7.9 ± 0.5**# 8.5 ± 1.0^#	6.4 ± 0.4 6.1 ± 0.5 6.9 ± 0.8

PC decreased throughout ME1 and there were no significant differences in PC, PN, or Carbon: Nitrogen (C:N) between treatments and the Control (see Phase 3 mean values in Table 5, data not shown). Conversely, PC and C:N increased throughout ME2, with a significant difference in PC in the GAMM fits for *pH* and the Control ($p < 0.01$), and a significantly higher Phase 3 mean PC in *pH* (see Figure 15) and an indicative increase in C:N ($p = 0.125$).

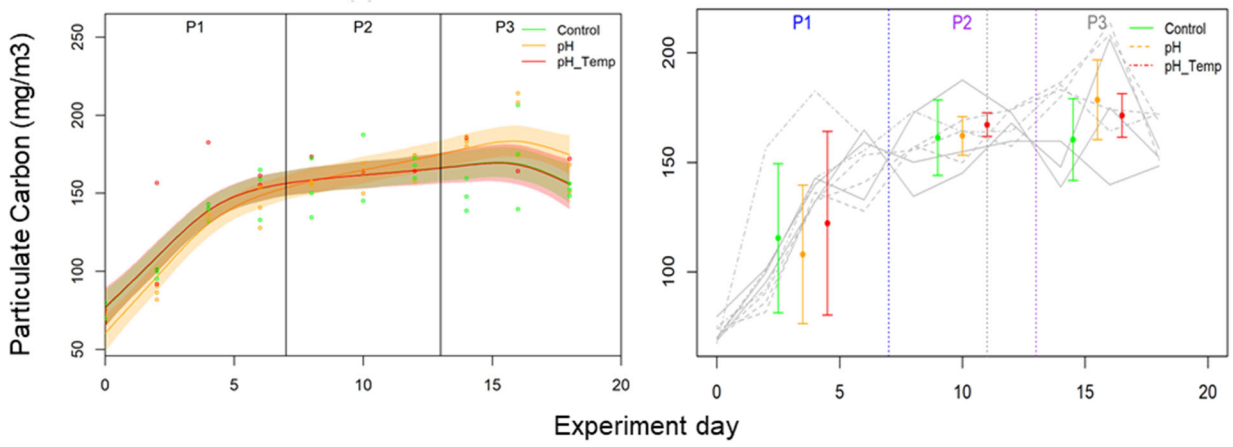

Figure 15: **Particulate Carbon during ME2, with treatments colour-coded (Control – green, *pH* – orange, *pH/T* – red). Individual data points for each replicate bag are overlain by the GAMM fits (mean and error) in the left figure, and the mean of the replicates for the Control and treatments, overlain by the mean and standard deviation for each phase are shown in the right figure. The different phases, P1, P2, and P3 are delineated by the vertical lines. Note that the *pH/T* results are based upon only one replicate in Phase 2 and 3 and so the results are not considered.**

ME3 exhibited the most significant treatment effects in particulate content, with the GAMM fit for PC differing from the Control for both *2100* ($p < 0.01$) and *2150* ($p < 0.01$, see Figure 16A), driven by lower PC in Phase 2 and higher PC at the end of ME3 (see Figure 16B). Conversely, the GAMMs for PN were only significantly different for *2150* ($p < 0.01$, Figure 16C), and this corresponded to a lower Phase 3 mean ($p = 0.00003$, Figure 16D). The elevated PC and lower PN resulted in significantly different GAMM fits ($p < 0.01$) for C:N, for both treatments (Figure 16F), with lower ratios in Phase 2 and significantly higher ratios in Phase 3 (Figure 16F). PC, PN, and C:N all decreased from initial high

values in response to bloom collapse at the start of ME4, but there were no significant treatment effects (see Appendix 4).

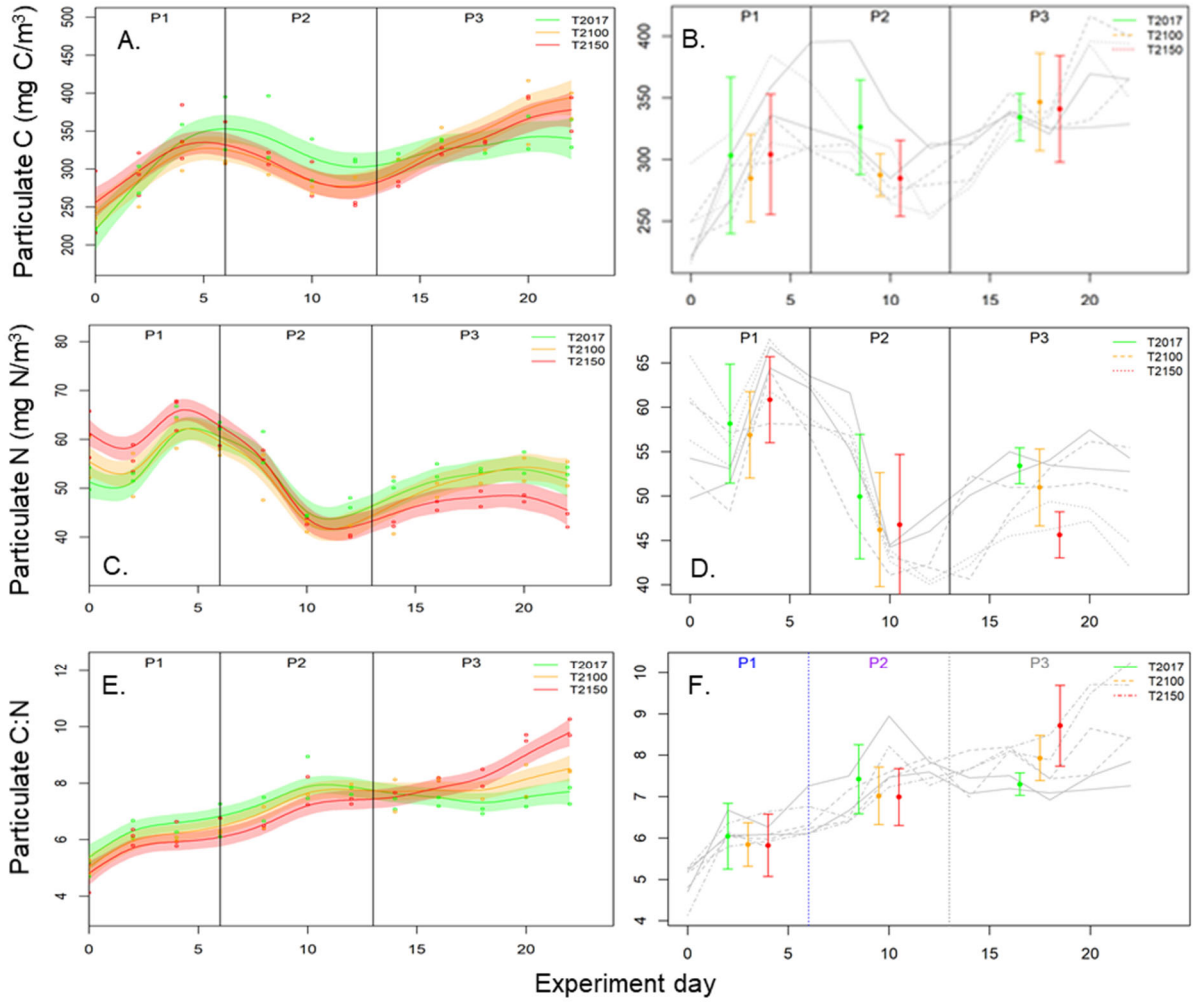

Figure 16: A, B. Particulate Carbon (PC), C, D. Particulate Nitrogen (PN), and E, F. C:N during ME3, with treatments colour-coded (Control – green, *2100* – orange, *2150* – red). Individual data points from each replicate bag are overlain by the GAMM fits (mean and error) in A, C, and E, and B, D, and F show the mean of the replicates for the Control and treatments, overlain by the mean and standard deviation for each Phase (using same colour scheme). The different phases, P1, P2, and P3 are delineated by the vertical lines. Note the different vertical axis scales.

Changes in CO_2 have been previously shown to alter C:N uptake and particulate stoichiometry of phytoplankton in natural community and unispecific culture studies (Riebesell et al. 2007, Bellerby et al. 2008, Li et al. 2012). A decrease in C:N may lead to a decrease in food quality, with implications for other components of the food web; however, this response was only evident in one (ME3) of the four experiments in the current study.

Amino acids

Particulate organic matter is a source of organic molecules such as amino acids, fatty acids, carbohydrates and sugars to consumers in coastal food webs. Amino acids (AAs) are structural components of proteins that provide an important nitrogen (N) source for marine organisms, as they represent a relatively labile component of particulate organic matter (McClelland & Montoya 2002). There are about 20 different types of amino acids, approximately half of which are essential, as they cannot be synthesized by most organisms (Jónasdóttir 2019). Both essential and non-essential AAs are synthesised by autotrophs, whereas heterotrophs can only synthesise non-essential AAs and thus are reliant on their diet (autotrophs) to acquire essential AAs. Measurement of AA concentration provided an indication of food quantity and its nutritional value at the base of the food web that was complemented

by measurement of Compound-specific Stable Isotope Analysis of Amino Acids (CSIA-AA), which indicated the source and transfer of essential organic compounds and energy through a food web, so providing information on trophic interactions (Eglite et al. 2018, Yamaguchi & McCarthy 2018).

The rationale behind CSIA-AA as a biogeochemical tool lies in the different fractionation behaviour of certain AAs, as they are synthesised by biological species and transferred through a food web. Briefly, AAs that are central to metabolic N cycling, such as alanine, aspartic acid, glutamic acid, isoleucine, leucine, proline, and valine (McClelland & Montoya 2002) are strongly ^{15}N-enriched in consumers relative to their diet during trophic transfer and are collectively known as 'trophic' AAs (Popp et al. 2007). In contrast, several other AAs (mostly notably phenylalanine, *Phe*) undergo little ^{15}N trophic enrichment and provide a direct proxy for the δ^{15}N value at the base of food webs and so are known as 'source' AAs. A third type of AA, threonine, shows ^{15}N depletion relative to food source and is regarded as a 'metabolic' AA (Germain et al. 2013, McMahon et al. 2015). Based on an understanding of the various AA metabolic pathways (McMahon & McCarthy 2016, O'Connell 2017), it is possible to create CSIA-AA-based proxies to decipher the origin and fate of organic matter within food webs.

CSIA-AA can also be used to estimate the trophic position (TP), which provides an indication of the trophic status of an organism based on the known isotopic fractionation of N in specific AAs during trophic transfer. In the case of particulate organic matter, the TP is used to assess the origin and quality of food at the base of the food web. CSIA-AA has been used to provide insights into the biochemistry and cycling of particulate organic matter (POM) under differing environmental conditions in marine systems (Eglite et al. 2018, Yamaguchi & McCarthy 2018), and also on the effect of ocean warming on planktonic food web structure (Loick-Wilde et al. 2019).

The observed differences in bulk particulate C and N in ME3 (Figure 16) may reflect changes in AA content, with potential food web implications if these essential dietary components are altered by future change. The impact of future warming and acidification on particulate AA concentrations was determined in ME3, and CSIA-AA in ME3 and ME4, with zooplankton CSIA-AA also determined in ME4. POM quantity was assessed by examining AA composition and concentrations, and POM quality in terms of organic matter degradation and microbial reworking, with CSIA-AA providing insights into biogeochemistry and transformation of amino acids in POM. The authors understand that this is the first study to use CSIA-AA to characterise the effect of ocean acidification and warming on particulate matter (Sabadel et al. submitted).

THAA concentrations showed an increase throughout ME3, with some indication of a decrease in the treatments relative to the Control during Phase 2 (Figure 17). Although the *2150* GAMM showed indicative differences to the Control ($p < 0.1$, Table 6), this was influenced by variability in Phase 1, and there were no significant differences in Phase 3 means. Some differences were apparent in specific AAs, with lower alanine and leucine concentrations in Phase 2 and 3 in *2150* relative to the Control (Figure 18), but Phase 3 means were not significantly different ($p = 0.11$ and 0.12, respectively). These two AAs accounted for ~18–20% of THAA concentration, and so these decreases do not explain the observed significant decrease in PN in *2150* during ME3 (see Table 5, Figure 16C, D). Other AAs, including proline, serine, valine, and phenylalanine, also showed significant differences between the Control and *2150* in the respective GAMM fits (see Table 6), although some of these were also influenced by significant variability in Phase 1. Overall, the results show no evidence that particulate AA will be altered under conditions projected for 2100, although there may be a decline in certain AAs by the middle of the next century.

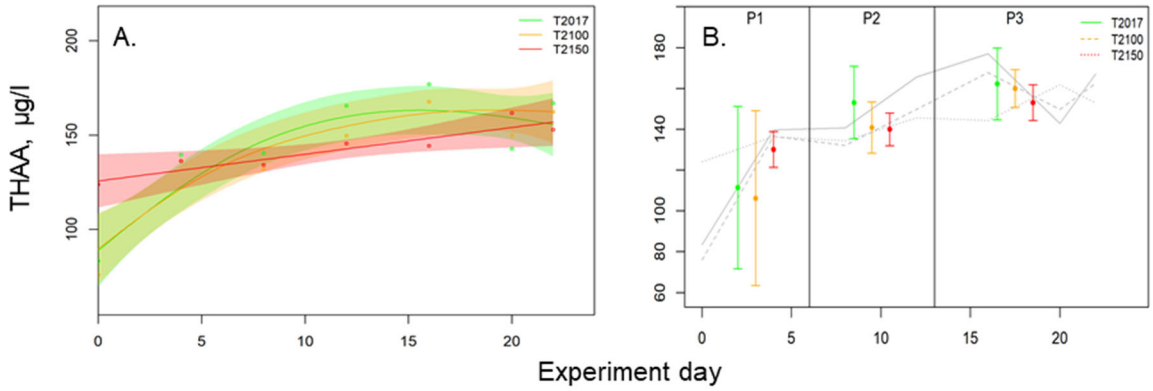

Figure 17: Total Hydrolysable Amino Acids (THAA, µg/l) during ME3 with treatments colour-coded (Control – green, *2100* – orange, *2150* – red). Individual data points from each replicate bag are overlain by the GAMM fits (mean and error) in A, C, and E, and B, D, and F show the mean of the replicates for the Control and treatments, overlain by the mean and standard deviation for each phase (using same colour scheme). The different phases, P1, P2, and P3 are delineated by the vertical lines. Note the different vertical axis scales.

Table 6: Amino acids, defined by type, and response of particulate concentrations in ME3, with significant difference in GAMM fits between treatment and Control indicated by *p* value, with blank cell indicating no significant difference. THAA: Total Hydrolysable Amino Acids.

	AA		GAMM Control vs.	GAMM Control vs.
Species		Type	*2100*	*2150*
Alanine	Non-Essential	trophic		<0.1
Aspartic acid	Non-Essential	trophic		
Glutamic acid	Non-Essential	trophic		
Glycine	Non-Essential	other		
Isoleucine	Essential	trophic		
Leucine	Essential	trophic		<0.1
Proline	Non-Essential	trophic		<0.1
Serine	Non-Essential	other	<0.1	<0.1
Threonine	Essential	metabolic		
Valine	Essential	trophic		<0.1
Phenylalanine	Essential	source		<0.01
THAA				<0.1

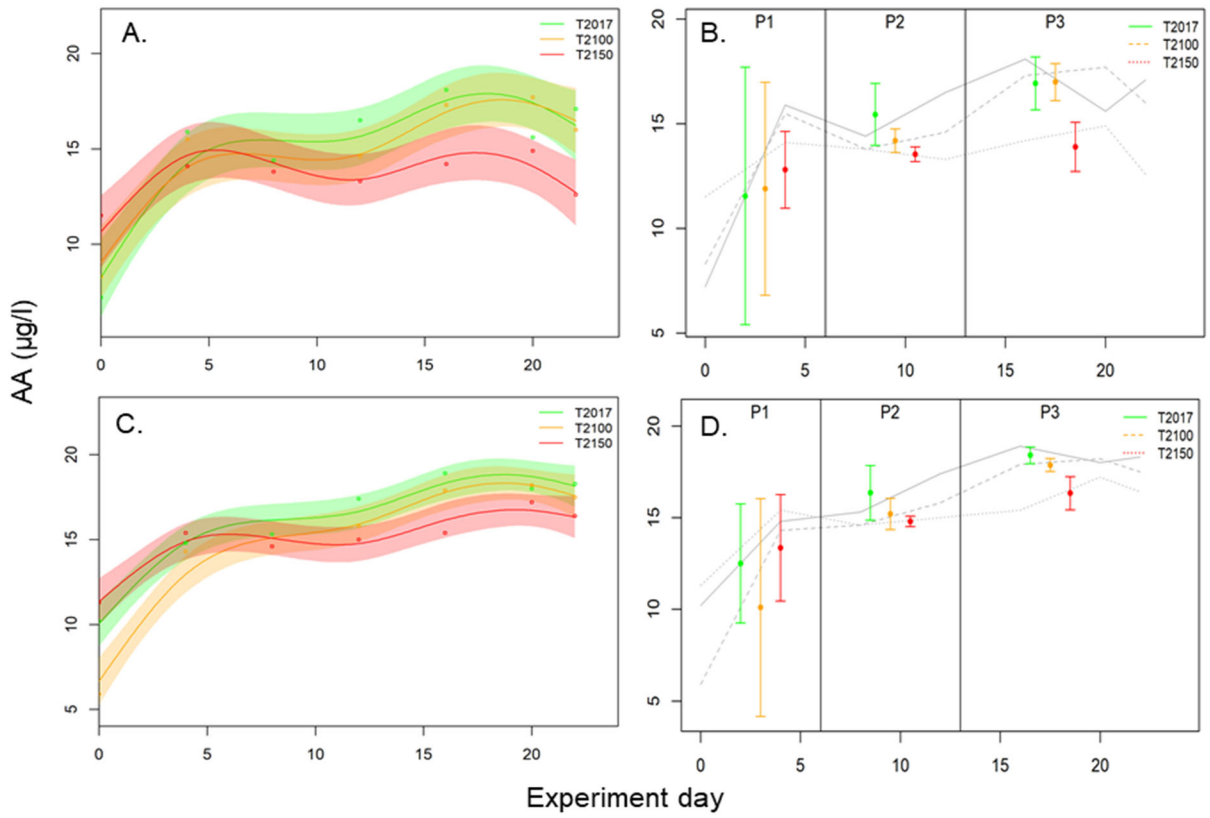

Figure 18: Trends in concentrations (µg/l) of alanine (A, B) and leucine (C, D). with treatments colour-coded (Control – green, *2100* – orange, *2150* – red). Individual data points from each replicate bag are overlain by the GAMM fits (mean and error) in A, C, and E, and B, D, and F show the mean of the replicates for the Control and treatments, overlain by the mean and standard deviation for each phase (using same colour scheme). The different phases, P1, P2, and P3 are delineated by the vertical lines. Note the different vertical axis scales.

Compound-Specific Isotopic Analysis of Amino Acids (CSIA-AA)

There was a general decrease in particulate $\delta^{15}N_{AA}$ values, with a decline of 4–6‰ in ME3 and 2‰ in ME4 (see Figure 19), that may reflect adjustment to the $\delta^{15}N$ values of the added dissolved inorganic nitrogen (see Table 2). As with the AA concentrations, there were no significant differences in $\delta^{15}N$ for all particulate AA species in Phase 3 means between the treatments and Controls in both experiments.

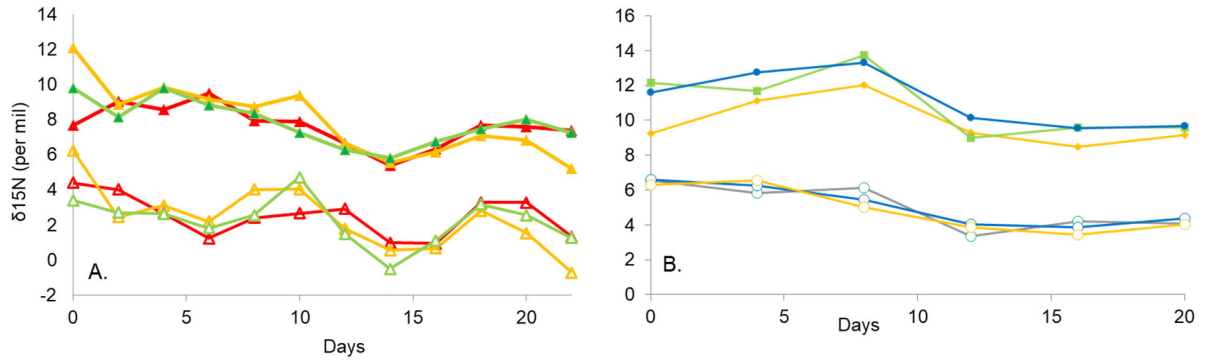

Figure 19: Temporal trends (mean values) in δ^{15}N-Glutamic acid (closed symbols) and δ^{15}N-Phenylalanine (open symbols) during A. ME3 (Control – green, *2100* - orange, *2150* - red) and B. ME4 (Control - green, *pH* - blue, *pH/T* - orange).

The only $\delta^{15}N_{AA}$ to show a difference in Phase 3 mean was threonine (*Thr)*, an enigmatic 'metabolic' amino acid that exhibits opposing behavior to other trophic AAs. Unlike the other $\delta^{15}N_{AA}$ values, $^{15}N_{Thr}$ deviated from Day 16 onwards, with higher values in the treatments relative to the Control (see

Figure 20). In other studies, $\delta^{15}N_{Thr}$ tends to decrease with trophic transfer (Hare et al. 1991, Styring et al. 2010), and this has been attributed to changes in planktonic community structure (Batista et al. 2014). This deviation between treatments and Control in $\delta^{15}N_{Thr}$ from Day 18 onwards coincided with increasing dominance of the diatoms, and particularly *C. closterium,* in the treatments during ME3 (see Figure 11A, B).

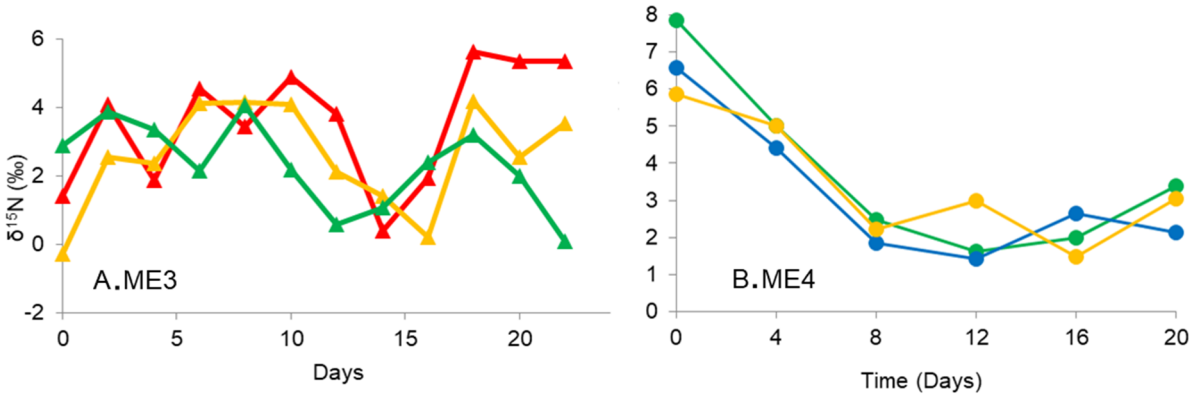

Figure 20: Temporal trend in $\delta^{15}N_{Thr}$ in A. ME3 (Control – green, *2100* - orange, *2150* - red), and B. ME4 (Control - green, *pH* - blue, *pH/T* - orange).

The potential influence of phytoplankton speciation on $\delta^{15}N_{Thr}$ is further supported by elevated $\delta^{15}N_{Thr}$ during the bloom at the start of ME4 (see Figure 11 C, D). Although there was no significant treatment effect on $\delta^{15}N_{Thr}$ in ME4 (Figure 20B), $\delta^{15}N_{Thr}$ was positively correlated with Particulate Carbon in both treatments (Pearson correlation, Control, $r = 0.92$ $p < 0.01$; *pH,* $r = 0.98$, $p < 0.01$; *pH/T,* $r = 0.92$, $p < 0.01$). In addition, $\delta^{15}N_{Thr}$ exhibited a significant positive relationship with diatom biomass (Control, $r = 0.96$, $p < 0.01$; *pH*, $r = 0.94$ $p < 0.01$, *pH/T,* $r = 0.89$ $p < 0.01$), and a negative relationship with small flagellate biomass (Control, $r = -0.70$, $p < 0.01$; *pH,* $r = -0.82$, $p < 0.01$; *pH/T,* $r = -0.87$, $p < 0.01$) (see Figure 21). These results support previous observations that different phytoplankton species may synthesise threonine using different metabolic pathways (Batista et al. 2014) and highlight the potential utility of $\delta^{15}N_{Thr}$ as a biomarker for phytoplankton community composition (Sabadel et al. in press).

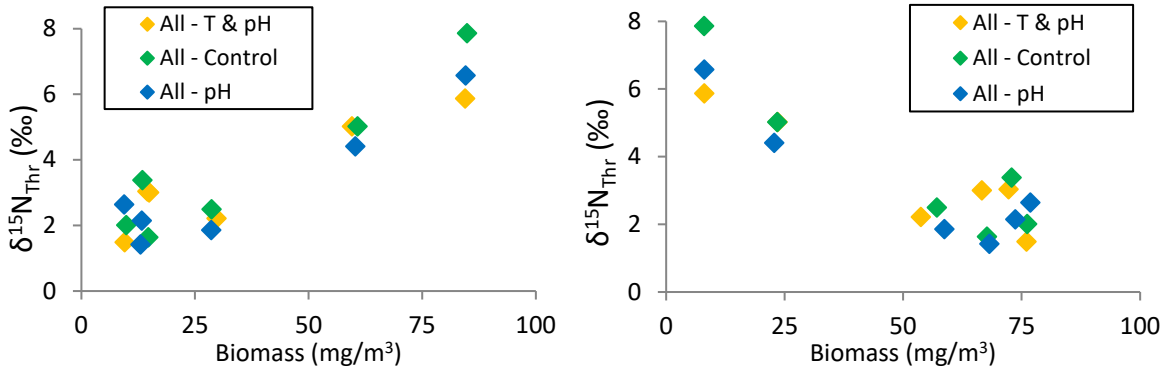

Figure 21: Relationship between $\delta^{15}N_{Thr}$ and A. Diatom biomass, and B. small nanoflagellate biomass during ME4 (Control – green, *pH* - blue, *pH/T* – orange).

δ15N - Trophic Position (TP)

TP provides information on the origin of POM. It is generally accepted that the 'trophic' amino acid (glutamic acid, *Glu*) and 'source' amino acid (phenylalanine, *Phe*) are the most representative AAs, and so their $\delta^{15}N$ values are used to calculate TP as in the following equation (Chikaraishi et al. 2009):

$$TP_{Glu-Phe} = \frac{(\delta^{15}N_{Glu} - \delta^{15}N_{Phe} - \beta)}{TEF_{Glu-Phe}} + 1$$

where β represents the isotopic difference between *Glu* and *Phe* in primary producers ($\delta^{15}N_{Glu}$ - $\delta^{15}N_{Phe}$ = 3.4‰ for aquatic cyanobacteria and algae). A trophic enrichment factor (TEF) of 7.6‰ is commonly used in aquatic food web studies for low TP (McMahon & McCarthy 2016, Ohkouchi et al. 2017).

Both ME3 and ME4 showed a TP between 1 and 1.5, indicative of POM dominated by fresh phytoplankton biomass (Hannides et al. 2013), with similar temporal trends of a TP maximum around Days 6–8 (see Figure 22). However, there were no significant differences between treatments in either experiment, indicating no effect of lower pH and warming on trophic position.

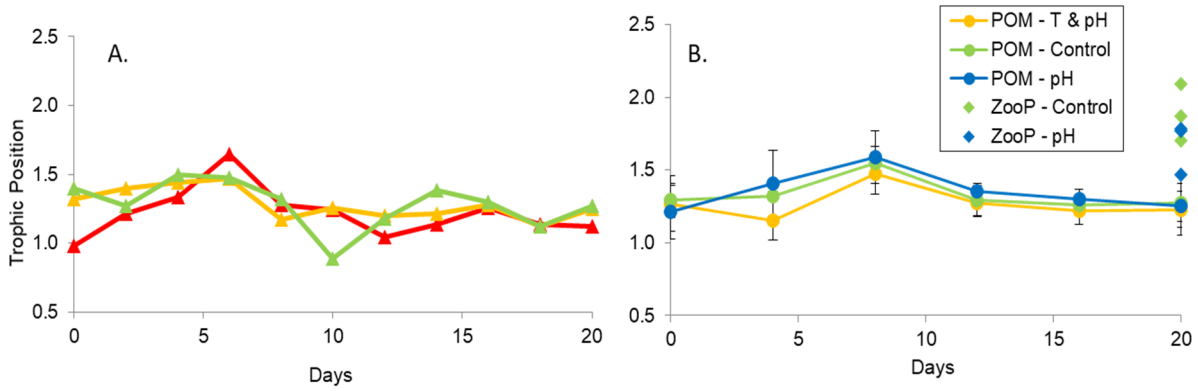

Figure 22: Trophic Position (TP) of particulate organic matter (POM), based upon $\delta^{15}N_{AA}$ during A. ME3 (Control – green, *2100* - orange, *2150* - red) and B. ME4 (Control - green, *pH* - blue, *pH/T*- orange, with the diamond symbols representing zooplankton TP on Day 20).

Zooplankton $\delta^{15}N_{AA}$ collected at the beginning and end of ME4 were compared with $\delta^{15}N_{AA}$ for POM to examine the interaction between primary producers and grazers (see Figure 23). At the start of ME4, the TP for POM was similar across treatments and replicates, with an average value of 1.23 ± 0.14 (range 1.08–1.42). However, there was a distinct separation between Day 0–8 and Day 12–20, with $\delta^{15}N$ of the POM in all treatments decreasing and becoming less variable (see 'direction of change' arrow and clusters in Figure 23). The convergence of POM $\delta^{15}N_{AA}$ in replicates and treatments may reflect the general decrease in phytoplankton community diversity.

Conversely, the zooplankton data showed different trends between the treatments in ME4 (see Figure 23). Although zooplankton $\delta^{15}N_{AA}$ values were scattered in the Control, the *pH* and *pH/T* values were more constrained and, although $\delta^{15}N_{Phe}$ values did not vary in *pH*, it became more depleted in *pH/T*. This depletion in zooplankton $\delta^{15}N_{Phe}$ tracked the temporal decrease in POM $\delta^{15}N_{Phe}$, suggesting rapid transfer of the particulate $\delta^{15}N$ composition to the zooplankton in *pH/T*. This may reflect more rapid grazing and metabolism in *pH/T* in response to elevated temperature, although this attribution is tempered by other results from ME4 which show contrary responses. For example, copepod gut content showed no significant difference between the Control and treatments (see Figure 36), and short-term grazing rate incubations in ME4 using a single copepod species showed a significant decline in grazing in *pH* but no difference in *pH/T* (see Figure 37). Although this confounds interpretation, these results still indicate a potentially valuable analytical role of $\delta^{15}N_{Phe}$ and TP as tracers of metabolism when determining climate impacts on trophic transfer (Sabadel et al. in press).

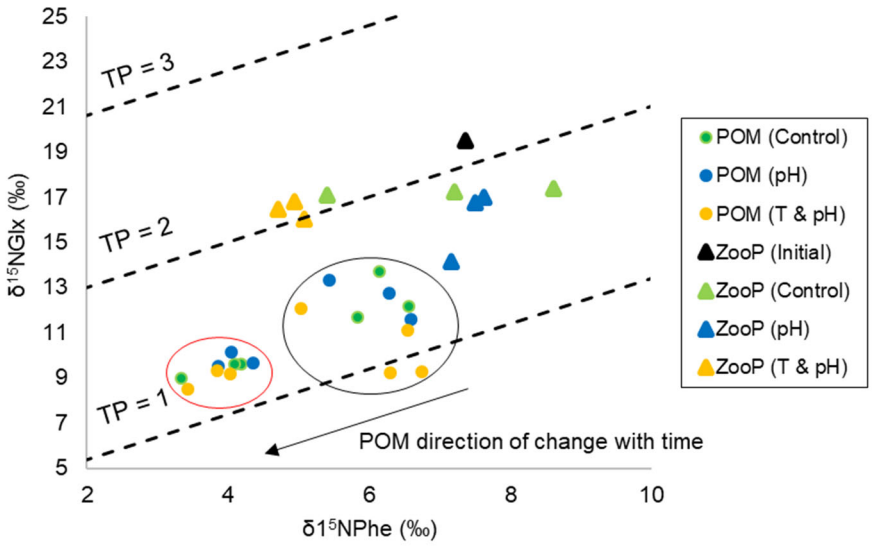

Figure 23: A cross-plot of $\delta^{15}N_{AA}$ for the canonical trophic and source amino acids glutamic acid (*Glx*) and phenylalanine (*Phe)*, respectively, in particulate organic matter (POM) (circles) and zooplankton (Zoop, triangles) during ME4. The larger black circle highlights the cluster of POM $\delta^{15}N$ values during Days 0–8, while the smaller red circle shows the cluster of POM $\delta^{15}N$ values during Days 12–20. The arrow indicates the direction of change in POM $\delta^{15}N$ between during the experiment and TP = trophic position.

Particulate fatty acids

Lipids are a broad range of compounds that support several functions in organisms, including energy storage, digestion, membrane structure and pigments, and are composed of fatty acids (FAs) (Jónasdóttir 2019). FAs are an important biomolecule, but their contribution to the dietary requirements and physiological status of an organism is dependent upon their molecular structure. Saturated FAs (SFA) lack a double bond and monounsaturated FAs (MUFA) contain one double bond whereas Polyunsaturated FAs (PUFA) contain 2 or more double bonds, which influences their dietary value. PUFA particularly play a crucial role, as the primary source of the essential omega-3 and omega-6 groups which most consumer species are unable to synthesise and can only obtain via their diet (Jónasdóttir 2019). Omega-3 PUFA (n3PUFA) are produced by phytoplankton groups including diatoms, cryptophytes, and dinoflagellates (Brett & Muller-Navarra 1997, Jónasdóttir 2019) and are known to enhance growth and reproductive rates in marine organisms (Ballantyne et al. 2003). For example, the lipid fraction in green-lipped mussels contains a high proportion of n3PUFA (Miller & Tian 2018), with the ratio of n3PUFA species varying with location and diet in New Zealand waters (Taylor & Savage 2006).

Previous studies have shown that lower pH may alter phytoplankton community composition with associated changes in particulate FAs (Rossoll et al. 2012, Leu et al. 2013; Wang et al. 2017), and so it is critical to establish the impact of future change in New Zealand coastal waters. Particulate FAs were measured every four days during ME2, ME3, and ME4, with the data summarised in terms of the major FA groups, with respect to volumetric concentration and also proportional concentration relative to TFA. Treatment effects are summarised in Table 7, with temporal trends for the different FA groups shown graphically in Figures 24–26. Due to variability between replicates in Phase 1 the GAMMs were not used in this analysis, and only Phase 3 means are considered.

Table 7: **Treatment responses of fatty acid groups in ME3 and ME4 as indicated by Phase 3 means with significant differences (p < 0.1, upward green arrows: increase; downward red arrows: decrease) between treatment and Control, and also indicative differences (< 0.15 italics, white arrows). Results are not included for ME2 and ME4 *pH/T* as there were no significant treatment effects. TFA: total fatty acids; MUFA: monounsaturated fatty acids; SFA: saturated fatty acids; PUFA: polyunsaturated fatty acids; n3PUFA: PUFA containing a double bond three atoms from the terminal methyl group. C indicates absolute concentration of each FA group and P indicates the proportional concentration each relative to Total FA concentration (TFA).**

		ME3		ME4
		2100	*2150*	*pH*
	Concentration (C) Proportion (P)	Phase 3 Mean	Phase 3 Mean	Phase 3 Mean
TFA	C		0.05 ↑	*0.12* ↓
SFA	C		*0.12* ⇧	*0.12* ⇩
	P		0.05 ↓	
MUFA	C		0.01 ↑	*0.12* ⇩
	P		0.01 ↑	
PUFA	C			
	P	0.03 ↓		
n3PUFA	C			
	P	0.08 ↓		

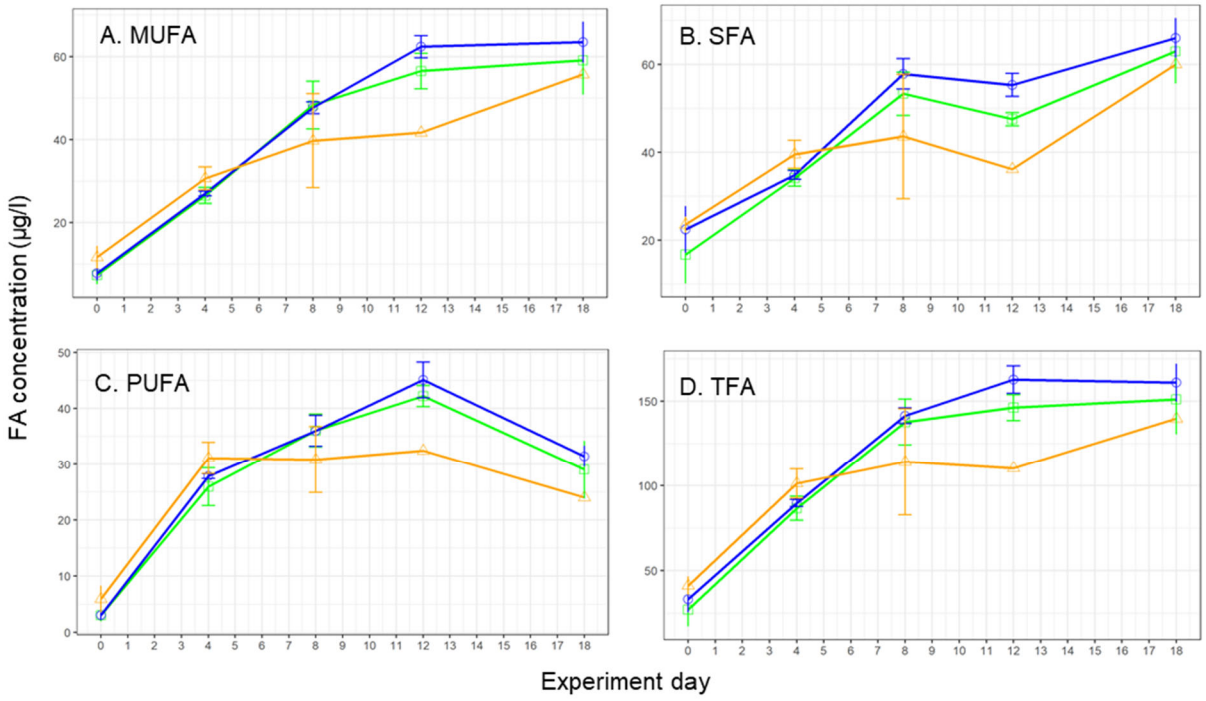

Figure 24: **ME2 FA concentrations (µg/l) showing the mean and standard deviation of replicates for each treatment at 4-day intervals (Control – green, *pH* – blue, *pH/T* – orange) for A. MUFA, B. SFA, C. PUFA and D. TFA. Note that there are no replicates for *pH/T* from D8 onwards. Abbreviations are identified in the Table 7 legend.**

In ME2, there was evidence of a decline in all major FA groups in *pH/T* relative to the Control (see Figure 24); however, the loss of two of the three replicates from Day 8 onwards meant that there was insufficient data to confirm whether this trend was significant and ME2 *pH/T* data were omitted from further

interpretation. There was some indication of an increase in all major FA groups in *pH* relative to the Control in the latter half of ME2, but no significant difference in Phase 3 means. Contrary to the response in ME2, and, despite variability between duplicates, ME3 showed significant treatment responses (see Table 7, Figure 25), with higher total concentrations for the major FA groups in *2150*. The relative proportions of MUFA and SFA were also altered in *2150*, with a significant increase in MUFA and decrease in SFA in the Phase 3 means. Conversely, these FA groups showed no significant responses in *pH/T* in ME4, although Phase 3 mean concentrations of MUFA, SFA and TFA were all lower in *pH* (p = 0.12, see Figure 26).

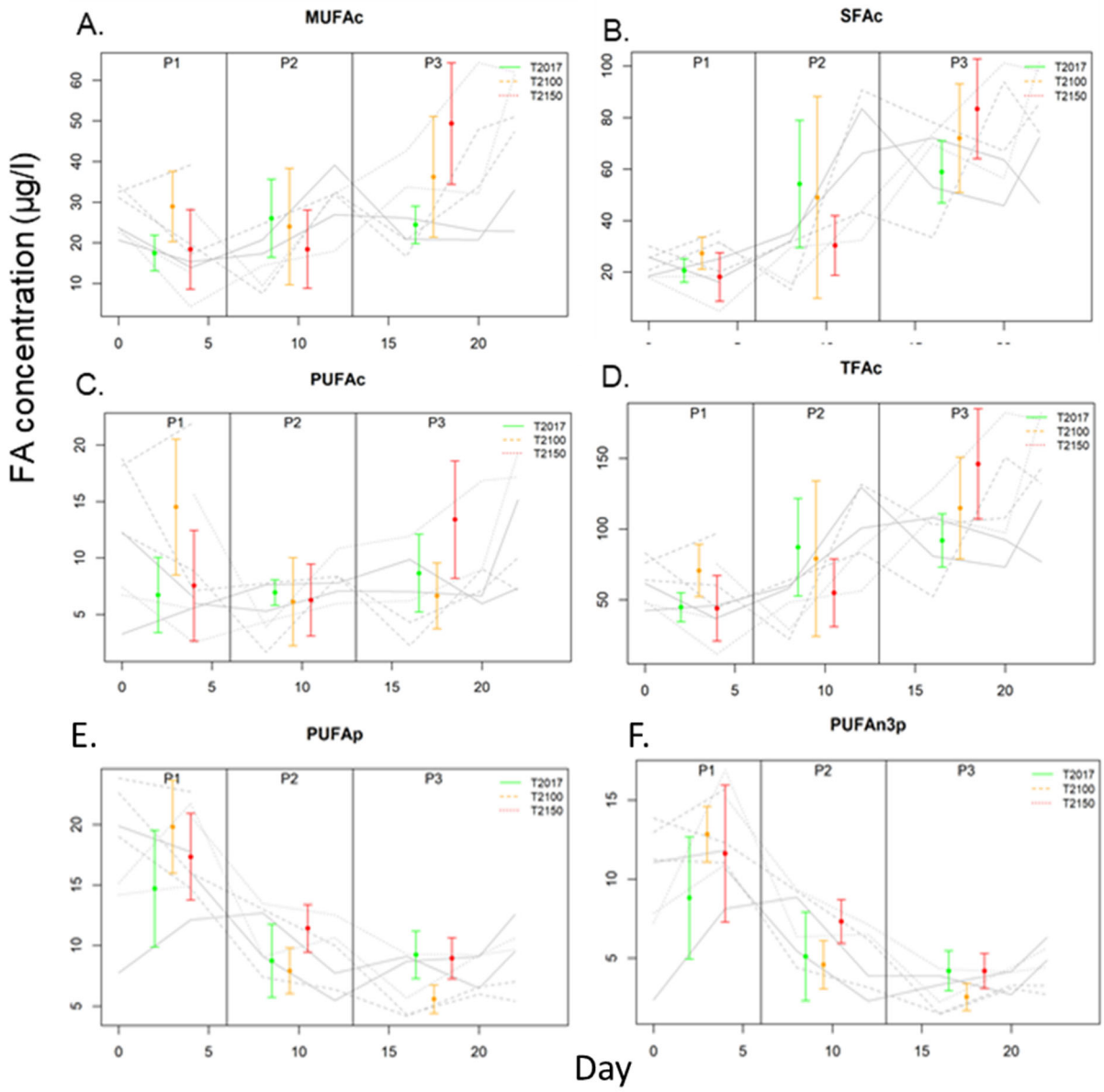

Figure 25: ME3 fatty acid concentrations (µg/l) for A. MUFA, B. SFA, C. PUFA, and D. TFA and also proportional concentration for PUFA and n3PUFA in E. and F.; respectively. Treatments are colour-coded (Control – green, *2100* – orange, *2150* – red), showing the replicates for the Control and treatments, overlain by the mean and standard deviation for each phase (using same colour scheme, as indicated in the legends). The different phases, P1, P2, and P3 are delineated by the vertical lines. Note the different vertical axis scales. Abbreviations are identified in the Table 7 legend.

The responses in PUFA were more variable than for the other FA groups in ME3. Despite no significant difference between Control and treatments for PUFA (Figure 25C) and n3PUFA concentration (data not shown) proportional concentrations were significantly lower for both PUFA (p = 0.03) and n3PUFA (p = 0.08) in *2100* (Figure 25E, F) due to relative increases in the other FA groups. However, neither absolute or proportional concentration of PUFA or n3PUFA exhibited any differences between the

Control and *2150* (see Figure 25C). As with the other FA groups in ME4, there were no significant treatment responses for n3PUFA and PUFA, due in part to the high variability in the replicates in Phase 3 (Figure 26).

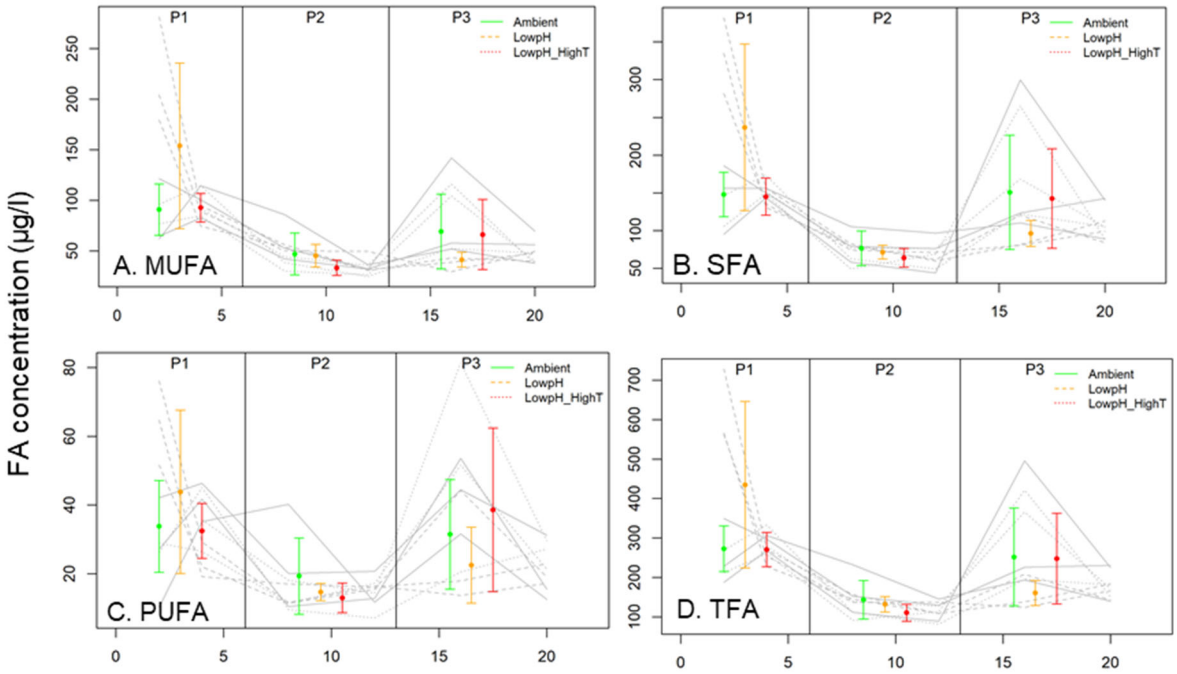

Figure 26: ME4 fatty acid concentration (µg/l) showing the mean and standard deviation (Control – green, *pH* – blue, *pH/T* – orange) and the mean and standard deviation for each phase (as indicated by labels P1, P2, and P3 and vertical divisions) for A. MUFA, B. SFA, C. PUFA, and D. TFA. Anomalously high initial concentrations for all FA classes on Day 2 in *pH* were discounted. Abbreviations are identified in the Table 7 legend.

As *C. closterium* dominated the diatom response in ME3, it was subsequently maintained in the laboratory under *Now* (Control) and *Future* conditions (750 ppm CO_2, +2.7 ºC; see Methods section 2.1) for 19 days, to determine whether responses in particulate FA are maintained over longer periods, and also whether bulk community changes in FAs observed in ME3 reflect the response of the dominant phytoplankton species. Results were consistent with ME3, with significantly higher SFA ($p = 0.027$), MUFA ($p = 0.034$) and TFA ($p = 0.031$) concentrations on a per cell basis in *Future* (see Figure 27). However, although PUFA and n3PUFA cell concentrations were also higher in *Future*, there was no significant difference from *Now*.

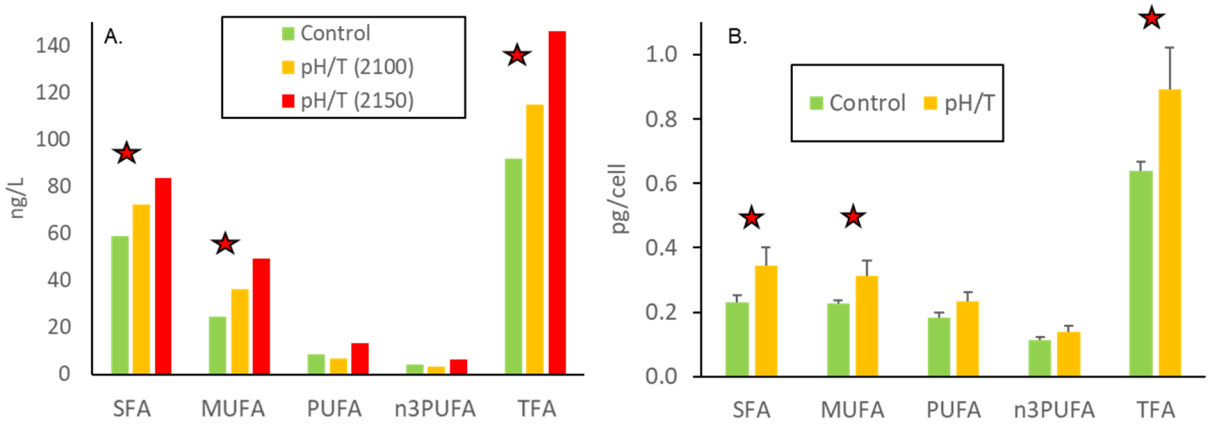

Figure 27: Comparison of FA groups in A. ME3 Phase 3 means (µg/l), and B. *C. closterium* incubations (pg/cell) after 19 days. Treatments are shown in the legends, and a red star indicates significant differences between treatments and Control in the Phase 3 Means ($p < 0.15$) in A.; and between the *Now* (Control) and *Future* (pH/T) in the *C. closterium* incubations ($p < 0.05$) in B. Abbreviations are identified in the Table 7 legend.

Although MUFA, SFA, and TFA concentrations decreased under *pH* in ME4, there were no corresponding decreases under *pH/T.* In addition, these FA groups responded positively to combined lower pH and elevated temperature in *2100* and *2150* in ME3, and *Future* in the *C. closterium* incubations. This suggests that warmer temperatures may compensate or ameliorate the influence of low pH on these FA groups, in agreement with previous mesocosm studies that incorporated both warming and low pH (Garzke et al. 2016).

Despite the decline in the main FA groups in *pH* during ME4, there was no corresponding decline in PUFA concentration or proportion. Combined with the absence of an effect of *pH* in ME2 (Figure 24C), this suggests that PUFA concentration is relatively insensitive to changes in pH. These results are consistent with a lack of response in PUFA to low pH in different phytoplankton species (King et al. 2015), although other studies have shown significant changes, with increases in PUFA in response to increased pCO_2 (Leu et al. 2013, Wang et al. 2017), and negative impacts on the ratio of PUFA to SFA and TFA (Rossoll et al. 2012, Bermudez et al. 2016). Overall, the reported variation in PUFA sensitivity to low pH, combined with the results of the current study, suggests the response of PUFA to future reductions in pH may be location-specific and dependent upon phytoplankton species or environmental factors, such as nutrient status.

Although proportional concentrations of PUFA may increase under warming and low pH (Garzke et al. 2016), other studies suggest that warming will lead to a reduction in PUFA and corresponding increase in SFA as a response to maintaining structural rigidity of the phytoplankton cell membrane (Rousch et al. 2003, Fuschino et al. 2011). This is supported by a global synthesis that identified decreasing proportional n3PUFA and increasing SFA as temperature increases (Hixson & Arts 2016). The ME3 results provide some support for this, with an increase in SFA in *2150* and a decrease in proportional PUFA concentration in *2100,* and the *C. closterium Future* incubation also showing significantly higher SFA on a per cell basis. Further studies are required to determine whether the balance between essential and non-essential FAs will be altered by future temperature increases but, overall, the results suggest that essential FAs in phytoplankton will not be significantly affected in New Zealand coastal waters over the next century.

Zooplankton fatty acid composition

Since the proportion of FAs in the tissues of crustaceans shows a relationship with that of their diet, and they lack the capability to synthesise n3PUFA (Sargent & Falk-Petersen 1988, Fraser et al. 1989), then any change in phytoplankton FAs will likely be reflected in the consumers that graze upon phytoplankton. Consequently, zooplankton FA composition was determined in copepods at the start and end of ME3 and ME4 to determine if the trends reflect that of the particulate FAs. FA content is reported as % of total FA (TFA), as the sampling approach precluded quantitative measurement of FA per zooplankton biomass.

In ME3, the relative proportion of SFA increased in all treatments from ~32% at the start to an average of 55% in the Control, 59% in *2100*, and 64% in *2150* by the end of the experiment (Figure 28). The relative proportion of MUFA in zooplankton also increased across all treatments, with MUFA proportions increasing from 13% to final proportions of 33% (Control), 36% (*2100*), and 31% (*2150*). The opposite trend was seen for PUFA, which decreased from initial proportions of ~54% to 11%, 5%, and 4% in the Control, *2100*, and *2150*, respectively, with a similar trend in n3PUFAs (Figure 28). Overall, there were no significant differences between control and treatments, and the significant reduction observed in phytoplankton proportional PUFA content in *2100* (Table 7) was not reflected in the zooplankton.

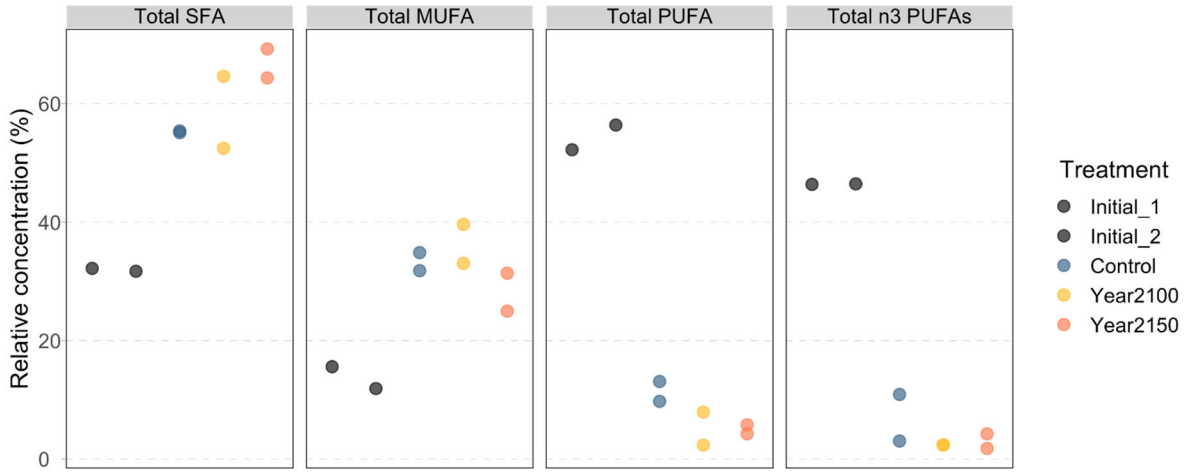

Figure 28: a) Relative proportions of SFA, MUFA, PUFA, and n3PUFA (as labelled, from left to right) for zooplankton in ME3. Initial values are shown in black, and final values are shown in blue (Control), yellow (*2100*), and pink (*2150*). Abbreviations are identified in the Table 7 legend.

ME4 showed similar trends to ME3 with an increase in zooplankton SFA across the experiment and higher, but not significantly different SFA proportion in the treatments, and no significant treatment effects in MUFA (Figure 29A, B). However, zooplankton PUFA was significantly lower in *pH/T* relative to the Control (p <0.01, Figure 29C), as confirmed by Principal Component Analysis which showed differences between the Control and *pH/T* driven by higher proportions of PUFA in the Control versus higher proportions of SFA in *pH/T* (Figure 29D).

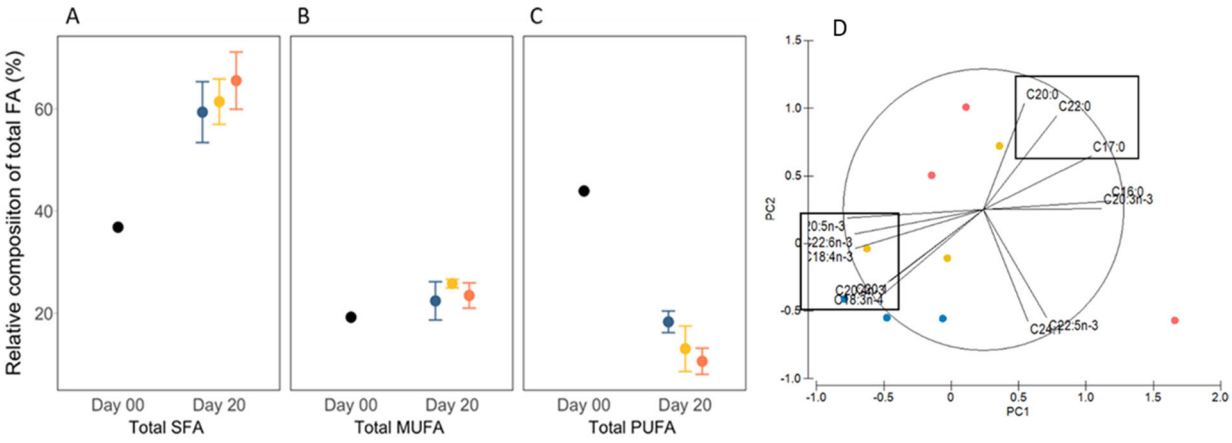

Figure 29: Relative proportions (mean % ± standard deviation) of A. SFA, B. MUFA, and C. PUFA in zooplankton in ME4. Initial values are shown in black and final values in blue (Control), yellow (*pH*), and pink (*pH/T*); D. Principal Component Analysis of individual FA proportions of TFA. PC1 describes 36.7% and PC2 describes 25.6% of the variation, respectively (cumulative = 62.3%). Vectors indicate Pearson correlations > 0.8. Boxes show groupings of individual PUFA (lower left) and SFA (upper right) vectors. Abbreviations are identified in the Table 7 legend.

ME3 treatment responses were similar between zooplankton and their particulate diet, with significant increases in SFA. Previous studies have reported that changes in phytoplankton FAs, including PUFAs, in response to elevated CO_2 transfer to zooplankton grazers, and influence their growth and reproduction (Rossoll et al. 2012, Bermudez et al. 2016). However, particulate and zooplankton FA appear decoupled in the current study with the significant decrease in phytoplankton PUFA in *2100* in ME3 not reflected in a similar response in zooplankton content (see Figures 24 & 25, Table 7), and the decrease in zooplankton PUFA in *pH/T* in ME4 not reflected in particulate PUFA (see Figure 29).

Linear regression analysis showed a significant relationship between particulate FA and zooplankton FA composition in both ME3 and ME4 (Figure 30A, B). As this relationship was unaffected by treatment, this infers that zooplankton FA profiles may be predicted from the FA profile of their diet under future ocean conditions. Although the combination of low pH and warmer temperatures decreased zooplankton PUFA content in ME4, it did not influence the overall relationship between diet and consumer FA composition. As copepods are an important dietary source of essential FAs for higher trophic levels (Rocha et al. 2017), these results indicate that the transfer of essential dietary components in New Zealand coastal planktonic food webs may not be significantly impacted in the future.

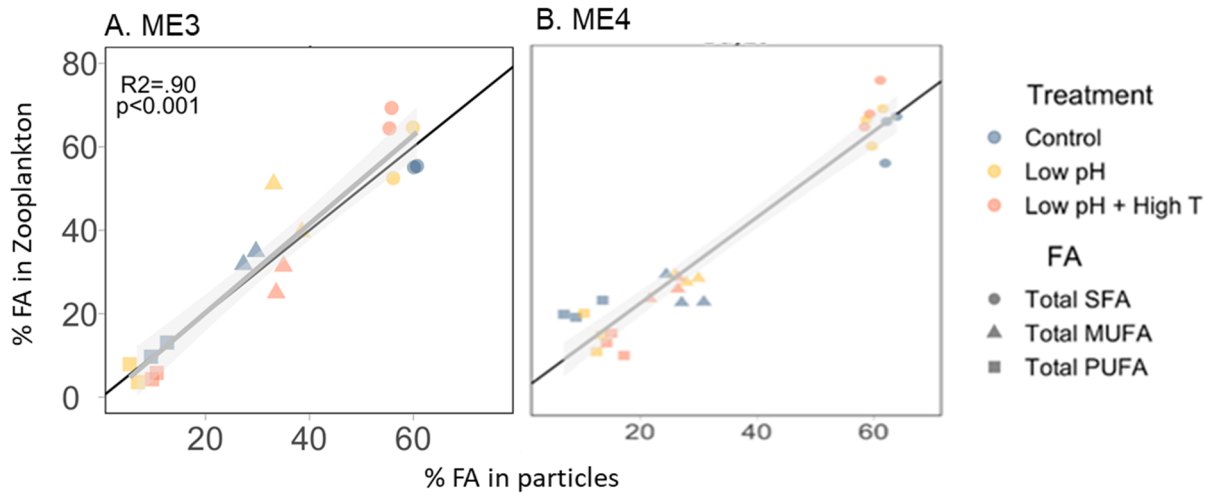

Figure 30: Linear regression models of the relationship between zooplankton and particle FA proportional concentration fitted to the combined data set (grey line + 95% confidence interval), for the final experiment day of A. ME3 and B. ME4. The reference line of 1 is shown in black in both figures, with the treatments and FA groups identified in the respective legends. Abbreviations are identified in the Table 7 legend.

3.2 Specific Objective 3: Projecting future impacts on green-lipped mussels

Specific Objective 3 is presented after Specific Objective 1 for continuity, as the significant treatment effects observed in the mesocosm experiments were subsequently applied in a Dynamic Energy Budget (DEB) model. The DEB model for green-lipped mussel (Ren et al. 2020) was used to assess the implications of the observed changes in particulate composition in response to lower pH and warmer temperatures for the commercially important Greenshell™ mussel. The DEB model was applied in two independent simulations using significant treatment effects observed in Phase 3 of ME1, ME3, and ME4, for a) Chl-*a* biomass and b) Phytoplankton carbon > 2µm (estimated from the 2–5-µm Chl-*a* fraction plus > 5-µm Phytoplankton Carbon in Appendix 5) as input parameters, with the input data given in Table 8.

Table 8: Input variables for the DEB model simulations. Mean values for Phase 3 are shown where treatment results were significantly different from the Control in Phase 3, with n/s indicating non-significant results.

	ME1		ME3			ME4		
	Control	*pH/T*	Control	*2100*	*2150*	Control	*pH*	*pH/T*
Temperature (°C)	17.1	20.1	15.6	18.2	21.1	12.1	12.1	15.6
Chl-*a* (µg/l)	0.86	1.03	2.42	n/s	3.65	2.46	n/s	3.31
Phytoplankton C	n/s	n/s	125.7	169.7	n/s	205.4	230.1	n/s

Chlorophyll-*a* (Model 1)

The DEB model predicted that the uptake rate of mussels would be 61.7%, 84%, and 81.7% greater in *pH/T* relative to the Control for ME1, ME3 (*2150*) and ME4, respectively (Figure 31A), and consequently the energy allocated for reproduction in *pH/T* would increase by 196.3%, 225.7% and 203% for ME1, ME3 (*2150*), and ME4, respectively (Figure 31B). The lower increase in length and flesh weight in ME1 reflects lower chlorophyll concentration relative to the other experiments, and so the overall difference in energetics between control and treatments reflect difference in both chlorophyll concentrations and temperature.

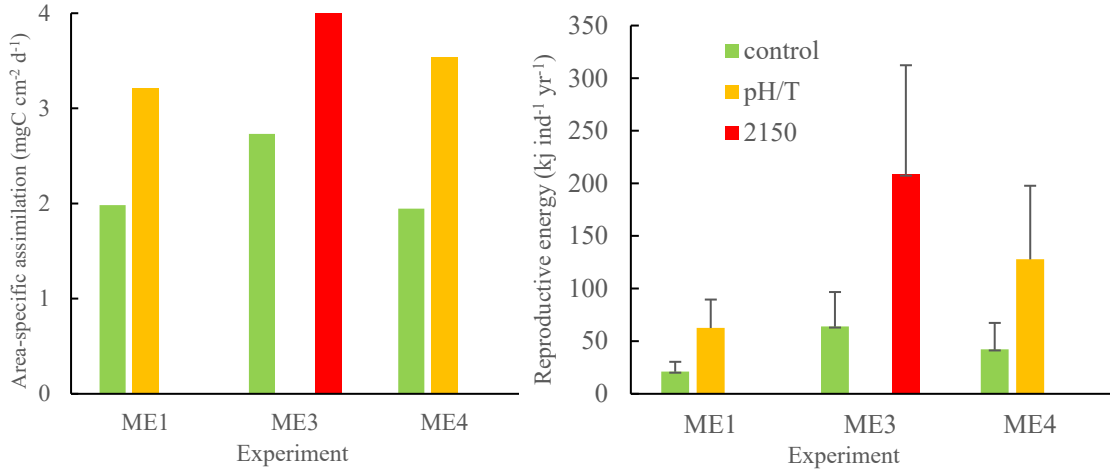

Figure 31: A. (left) Mean food uptake rate and B. (right) Energy allocation (mean and standard deviation) for reproduction in Model 1 based upon Phase 3 Chl-*a* results from ME1, ME3 (*2150*) & ME4 (Control – green, *pH/T or 2100* – orange, *2150* – red). There are no error bars in A as constant food input was used over the entire simulation period.

Model 1 output indicated shell length would be 33.3%, 30.7%, and 22.7% higher in *pH/T* relative to the Control for ME1, ME3 (*2150*), and ME4, respectively, at the end of simulations (Figure 32A). Similarly, dry flesh weight was projected to be 168.9%, 171.1%, and 115.6% higher under *pH/T* relative to the Control for ME1, ME3 (*2150*), and ME4 (Figure 32B).

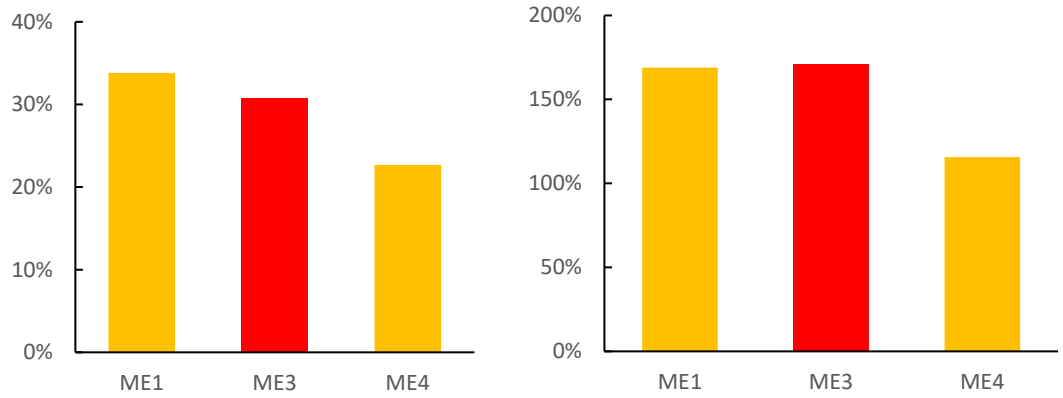

Figure 32: Percentage changes in A. (left) shell length and B. (right) dry flesh weight in *pH/T* relative to the Control at the end of 5-year Model 1 simulation based upon Chl-*a* results for ME1, ME3 (*2150*) and ME4 (*pH/T* – orange, *2150* – red).

Model 1 simulations indicate that growth was significantly faster and reproduction higher under future conditions relative to control conditions ($p < 0.01$ for all tests). These results provisionally appear contrary to previous studies of the effects of low pH, which reported negative impacts on shellfish physiology (Pörtner et al. 2004, Gu et al. 2019, Shang et al. 2020) and also on growth and reproduction (Pan et al. 2015, Sui et al. 2016, Ren et al. 2020). This apparent discrepancy reflects the role of temperature in driving differences between the Control and treatments in this study. The ME results show that Chl-*a* was significantly higher in *pH/T* relative to the Control, but not in *pH*, and consequently

there is elevated food supply in *pH/T*. High temperature in combination with elevated food supply has a positive effect on bivalve growth (Shpigel et al. 1992, Pilditch & Grant 1999). Although high temperature would generate higher energy costs via respiration, the energy uptake would be greater than the additional respiration cost when food is available. Consequently, the positive influence of temperature may have overridden the negative effects of pH on mussel growth. This is also consistent with reports that the effects of ocean acidification on energetics are greater when food is limited, but weaker when food is abundant (e.g.; Ramajo et al. 2016, Brown et al. 2018). It should be noted that Chl-*a* concentration, and so food levels during Phase 3 in *pH/T*, were moderate (above average) relative to in situ regional concentrations around aquaculture farm regions in the Marlborough Sounds (Zeldis et al. 2008, Ren et al. 2010, 2012, Zeldis et al. 2013).

As food and temperature are the major drivers in the DEB model, increases in both parameters would drive higher growth and reproduction than in controls. However, it is important to note that the Model 1 results are only based upon the significant increases in Chl-*a* observed in three of the mesocosm experiments and so reflect the maximal response under these conditions; under different nutrient regimes and plankton communities the response may not be significant. Nevertheless, the model simulation highlights the importance of considering indirect climate effects, such as changes in food quantity, on shellfish physiology and growth in future projections. The results also highlight the importance of considering lower pH and higher temperature together (plus other stressors) for robust projection of future shellfish population success.

Phytoplankton carbon (Model 2)

DEB Model 2 predicts that food uptake rate would be 55.2% greater in *2100* relative to the Control in ME3 and 6.8% higher in *pH* in ME4 (Figure 33A) based upon the significant responses in phytoplankton carbon (Table 8). This would result in an increase of 142.9% in energy allocation for reproduction in *2100* relative to the Control in ME3, and 19.1% more in *pH* in ME4 (Figure 33B). Similarly, shell length in *2100* in ME3, and *pH* in ME4, would be 23.2% and 6.3% larger than in the Control (Figure 34A). Corresponding dry flesh weights in these treatments would be 111.4% and 21.6% greater than in the Control for ME3 and ME4 (Figure 34B).

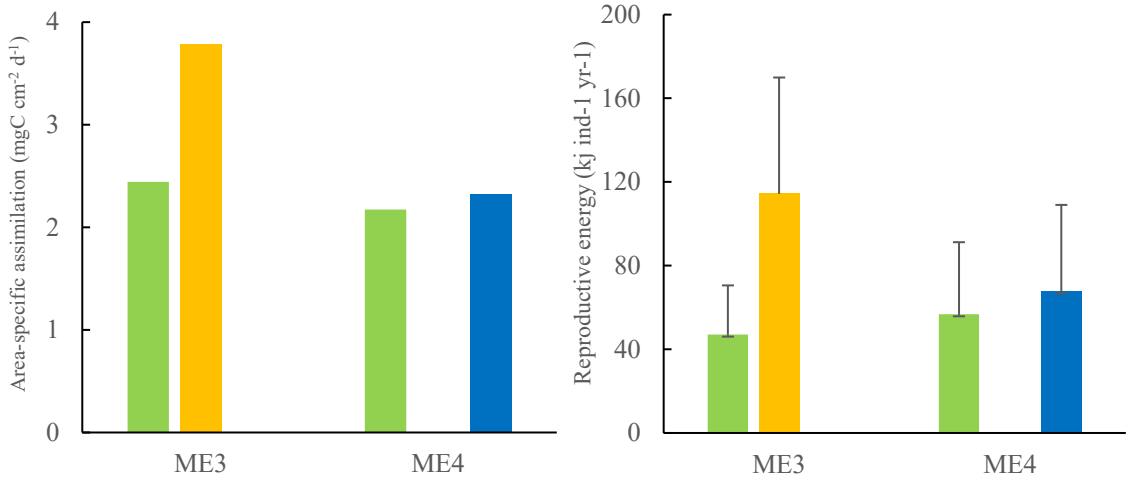

Figure 33: A. (left) Area-specific food uptake rate (Note that there are no error bars as constant food input was used over the entire simulation period), and B. (right) Energy allocation for annual reproduction in Model 2 simulations based upon phytoplankton carbon results from ME3 and ME4 (Control – green, *pH* – blue, *2100* – orange).

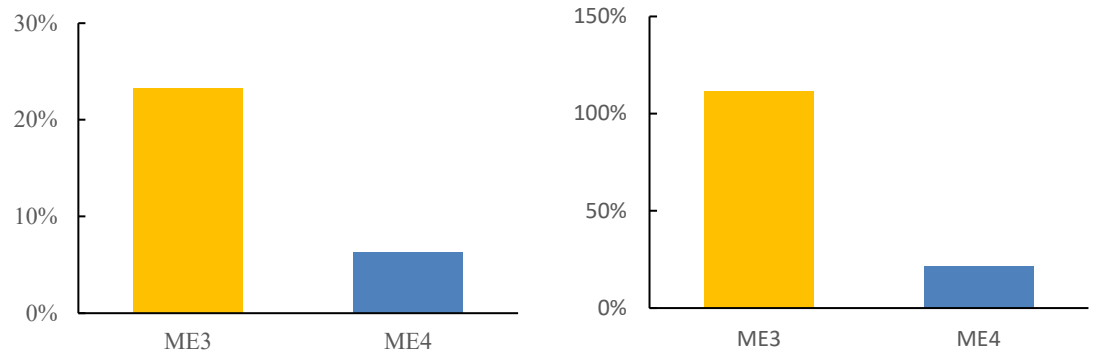

Figure 34: A. (left) Percentage changes in shell length and B. (right) dry flesh weight in *2100* (orange) in ME3 and *pH* (blue) in ME4, relative to the Controls, at the end of 5-year Model 3 simulation, based upon phytoplankton carbon results from ME3 and ME4.

These results are generally consistent with the outputs of DEB Model 1 based upon Chl-*a*, although there are some contradictions. In ME3, the *2100* treatment did not show a significant increase in Chl-*a* but did in phytoplankton carbon, hence there is an increase in mussel energetics in *2100* with phytoplankton carbon but not chlorophyll. In ME4, a significant increase in Chl-*a* in *pH/T* relative to the Control resulted in an increase in mussel energetics; conversely, phytoplankton carbon showed a significant increase in *pH*, and consequently ME4 phytoplankton carbon provided the only positive effect on mussel energetics for low pH only. Although the sign and significance of these results is robust, the resulting relative magnitude of chlorophyll and phytoplankton carbon results in the two DEB model simulations is less certain. This may arise in part from assumptions, such as the use of a fixed C:Chl ratio, which may vary with phytoplankton species composition (Mackenzie et al. 1986).

Overall, the DEB model results summarised in Table 9 indicate a positive effect of future conditions that is driven primarily by elevated temperature, as lower pH alone (e.g.; *pH*) results in lower increases (based upon ME4 results only). The model simulations predict future food intake increases of +6.8% to +84% and increases in mussel energetics ranging more widely from +19.1 to +225.7%. Changes in shell length and dry flesh weight are also variable, ranging from +6.3% to +33.3%, and +21.6% to +168.9%, respectively. This range reflects variability in response of the two food input parameters to future conditions and also the differing temperatures between experiments. It should be noted that the DEB model is uncalibrated for these food inputs and includes assumptions regarding conversion of the parameters to food in the model. It is important to note that only the observed significant results from the mesocosm experiments were used, and so the DEB model results represent the maximum changes that could be expected in the future. The majority of the significant responses were observed in ME3 and ME4 in which nutrient supply was maintained, and so the corresponding responses in mussels may be different if nutrient supply is reduced in the future (as indicated by ME1 and ME2). Nevertheless, this application of the DEB model highlights the importance of considering indirect effects of future changes in food supply, in addition to the direct effects of temperature and pH change (Ren et al. 2020), when assessing future performance of this important aquaculture species (White 2017, New Zealand Government 2019, Seafood New Zealand 2019).

Table 9: Predicted increase (%) in physiological and morphological parameters for green-lipped mussel by the DEB model simulations, based upon input of significant treatment responses to lower pH and higher temperature in mesocosm experiments ME1, ME3, and ME4. Abbreviations: *pH*: lower pH relative to ambient value; *pH/T*: lower pH and warmer temperature relative to ambient value; *2100*: lower pH and warmer temperature based upon projections for Year *2100*; *2150*: lower pH and warmer temperature based upon projections for Year 2150; Chl-*a*: Chlorophyll-a biomass.

Green-lipped Mussel	Parameter/ Model	ME1	ME3		ME4	
		pH/T	*2100*	*2150*	*pH*	*pH/T*
Food intake	Chl-*a*/Model 1	+61.7		+84		+81.7
	Phytoplankton Carbon/Model 2		+55.2		+6.8	
Energy Allocation	Chl-*a*/Model 1	+196.		+225.7		+203
	Phytoplankton Carbon/Model 2		+142.9		+19.1	
Shell length	Chl-*a*/Model 1	+33.3		+30.7		+22.7
	Phytoplankton Carbon/Model 2		+23.2		+6.3	
Dry Flesh weight	Chl-*a*/Model 1	+168.		+171.1		+115.6
	Phytoplankton Carbon/Model 2		+111.4		+21.6	

3.3 Specific Objective 2: Influence of future changes on rates

Microzooplankton grazing

Microzooplankton occupy a critical role at the base of marine food webs facilitating the trophic transfer of phytoplankton carbon and energy. Grazing represents the main source of phytoplankton mortality, which on average accounts for 66% of daily primary production, and microzooplankton are also important prey for mesozooplankton grazing (Calbet & Landry 2004); consequently, microzooplankton represent an important trophic connection in marine food webs. Phytoplankton growth and microzooplankton grazing tend to be dynamically coupled at both the community and group level (e.g.; faster growing phytoplankton groups being consumed at higher rates), and perturbations altering this coupling influence the onset and development of phytoplankton blooms (Irigoien et al. 2005, Behrenfeld & Boss 2014). Despite the pivotal importance of the phytoplankton-microzooplankton coupling for pelagic ecosystem functioning, little is known about how future ocean conditions will affect this balance (Caron & Hutchins 2012, Steinberg & Landry 2017).

Experiments were carried out to estimate changes in phytoplankton growth and microzooplankton grazing at different stages of the plankton community growth trajectory in three ME experiments. The response for the total phytoplankton community and the effect of nutrient addition are briefly summarised in Table 10, with more detailed discussion of the results, including consideration of the response of specific phytoplankton groups (*Synechococcus,* picoeukaryotes, and nanoeukaryotes) in Appendix 6.

Table 10: Treatment responses of microzooplankton grazing experiments in ME1, ME2, and ME3. n/s: non-significant.

Experiment/ duration	Sample Days	Phytoplankton growth rate	Grazing rate	Net growth rate
ME1 18 days	0, 5, 11, & 17	Higher in *pH/T* relative to *pH* but n/s (One-way ANOVA, $p = 0.18$) nutrient addition: higher in treatments, but n/s (Two-way ANOVA, $p = 0.10$).	Lower in Phase 2 in *pH/T* but n/s *(*One-way ANOVA, $p = 0.21$).	Higher in *pH/T* (Two-way ANOVA, $p = 0.08$).
ME2 18 days	0, 4, 8, 12, 16, & 18	n/s	n/s	n/s
ME3 22 days	2, 8, 14, & 22	n/s	Higher in *2150* relative to Control and *2100,* particularly towards end of experiment (One-way ANOVA, F=5.98, $p = 0.09$).	Lower in *2150* relative to Control and *2100* (Two-way ANOVA, $p < 0.005$), particularly at end of experiment.

Responses varied between experiments, in part reflecting their differing nutrient status and initial planktonic community composition. In terms of treatment effects, warmer temperatures had greater impact on growth and grazing than lower pH alone, particularly in ME1 and ME3. This is consistent with observations that microzooplankton respond more rapidly to increases in phytoplankton biomass at higher temperatures, whereas lower pH has no effect on microzooplankton (Horn et al. 2015). However, the actual response of the microzooplankton in *pH/T* varied between experiments, with higher net community growth in ME1 but lower in *2150* in ME3, which is surprising given that the higher nutrient availability in ME3 might be expected to have accelerated phytoplankton growth rates. The latter result may reflect that grazing rate was also significantly higher in *2150* in ME3 (see Table 10), potentially due to higher grazer metabolism at elevated temperature, and so tighter coupling between growth and grazing at higher temperature. These results concur with model studies of Chen et al. (2012) which identified that warming may increase microzooplankton herbivory under nutrient-replete conditions. Tighter coupling may lead to more efficient transfer of food and energy into the lower food web under future conditions, but also lower phytoplankton biomass accumulation. As an increase in total Chl-*a* biomass was apparent in both ME1 and ME3 (see Figure 5), tighter coupling may alternatively result in more rapid recycling of nutrients that sustain phytoplankton growth.

In terms of the picophytoplankton community, significant treatment effects were apparent for *Synechococcus* and the picoeukaryotes, which both showed increased growth rate in *pH* and *pH/T* in ME1 (see Appendix 6). Their small size may have provided an additional advantage in that they were better able to compete under the low nutrient conditions in ME1, and so able to grow more rapidly under higher temperature and lower pH. This suggests that the enhanced growth rate of small phytoplankton groups under nutrient-limited conditions could decouple growth and grazing in the future, although this effect may be limited as grazing on picoeukaryotes also increased in both *pH* and *pH/T* in ME1.

Copepod grazing estimates from gut content analysis

The pigment content (Chl-*a* and phaeopigments) of copepod guts was examined at time points during three mesocosm experiments (ME1, 2, and 3) to determine whether there was a treatment effect upon mesozooplankton grazing. There were clear differences in the magnitude of grazing between each experiment arising from the differing initial phytoplankton biomass and community composition.

Grazing trends in the two zooplankton size fractions, > 64 µm and > 80 µm, showed similar trends durng ME1 with an increase on Day 6 in *pH/T* (Figure 35A and B); however replicates were highly variable for both fractions on this day and there was no significant treatment effect overall (one-way ANOVA). This was also the case for ME2 and ME4, which despite higher grazing rates in the latter, also showed no significant treatment effect (Figure 35C and D).

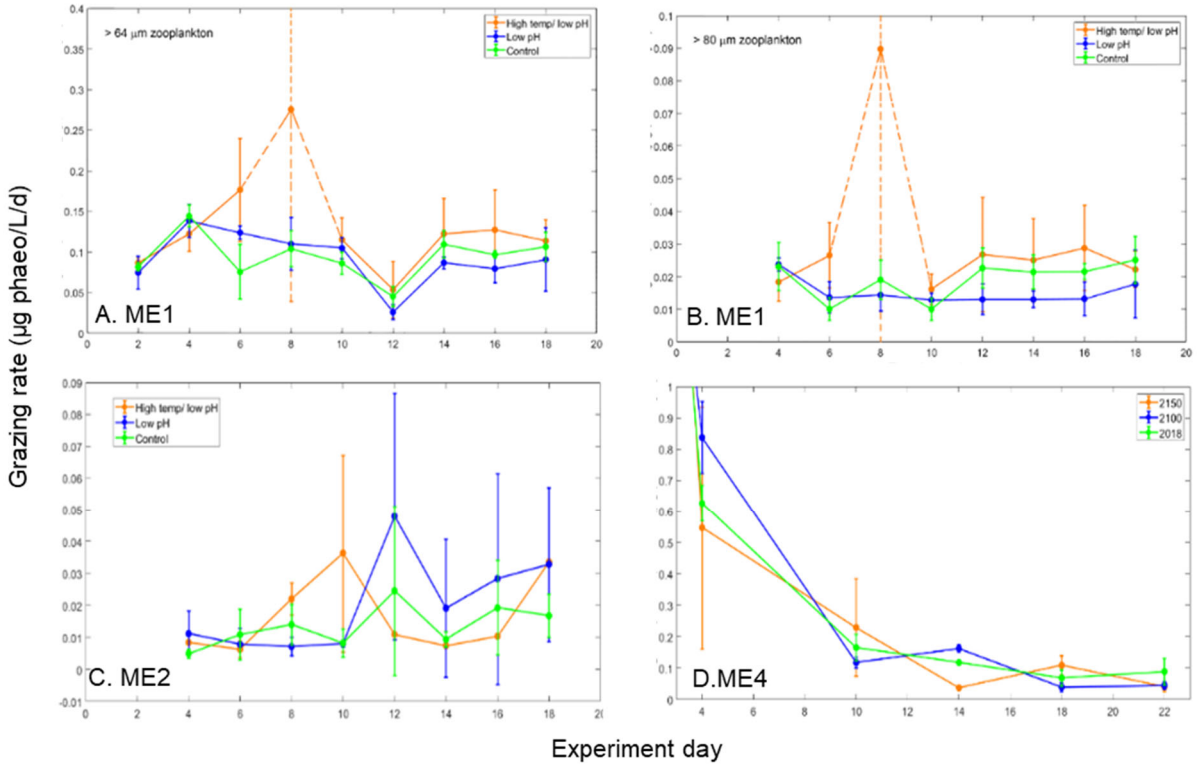

Figure 35: Zooplankton grazing rate based upon pigment gut content in A. > 64 µm zooplankton in ME1, B. > 80 µm zooplankton in ME1, C. >80µm zooplankton in ME2 and D. >80µm zooplankton in ME4.

Copepod grazing rate incubations

The effect of future conditions on copepod grazing rate was also examined in three short-term incubations during ME3 and ME4. In general the ME3 results show lower net grazing by copepods in *2100* compared with Control conditions (Figure 36), with copepods ingesting less carbon in *2100* than in the Control during Incubations 1 ($p = 0.07$) and 3 ($p < 0.001$). There was also no evidence of treatment differences in copepod grazing selectivity among different sizes and shapes of phytoplankton. The results also reveal unique treatment responses of the complex network of plankton interactions contained in the incubations. For example, there were differences in the balances between phytoplankton growth and grazing mortality between the Control and *2100*, which gave rise to instances of negative rates in Incubations 2 and 3 (Figure 36). These patterns could indicate that the pathway of energy transfer within the plankton community is sensitive to future environmental temperature and pH.

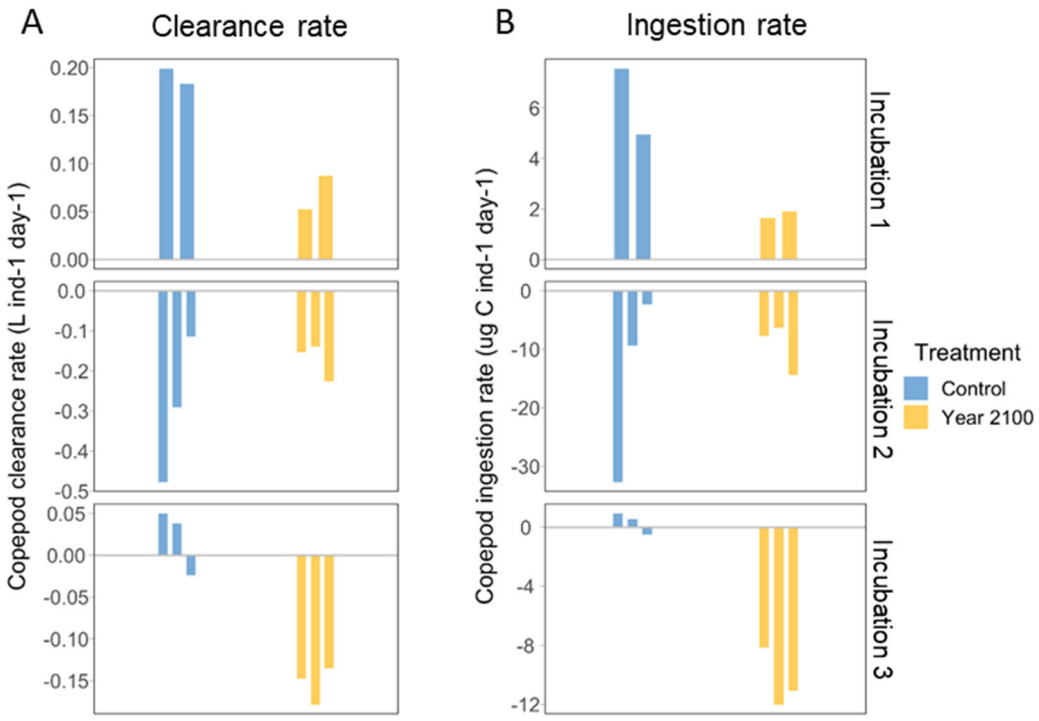

Figure 36: Copepod grazing during ME3 showing A. clearance rates (L/individual/day) and B. ingestion rates (µg C /individual/day) for the total prey field for Incubations 1, 2, and 3 (upper, middle, and lower plots, respectively). Each bar represents a single treatment replicate. Rates that fall below zero indicate a shift in the balance between phytoplankton growth and mortality within the incubation jar.

Similar grazing incubations were carried out in ME4 to investigate zooplankton grazing dynamics. The results indicated an effect of lower pH on copepod grazing with different responses in *pH* relative to the Control and *pH/T* (Figure 37). In Incubation 1, this difference was characterised by greater variability in clearance rates and ingestion rates in *pH*, whereas in Incubation 2, net clearance and ingestion rates were lower in *pH*. There was also evidence of a shift in the balance between phytoplankton growth and mortality in Incubation 2 that resulted in negative grazing rates in *pH* (Figure 37).

Grazing rates have been previously reported to decrease under elevated pCO_2 in *Calanus* spp. (Li & Gao 2012, de Klujver et al. 2013), although the effects of low pH on ingestion rates were non-linear and varied with region and food concentration for *Pseudocalanus acuspes* (Thor & Oliva 2015). The unique patterns in ME4 (Figure 37) suggest that energy transfer within the plankton community may be sensitive to future acidification, as shown in *pH*, but that this may be compensated for by warmer temperatures in *pH/T*. The results of ME3 differ, with a shift in grazing dynamics in *2100* (Figure 36) that is absent from the analogous *pH/T* treatment in ME4 (Figure 37). However, the plankton community composition and biomass differed in these experiments, with a mixed community including *Temora turbinata* and *Paracalanus* sp. in ME3, and only *T. turbinata* in ME4. Consequently, innate taxonomic differences in grazing behaviour may have contributed to the observed differences. Another contributing factor could be different treatment temperatures; although the plankton community was exposed to warmer than normal temperatures for the time of year (15.6 °C as opposed to 12.1 °C) in *pH/T* in ME4, *2100* temperatures were higher in ME3 (18 °C).

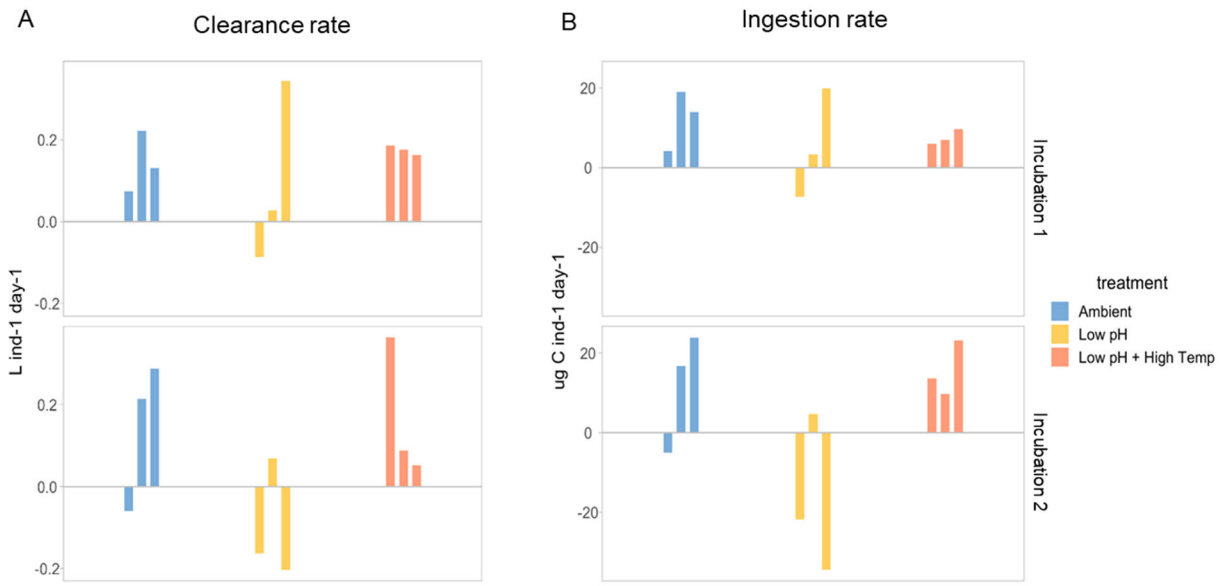

Figure 37: Copepod grazing showing A. clearance rates (L/individual/day) and B. ingestion rates (µg C/individual/day) for the total prey field for Incubations 1, 2, and 3 (upper, middle, and lower plots, respectively) in ME4. Each bar represents a single treatment replicate. Rates that fall below zero indicate a shift in the balance between phytoplankton growth and mortality within the incubation jar.

The discrepancy in results between the different approaches of whole-community grazing estimates, based upon gut pigments, and bottle incubations may reflect different inherent sources of variability. The whole-community grazing estimate provided an integrated measure of the pigment contained in an aliquot of all zooplankters, and so integrates the responses of the microplankton community and mesozooplankton community which may have varied. So, although differences were apparent in the whole community estimates, i.e.; high microzooplankton grazing in *2150* in ME3 (see Table 10), the variability among treatment bags precluded detection of significant trends. In addition, the bottle incubations typically used one species (*T. turbinata* or *Paracalanus* sp.) and, excepting Incubation 1 in ME3, the replicates were three bottles within only one mesocosm bag. This means that the replication only included that of the zooplankton investigated, whereas the plankton community was held constant. For example, Incubation 1 of ME3, which was replicated in all 9 treatment bags, showed significant difference, but only assessed the response of one species (*T. turbinata*) to differing phytoplankton communities under *pH/T*.

Comparison of the response of ME3 with that of ME4 suggests that *T. turbinata* is negatively affected by higher temperatures, and this result was robust to differences among microplankton communities in each treatment. However, *T. turbinata* was collected from Ākautangi/Evans Bay, and not the mesocosm bags, as zooplankton numbers were too low to ensure sufficient numbers for incubations in ME3. Thus, although these short-term grazing results were robust in indicating response of *T. turbinata* to future conditions, the response of the whole-community grazing estimate for ME3 did not include this copepod species.

Incubations carried out with whole communities (such as Incubation 3 ME3, Figure 36), provide a more comparable grazing estimate to the whole-community gut pigment estimates; however, the observed negative grazing rates are indicative of changing conditions in the incubations and cannot determine the actual grazing rates of the whole zooplankton community. In ME4, *T. turbinata* was collected from bags for the bottle incubations and the results of the whole community estimates and the bottle incubations are more consistent between the Control and *pH/T*, showing comparable grazing rates (negative rates excluded), and so no significant difference.

The observed reduction in grazing rate under future conditions in the short-term incubations appears to contradict the comparison of zooplankton and particulate amino acid δ^{15}N signatures which suggested

more rapid transfer and incorporation of the dietary isotopic signal into zooplankton under future conditions (Figure 23), indicative of accelerated grazing and metabolism at warmer temperatures. Again, these conflicting results may be due to different scales (temporal, spatial, species versus communities) associated with the different measurement approaches.

The inherent complexity of pelagic food webs, consisting of different components with differing sensitivities, may obscure prediction of the effects of future conditions on plankton. Nevertheless, understanding the range of responses and the net effect of the interaction of these sources of variability is necessary for projection of the effects of warming and lower pH on coastal marine ecosystems.

Performance of green-lipped mussel veliger larvae under future conditions

Green-lipped mussel veliger larvae were incubated in situ in selected bags during ME4. Survival and successful recovery of larvae was initially high with over 70% of stocked larvae alive following 2 days immersion in the mesocosms (4 days post-fertilisation, dpf; Figure 38A). Final survival rates did not differ significantly between the Control and treatments (Tukey HSD P = 0.08); however, after 11 days net survival in *pH/T* was significantly lower than in *pH* ($F_{2, 42}$ = 5.64, P = 0.0068; Table 11). The incidence of abnormality remained below 20% of the living population throughout the trial (Figure 38B), decreasing to less than 5% by the end of the trial, presumably due to selective mortality.

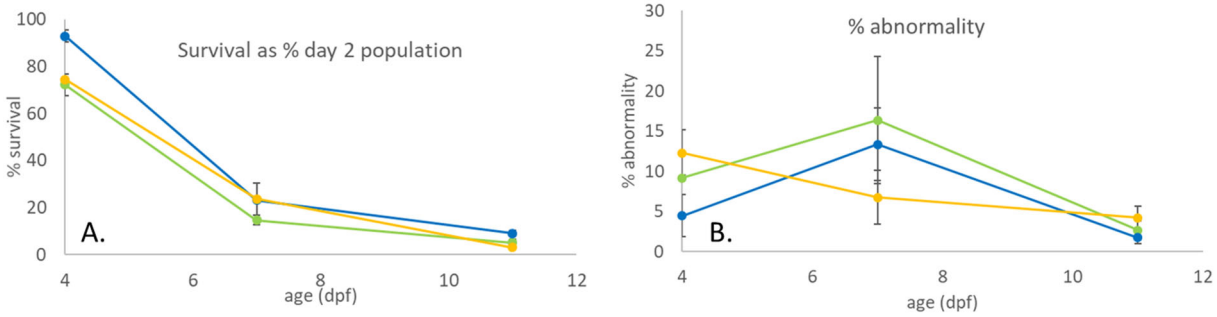

Figure 38: A. Larval survival expressed as a percentage of apparent stocking population 2 dpf (days post-fertilisation). (Mean ± standard error). B. Proportion of living larvae presenting with obvious malformations of the velum or shell. (Control – green, *pH* – blue, *pH/T* – orange)

Average shell length increased slowly in the Control and *pH*, and plateaued after 5 days (Figure 39A), whereas faster growth was apparent in *pH/T* up to one week post-fertilisation with a subsequent decrease, suggesting selective mortality of larger individuals in this treatment (Figure 39B). However, substantial size variability occurred between individuals and replicates, and consequently no significant size difference was detected between treatments ($F_{2, 21}$ = 0.89, P = 0.43) or sample times following immersion in the mesocosms ($F_{1, 21}$ = 0.08, P = 0.75).

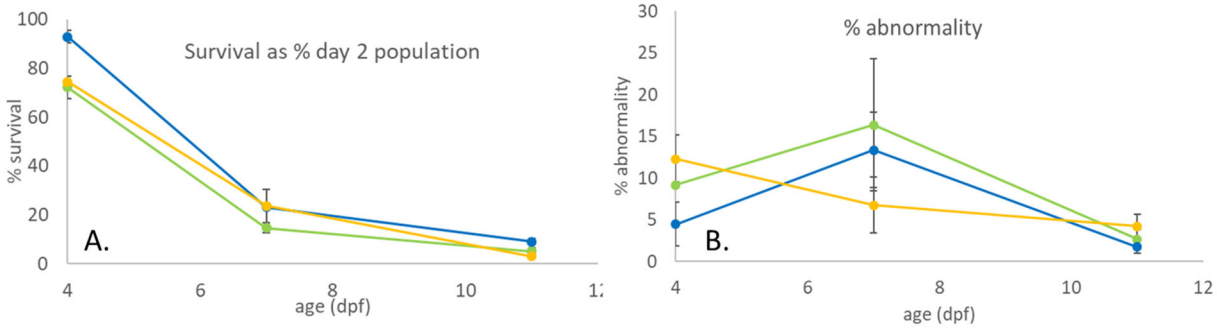

Figure 39: A. Mean shell length of larvae (± sem). Typical sample size ≥ 25. B. Maximum shell length of larvae, i.e.; largest measured individual in each cage.

The largest size attained within each treatment followed the same pattern as the mean size, except for the Control larvae towards the end of the assessment period, which attained a larger size than the treatments (Figure 39, Table 11). This suggests that some individuals continued to grow in the Control

cages, despite little change in the average size. Treatment significantly affected maximum final size ($F_{2, 37} = 3.83$, P = 0.03), whereas within-mesocosm replicate cages were not significantly different from each other ($F_{3, 37} = 0.02$, P = 0.99), and specific contrasts showed that larvae in *pH/T* attained a significantly smaller maximum size compared with Controls (Tukey HSD P = 0.036).

Table 11: Final larval assessment values (mean ± sem) at 11 days post-fertilisation (dpf), following 9 days in target mesocosm.

Treatment	Survival (% of cage population 2 dpf)	Abnormal larvae (% of living population)	Mean final shell size (µm)	Maximum final shell size (µm)
Control	5.0 ±1.5	2.7 ±1.2	98.5 ±1.4	107.9 ±2.8
pH	9.1 ±1.1	1.8 ±0.8	96.7 ±0.7	101.0 ±0.1
pH/T	3.0 ±1.1	4.2 ±1.5	96.9 ±1.2	100.0 ±0.8

This experiment provided a relatively unique test of the effect of future conditions on mussel larvae by trialling them under in situ conditions. Most studies to date have been laboratory batch culture studies where food availability is maintained at high or above ambient levels, and both competitors and predators are excluded. These challenges were reflected in the larval performance, but treatment effects were still apparent. In the Control, a small number of individuals appeared to develop separately from the main population by end of trial, as indicated by shell length; the reasons for this observation remain unclear but may reflect natural variation in populations. Both the mean and range in final shell size were significantly lower in the treatments suggesting future conditions may override this natural variability. Furthermore, because this occurred in both treatments, the reduced carbonate availability associated with low pH may have played a role in reduced shell formation. Despite this, percentage survival was highest in *pH*, significantly larger and three times greater than in *pH/T*. Although phytoplankton carbon was higher in *pH* relative to the Control in ME4 (see Table 8), total Chl-*a* was lower in *pH* relative to *pH/T* (see Figures 5 and 9) indicating that food supply may be lower. This may reflect that although elevated temperature in *pH/T* accelerated mussel growth (see Figure 39), this was not sustainable and consequently mortality of larger individuals was elevated (Ragg et al. 2010).

4. SUMMARY AND CONCLUSIONS

This report summarises the results of four mesocosm experiments carried out over three years to establish the response of coastal plankton communities to projected warming and acidification, with a focus on how changes in phytoplankton biomass, community and cell composition may affect grazers in the higher food web (see summary in Table 12). Selected significant responses observed in the mesocosm experiments were subsequently applied in a Dynamic Energy Budget Model to predict the potential indirect effects of warming and low pH on green-lipped mussels (see Table 9).

- Total chlorophyll-*a* was not affected by lower pH (-0.3 to -0.5) in all four experiments, confirming that projected changes in pH alone will not alter future phytoplankton biomass in coastal waters, and indicating resilience of coastal phytoplankton to pH variation.
- There was a significant increase in chlorophyll-*a* biomass and an accompanying shift in the size spectrum of the phytoplankton community in three of the four experiments when low pH was combined with elevated temperature (+2.7 to +4.5 °C). These results confirm that future changes in temperature will be a more significant driver of future coastal plankton biomass than pH and highlight the shortcomings of using results from pH only experiments. The observed 20–64% increase in total chlorophyll- *a* under future conditions suggests increased food availability at the base of the coastal food web, and so potential for increased carbon and energy flow within coastal food webs. However, an increase in biomass may also enhance eutrophication in regions that are subject to high nutrient loading.
- Projected temperature and pH for the year 2150 (-0.5 pH, +4.5 °C) resulted in the highest number of significant responses, highlighting that change beyond the end of the century should be considered.
- The response of phytoplankton community and speciation to future lower pH/higher temperature was influenced by nutrient availability. Overall, there was a decrease in phytoplankton size spectrum under future conditions when nutrients were depleted, whereas there was an increase when nutrient supply was maintained. Consequently, future changes in coastal nutrients, and management of terrestrial nutrient input, will influence plankton community composition response to warming and acidification.
- The change in phytoplankton size spectrum under future conditions was partly driven by an increase in pennate diatoms in the > 5-µm size range, and particularly the species *Cylindrotheca closterium*, which dominated diatom biomass at the end of most experiments. Diatom biomass increased in both pH only and combined low pH/elevated temperature treatments in two experiments, indicating that increased CO_2 availability may benefit this group. A shift to a phytoplankton community dominated by pennate diatoms may have implications for coastal food webs with a potential shift in consumers reflecting diet size-specificity.
- Particulate composition was altered by future conditions with lower particulate Carbon: Nitrogen ratios in two of the four experiments. This suggests future decreases in food quality with potential flow-on effects for higher trophic level consumers; however, the depletion of nitrogen relative to carbon was not reflected in particulate amino acid concentrations or the associated amino acid $\delta^{15}N$ signature.
- Particulate monounsaturated, saturated, and total fatty acids were relatively insensitive to a reduction in pH alone but were more sensitive to temperature, with significant increases under low pH and warming projected for 2150. This response was replicated in incubations of the diatom species *Cylindrotheca closterium* confirming that the response of the dominant phytoplankton may determine lower food web food quality under future conditions.
- Proportional concentrations of particulate polyunsaturated fatty acids (PUFA) and the essential n-3 PUFA group decreased under conditions projected for 2100 in one experiment. Although this may have implications for the food web, the variability in response to future conditions among experiments precludes definitive conclusions. Further studies are required to determine whether the sensitivity of essential fatty acids to future conditions is influenced by phytoplankton community composition and other environmental factors.
- The proportional fatty acid composition of zooplankton reflected some of the responses in particulate composition, with increases in saturated fatty acids but no changes in zooplankton

PUFA under future conditions. A linear relationship between zooplankton and particulate proportional fatty acid content confirmed that zooplankton composition reflects diet.

- The response of microzooplankton grazing was variable with a significant increase, and associated decrease in phytoplankton growth, apparent only under conditions projected for 2150 in one experiment. This response suggests an increase in coupling between phytoplankton growth and zooplankton grazing under more extreme future conditions (-0.5 pH, +4.5 °C).
- Despite the observed enhancement of phytoplankton biomass under future conditions, there was no corresponding effect on zooplankton community composition and abundance. This may be due to the limited experimental duration of 18–22 days, which is shorter than the generation time (one month) of copepods.
- Analysis of zooplankton gut pigment content showed high variability and no significant effect of future conditions after 18–22 days in three experiments. Conversely, short-term grazing incubations using a single copepod species identified lower grazing under future warming and lower pH, and under low pH in a second experiment. As there was no corresponding decrease in chlorophyll-*a* biomass, the lower grazing rate suggests a potential physiological or behavioural response to future conditions independent of diet. These results contrast with a comparison of zooplankton and particulate amino acid δ^{15}N signatures in one experiment, which indicated more rapid transfer of the isotopic signal from phytoplankton to zooplankton under future conditions, suggestive of accelerated grazing and metabolism at warmer temperatures.
- As the phytoplankton responses to future conditions were not reflected in the zooplankton overall, the lower food web in coastal waters appears relatively robust to projected future changes.
- The significant responses of chlorophyll-*a* and phytoplankton carbon (> 5 μm) in the mesocosm experiments were applied in a Dynamic Energy Budget model to simulate future change in green-lipped mussels (*Perna canaliculus)*. Warmer temperature influences mussels directly, via effects on mussel physiological processes, and indirectly via increased food availability under future conditions. The model outputs predicted future increases in food uptake rate, energy allocation, shell length, and flesh weight, with results varying with input parameter and temperature; however, these results are based solely upon the significant responses observed in selected experiments and do not consider the non-significant results. In addition, these results may not be representative for coastal waters with differing nutrient regimes and plankton communities.
- Although there were no significant differences in survival and abnormality in green-lipped mussel veliger larvae maintained under current and future conditions, survival at 11 days was lower in the combined low pH/warming treatment relative to the low pH only treatment, indicating a negative effect of temperature. In addition, the maximum final shell size was smaller in both the low pH only and low pH/elevated temperature treatments, supporting previous observations that future lower carbonate availability may limit larval shell growth.

Table 12: **Summary of significant treatment effects in Phase 3 means in the mesocosm experiments. The arrows indicate the direction of the response in the treatment relative to the Control, with significant increases ($p < 0.1$), shown by a green arrow and decreases a red arrow. White arrows show an indicative but non-significant difference ($p < 0.15$) between treatment and Control, and a blank cell no significant difference. *n/a* indicates where not assessed, and ^ where incubations of the dominant phytoplankton (*C. closterium*) confirmed significant responses in ME3. Abbreviations: *pH*: lower pH relative to ambient value; *pH/T*: lower pH and warmer temperature relative to ambient value; *2100:* lower pH and warmer temperature based on projections for Year 2100; *2150:* lower pH and warmer temperature based upon projections for Year 2150; Chl-*a:* Chlorophyll-*a*; SFA: saturated fatty acids; MUFA: monounsaturated fatty acids; PUFA: polyunsaturated fatty acids; n3PUFA: PUFA containing a double bond three atoms from the terminal methyl group; Conc.: concentration (of total fatty acids): Prop.: proportion (of total fatty acids).**

Experiment	ME1		ME2	ME3		ME4	
Parameter/Treatment	*pH*	*pH/T*	*pH*	*2100*	*2150*	*pH*	*pH/T*
Total Chl-*a*		⇧			↑		↑
0.2–2 µm Chl-*a*		↑		↓	↓	↑	
5–20 µm Chl-*a*					↑		
>20 µm Chl-*a*	↓	↓			↑	↑	↑
Diatom biomass				↑	↑	↑	↑
Dinoflagellate biomass	↓	↓			↑		
Small flagellates					↓		↓
Total phytoplankton Carbon (< 2 µm)				↑		↑	
Particulate Carbon			↑				
Particulate Nitrogen					↓		
Particulate Carbon: Nitrogen			⇩	↓	↓		
Particulate SFA (Conc.)	*n/a*	*n/a*			⇧^	⇩	
Particulate MUFA (Conc.)	*n/a*	*n/a*			↑^	⇩	
Particulate PUFA & n3PUFA (Prop)	*n/a*	*n/a*		↓			
Zooplankton PUFA (Prop.)	*n/a*	*n/a*	*n/a*				↓
Microzooplankton grazing rate					↑	*n/a*	*n/a*
Microzooplankton net growth rate					↓	*n/a*	*n/a*
Copepod grazing rate	*n/a*	*n/a*	*n/a*	↓	*n/a*	↓	

5. MANAGEMENT IMPLICATIONS AND NEXT STEPS

- This study considered the sensitivity of coastal planktonic communities only under certain conditions, e.g.; one location in two seasons and using two future climate scenarios. Although it is unrealistic to test all regions in all seasons, the observed results need to be confirmed in other New Zealand coastal areas to ensure they are representative. Further experimental studies in warmer coastal waters in the northern North Island, where productivity is already limited by nutrient availability, would be valuable.
- Although some parameters showed a significant response to changes in projected temperature and pH by the Year 2100, more significant responses were apparent in projected conditions for the Year 2150 (see Table 12). Consequently, further research is required to determine when tipping points in coastal planktonic communities and food webs may occur.
- The results highlight the shortcomings of relying on the outcomes of experiments that only assess changes in pH for future projections, as in many cases responses differed when combined with elevated temperature. Although it is important to disentangle the effects of pH and temperature, the results highlight the need to consider these stressors together, as well as other factors such as nutrient availability and turbidity. Although challenging experimentally and also from the perspective of temporal and regional variability, coastal stressors such as deoxygenation, nutrients, particles, and pollutants need to be incorporated into experimental assessments and models. New experimental approaches (Boyd et al. 2019) and application of regional stressor clusters should be used to assess the net impact of multiple stressors to ensure robust projections of the future status on coastal plankton.
- The results extend current understanding of the impacts of ocean acidification in New Zealand waters (Law et al. 2018a) and show that significant changes may occur in the biomass and species composition of primary producers in coastal pelagic waters. However, the impact of future changes on consumers in the overlying food web is obscured by the complexity and dynamics of the coastal plankton community. As zooplankton represent important intermediaries in the transfer of energy from primary producers to the higher food web, the observed reductions in zooplankton grazing and essential fatty acid content in response to warming and lower pH warrants further investigation in more focused experiments.
- Incorporation of the mesocosm experiment results into the Dynamic Energy Budget Model highlight the importance of considering the indirect impacts of climate change on food availability and quality, in addition to the direct effects of changes in temperature and pH, when assessing the future status of New Zealand's green-lipped mussel. This should be considered in climate studies of ecologically and economically important species and ecosystems by coordination and integration of experimental and model studies.

6. ACKNOWLEDGEMENTS

This work was completed under Fisheries New Zealand project ZBD2016-07 and funded by Fisheries New Zealand, and also MBIE via the CARIM (Coastal Acidification: Rate, Impacts and Management) project. We are particularly grateful to NIWA for supporting and funding the mesocosm facility, and to NIWA staff and scientists who assisted with the experiments including Jane Halliday, Andrew Marriner, Rory Graham, Phil Fisher, Karen Thompson, Mike Crump, Margaret McMonagle, Nick Eaton, Stacy Deppeler, Vonda Cummings, Kim Currie, Aaron Dalbeth, and Warwick Lyons. We also thank participating international scientists, including Karine Sellegri and Qingshan Lao, and all the students who assisted with this study, including Alexia Saint-Macary, Fenella Deans, Ro Allen, Baptiste Abboud, Johanna Parisi, Kolby Reddy, Paige Achiele, Sienna Kelly, Jonathan Velarde, Erin Houlihan, Sienna Kelly, Jennie Barr-Skeoch, and Zihan Fang. Finally, we thank Scott Nodder, Niall Broekhuizen, and Judy Hewitt for their review comments, and Jeanne Wissing and Suze Baird for editing.

7. REFERENCES

Alvarez-Fernandez, S.; Bach, L.T.; Taucher, J.; Riebesell, U.; Sommer, U.; Aberle, N.; Brussaard, C.P.D.; Boersma, M. (2018). Plankton responses to ocean acidification: The role of nutrient limitation. *Progress in Oceanography 165*: 11–18.

Armbrust, E.V. (2009). The life of diatoms in the world's oceans. *Nature 459(7244)*: 185–192.

Armengol, L.; Franchy, G.; Ojeda A.; Santana-del Pino, A.; Hernandez-Leon S. (2017). Effects of copepods on natural microplankton communities: do they exert top-down control? *Marine Biology 164(6)*: 136.

Bach, L.T.; Taucher, J. (2019). CO2 effects on diatoms: a synthesis of more than a decade of ocean acidification experiments with natural communities. *Ocean Science 15(4)*: 1159–1175.

Ballantyne, A.P.; Brett, M.T.: Schindler, D.E. (2003). The importance of dietary phosphorus and highly unsaturated fatty acids for sockeye (*Oncorhynchus nerka*) growth in Lake Washington a bioenergetics approach. *Canadian Journal of Fisheries and Aquatic Sciences 60(1)*:12–22.

Barton, A.; Hales, B.; Waldbusser, G.G.; Langdon, C.; Feely, R.A. (2012). The Pacific oyster, *Crassostrea gigas*, shows negative correlation to naturally elevated carbon dioxide levels: Implications for near-term ocean acidification effects. *Limnology and oceanography 57(3)*: 698–710.

Batista, F.C.; Ravelo, A.C.; Crusius, J.; Casso, M.A.; McCarthy, M.D. 2014. Compound specific amino acid δ15N in marine sediments: A new approach for studies of the marine nitrogen cycle. *Geochimica et Cosmochimica Acta 142*: 553–569.

Behrenfeld, M.J.; Boss, E.S. (2014). Resurrecting the ecological underpinnings of ocean plankton blooms. *Annual Review of Marine Science 6*: 167–194.

Bellerby, R.G.J.; Schulz, K.; Riebesell, U.; Neill, C.; Nondal, G.; Johannessen, T. Brown; K.R. (2008). Marine ecosystem community carbon and nutrient uptake stoichiometry under varying ocean acidification during the PeECE III experiment. *Biogeosciences (BG) 5(6)*:1517–1527.

Bermúdez, J.R.; Riebesell, U.; Larsen, A.; Winder, M. 2016. Ocean acidification reduces transfer of essential biomolecules in a natural plankton community. *Scientific Reports 6*: 27749.

Bermudez, J.R.; Winder, M.; Stuhr, A.; Almén, A.K.; Engström-Öst, J.; Riebesell, U. (2016). Effect of ocean acidification on the structure and fatty acid composition of a natural plankton community in the Baltic Sea. *Biogeosciences (BG) 13(24)*: 6625–6635.

Boyd, P.W.; Collins, S.; Dupont, S.; Fabricius, K.; Gattuso, J.-P.; Havenhand, J.; Hutchins, D.A.; McGraw, C.M.; Riebesell, U.; Vichi, M.; Biswas, H.; Ciotti, A.; Dillingham, P.; Gao, K.; Gehlen, M.; Hurd, C.L.; Kurihawa, H.; Navarro, J.; Nilsson, G.E.; Passow, U.; Portner, H.-O. (2019). SCOR WG149 Handbook to support the SCOR Best Practice Guide for 'Multiple Drivers' Marine Research. http://dx.doi.org/10.25959/5c92fdf0d3c7a

Brett, M.; Muller-Navarra, D. (1997). The role of highly unsaturated fatty acids in aquatic food web processes. *Freshwater Biology 38(3)*: 483–499.

Brown, J.H.; Gillooly, J.F.; Allen, A.P.; Savage, V.M.; West, G.B. (2004). Toward a metabolic theory of ecology. *Ecology 85*: 1771−1789.

Brown, N.E.M.; Bernhardt, J.R.; Anderson, K.M.; Harley, C.D.G. (2018). Increased food supply mitigates ocean acidification effects on calcification but exacerbates effects on growth. *Scientific Reports 8*: 1–9.

Calbet, A.; Landry, M. R. 2004. Phytoplankton growth, microzooplankton grazing, and carbon cycling in marine systems. *Limnology and Oceanography 49(1)*: 51–57.

Caron, D.A.; Hutchins, D.A. (2012). The effects of changing climate on microzooplankton grazing and community structure: drivers, predictions and knowledge gaps. *Journal of Plankton Research*, *35(2)*: 235–252.

Chen, B.; Landry, M.R.; Huang, B.. Liu, H. (2012). Does warming enhance the effect of microzooplankton grazing on marine phytoplankton in the ocean? *Limnology and Oceanography 57(2)*: 519–526.

Chikaraishi, Y.; Ogawa, N.O.; Kashiyama, Y.; Takano, Y.; Suga, H.; Tomitani, A.; Miyashita, H.; Kitazato, H.; Ohkouchi, N. (2009). Determination of aquatic food-web structure based on compound-specific nitrogen isotopic composition of amino acids. *Limnology and Oceanography: methods 7(11)*: 740–750.

Chivers, W.J.; Edwards, M.; Hays, G.C. (2020). Phenological shuffling of major marine phytoplankton groups over the last six decades. *Diversity and Distributions 26*(5): 536–548.

Clements, J.C.; Hicks, C.; Tremblay, R.; Comeau, L.A. (2018). Elevated seawater temperature, not pCO_2, negatively affects post-spawning adult mussels (*Mytilus edulis*) under food limitation. *Conservation Physiology 6(1)*: cox078.

Cripps, G.; Lindeque, P.; Flynn, K.J. 2014. Have we been underestimating the effects of ocean acidification in zooplankton? *Global Change Biology 20(11)*: 3377–3385.

Dam H.G.; Peterson W.T. 1988. The effect of temperature on the gut clearance rate constant of planktonic copepods. *Journal of Experimental Marine Biology and Ecology 123*: 1–14.

de Kluijver, A.; Soetaert, K.; Czerny, J.; Schulz, K.G.; Boxhammer, T.; Riebesell, U.; Middelburg, J. J. (2013). A 13C labelling study on carbon fluxes in Arctic plankton communities under elevated CO2 levels. *Biogeosciences 10 (3)*: 1425–1440.

Eglite, E.; Wodarg, D.; Dutz, J.; Wasmund, N.; Nausch, G.; Liskow, I.; Schulz-Bull, D.; Loick-Wilde, N. (2018). Strategies of amino acid supply in mesozooplankton during cyanobacteria blooms: a stable nitrogen isotope approach. *Ecosphere* 9: e02135.

Eppley, R.W.; Reid, F.M.H.; Strickland, J.D.H. (1970). The ecology of the plankton off La Jolla, California, in the period April through September 1967. *Bulletin of the Scripps Instititon of Oceanography 17*: 33–42.

Ericson, J. (2010). Effects of ocean acidification on fertilisation and early development in polar and temperate marine invertebrates [MSc thesis]. Dunedin: University of Otago. 117 p.

Feng, Y.; Hare, C.E.; Rose, J.M.; Handy, S.M.; DiTullio, G.R.; Lee, P.A.; Smith Jr, W.O.; Peloquin, J.; Tozzi, S.; Sun, J.; Zhang, Y. (2010). Interactive effects of iron, irradiance and CO_2 on Ross Sea phytoplankton. *Deep Sea Research Part I: Oceanographic Research Papers 57(3)*: 368–383.

Fraser, A.J.; Sargent, J.R.; Gamble, J.C.; Seaton, D.D. (1989). Formation and transfer of fatty acids in an enclosed marine food chain comprising phytoplankton, zooplankton and herring (*Clupea harengus* L.) larvae. *Marine Chemistry 27*: 1–18.

Frost, B. (1972). Effects of size and concentration of food particles on the feeding behavior of the marine planktonic copepod *Calanus pacificus*. *Limnology and Oceanography 17(6)*: 805–815.

Fuschino, J.R.; Guschina, I.A.; Dobson, G.; Yan, N.D.; Harwood, J.L.; Arts, M.T. (2011). Rising water temperatures alter lipid dynamics and reduce n-3 essential FA concentrations in Scenedesmus obliquus. *Journal of Phycology 47*: 763–774.

Galloway, A.W.; Winder, M. (2015). Partitioning the relative importance of phylogeny and environmental conditions on phytoplankton fatty acids. *PloS ONE 10(6)*: e0130053.

Garzke, J.; Hansen, T.; Ismar, S.M.; Sommer, U. (2016). Combined effects of ocean warming and acidification on copepod abundance, body size and fatty acid content. *PLoS ONE 11(5)*: e0155952.

Gazeau, F.; Sallon, A.; Pitta, P.; Tsiola, A.; Maugendre, L.; Giani, M.; Celussi, M.; Pedrotti, M.L.; Marro, S.; Guieu, C. (2017). Limited impact of ocean acidification on phytoplankton community structure and carbon export in an oligotrophic environment: Results from two short-term mesocosm studies in the Mediterranean Sea. *Estuarine, Coastal and Shelf Science 186*: 72–88.

Germain, L.R.; Koch, P.L.; Harvey, J.; McCarthy, M.D. (2013). Nitrogen isotope fractionation in amino acids from harbor seals: implications for compound-specific trophic position calculations. *Marine Ecology Progress Series 482*: 265–277.

Gu, H.; Shang, Y.; Dupont, S.; Wang, T.; Wei, S.; Wang, X.; Chen, J.; Huang, W.; Hu, M.; Wang, Y. (2019). Hypoxia aggravates the effects of ocean acidification on the physiological energetics of the blue mussel *Mytilus edulis*. *Marine Pollution Bulletin 149*: 110538.

Gutiérrez-Rodríguez, A.; Selph, K.E.; Landry, M.R. (2015). Phytoplankton growth and microzooplankton grazing dynamics across vertical environmental gradients determined by transplant *in situ* dilution experiments. *Journal of Plankton Research 38(2)*: 271–289.

Han, C.H.; Uye, S.I. (2010). Combined effects of food supply and temperature on asexual reproduction and somatic growth of polyps of the common jellyfish *Aurelia aurita* sl. *Plankton and Benthos Research 5(3)*: 98–105.

Hannides, C.C.S.; Popp, B.N.; Choy, C.A.; Drazen, J.C. (2013). Midwater zooplankton and suspended particle dynamics in the North Pacific Subtropical Gyre: A stable isotope perspective. *Limnology and Oceanography 58*: 1931–1946.

Hare, C.E.; Leblanc, K.; DiTullio, G.R.; Kudela, R.M.; Zhang, Y.; Lee, P.A.; Riseman, S.; Hutchins, D.A. (2007). Consequences of increased temperature and CO2 for phytoplankton community structure in the Bering Sea. *Marine Ecology Progress Series 352*: 9–16.

Hare, E.P.; Fogel, M.L.; Stafford Jr, T.W.; Mitchell, A.D.; Hoering, T.C. (1991). The isotopic composition of carbon and nitrogen in individual amino acids isolated from modern and fossil proteins. *Journal of Archaeological Science 18*: 277–292.

Hein, M.; Pedersen, M.F.; Sand-Jensen, K. (1995). Size dependent nitrogen uptake in micro- and macroalgae. *Marine Ecology Progress Series 118*: 247–253.

Hildebrandt, N.; Sartoris, F.J.; Schulz, K.G.; Riebesell, U.; Niehoff, B. (2015). Ocean acidification does not alter grazing in the calanoid copepods Calanus finmarchicus and Calanus glacialis. *ICES Journal of Marine Science 73(3)*: 927–936.

Hixson, S.M.; Arts, M.T. (2016). Climate warming is predicted to reduce omega-3, long-chain, polyunsaturated fatty acid production in phytoplankton. *Global Change Biology 22(8)*: 2744–2755.

Hofmann, G.E.; Smith, J.E.; Johnson, K.S.; Send, U.; Levin, L.A.; Micheli, F.; Paytan, A.; Price, N.N.; Peterson, B.; Takeshita, Y.; Matson, P.G.; et al. (2011). High-frequency dynamics of ocean pH: a multi-ecosystem comparison. *PloS ONE 6(12)*: e28983.

Horn, H.G.; Boersma, M.; Garzke, J.; Löder, M.G.; Sommer, U.; Aberle, N. (2015). Effects of high CO_2 and warming on a Baltic Sea microzooplankton community. *ICES Journal of Marine Science 73(3)*: 772–782.

Irigoien, X.; Flynn, K.J.; Harris, R.P. (2005). Phytoplankton blooms: a "loophole" in microzooplankton grazing impact? *Journal of Plankton Research 27(4)*: 313–321.

Jónasdóttir, S.H. (2019). Fatty Acid Profiles and Production in Marine Phytoplankton. *Marine Drugs 17*: 151. doi:10.3390/md17030151

King, A.L.; Jenkins, B.D.; Wallace, J.R.; Liu, Y.; Wikfors, G.H.; Milke, L.M.; Meseck, S.L. (2015). Effects of CO_2 on growth rate, C: N: P, and fatty acid composition of seven marine phytoplankton species. *Marine Ecology Progress Series 537*: 59–69.

Kingston, M.B. (2009). Growth and motility of the diatom *Cylindrotheca closterium*: implications for commercial applications. *Journal of the North Carolina Academy of Science 125(4)*: 138–42.

Kroeker, K.J.; Kordas, R.L.; Crim, R.; Hendriks, I.E.; Ramajo, L.; Singh, G.S.; Duarte, C.M.; Gattuso, J.P. (2013). Impacts of ocean acidification on marine organisms: quantifying sensitivities and interaction with warming. *Global ChangeBbiology 19(6)*: 1884–1896.

Landry, M.; Haas, L.; Fagerness, V. (1984). Dynamics of microbial plankton communities: experiments in Kaneohe Bay, Hawaii. *Marine Ecology Progress Series 16*: 127–133.

Landry, M.; Hassett, R. (1982). Estimating the grazing impact of marine microzooplankton. *Marine Biology 67*:2 83–288

Law, C.S.; Bell, J.J.; Bostock, H.C.; Cornwall, C.E.; Cummings, V.; Currie, K.; Davy, S.K.; Gammon, M.; Hepburn, C.D.; Hurd, C.L.; Lamare, M.; Mikaloff-Fletcher, S.E.; Nelson, W.A.; Parsons, D.M.; Ragg, N.L.C.; Sewell, M.A.; Smith, A.M.; Tracey, D.M. (2018a). Ocean Acidification in New Zealand waters. *New Zealand Journal of Marine & Freshwater Research 52(2)*: 155–195.

Law, C.S.; Rickard, G.J.; Mikaloff-Fletcher, S.E.; Pinkerton, M.H.; Gorman, R.; Behrens, E.; Chiswell, S.M.; Bostock, H.C.; Anderson, O.; Currie, K. (2018b). Climate Change projections for the surface ocean around New Zealand. *New Zealand Journal Marine and Freshwater Research 52(3)*: 309–335.

Leu, E.; Daase, M.; Schulz, K.G.; Stuhr, A.; Riebesell, U. (2013). Effect of ocean acidification on the fatty acid composition of a natural plankton community. *Biogeosciences 10(2)*: 1143–1153.

Lewandowska, A.; Sommer U. (2010). Climate change and the spring bloom: a mesocosm study on the influence of light and temperature on phytoplankton and mesozooplankton. *Marine Ecology Progress Series 405*: 101−111.

Li, W.; Gao, K. (2012). A marine secondary producer respires and feeds more in a high CO_2 ocean. *Marine Pollution Bulletin 64(4)*: 699–703.

Li, W.; Gao, K.; Beardall, J. (2012). Interactive effects of ocean acidification and nitrogen-limitation on the diatom *Phaeodactylum tricornutum*. *PloS ONE 7(12)*: e51590. doi:10.1371/journal.pone.0051590

Litchman E.; Klausmeier C.A.; Schofield O.M.; Falkowski P.G. (2007). The role of functional traits and trade-offs in structuring phytoplankton communities: scaling from cellular to ecosystem level. *Ecology Letters 10*: 1170–1181.

Loick-Wilde, N.; Fernández-Urruzola, I.; Eglite, E.; Liskow, I.; Nausch, M.; Schulz-Bull, D.; Wodarg, D.; Wasmund, N.; Mohrholz, V. (2019). Stratification, nitrogen fixation, and cyanobacterial bloom stage regulate the planktonic food web structure. *Global Change Biology 25(3)*: 794–810.

McClelland, J.W.; Montoya, J.P. (2002). Trophic relationships and the nitrogen isotopic composition of amino acids in plankton. *Ecology 83(8)*: 2173–2180.

Mackenzie, A.L.; Kaspar, H.F.; Gillespie, P.A. (1986). Some observations on phytoplankton species composition, biomass, and productivity in Kenepuru Sound, New Zealand, 1982–83. *New Zealand Journal of Marine and Freshwater Research 20*: 397–405.

McLeod, D.J.; Hallegraeff, G.M.; Hosie, G.W.; Richardson, A.J. (2012). Climate-driven range expansion of the red-tide dinoflagellate *Noctiluca scintillans* into the Southern Ocean. *Journal of Plankton Research 34(4)*: 332–337.

McMahon, K.W.; McCarthy, M.D. (2016). Embracing variability in amino acid δ^{15}N fractionation: mechanisms, implications, and applications for trophic ecology. *Ecosphere 7*: 1–26.

McMahon, K.W.; Thorrold, S.R.; Elsdon, T.S.; McCarthy, M.D. (2015). Trophic discrimination of nitrogen stable isotopes in amino acids varies with diet quality in a marine fish. *Limnology and Oceanography 60*(3): 1076–1087.

Menden-Deuer, S.; Lessard, E.J. 2000. Carbon to volume relationships for dinoflagellates, diatoms, and other protist plankton. *Limnology and Oceanography 45(3)*: 569–579.

Meunier, C.L.; Algueró-Muñiz, M.; Horn, H.G.; Lange, J.A.; Boersma, M. (2017). Direct and indirect effects of near-future pCO_2 levels on zooplankton dynamics. *Marine and Freshwater Research 68(2)*: 373–380.

Meyer, J.; Riebesell, U. (2015). Reviews and Syntheses: Responses of coccolithophores to ocean acidification: a meta-analysis. *Biogeosciences 12(6)*: 1671–1682.

Miller, M.R.; Pearce, L.; Bettjem, B.I. (2014A). Detailed Distribution of Lipids in Greenshell™ mussel (*Perna canaliculus*). *Nutrients 6*: 1454–1474.

Miller, M.R.;Tian, H. (2018). Changes in proximate composition, lipid class and fatty acid profile in Greenshell™ mussels (*Perna canaliculus*) over an annual cycle. *Aquaculture Research 49(3)*: 1153–1165.

Ministry for the Environment & Stats NZ (2019). *New Zealand's Environmental Reporting Series: Our Marine Environment 2019*. Available from www.mfe.govt.nz and www.stats.govt.nz.

Montagnes, D.J.; Franklin, M. (2001). Effect of temperature on diatom volume, growth rate, and carbon and nitrogen content: reconsidering some paradigms. *Limnology and Oceanography 46(8)*: 2008–2018.

Nejstgaard, J.; Naustvoll, L.J.; Sazhin A. (2001). Correcting for the underestimation of microzooplankton grazing in bottle incubation experiments with mesozooplankton. *Marine Ecology Progress Series 221*: 59–75.

O'Connell, T.C. 2017. 'Trophic' and 'source' amino acids in trophic estimation: a likely metabolic explanation. *Oecologia 184(2)*: 317–326.

O'Connor, M.I.; Piehler, M.F.; Leech, D.M.; Anton, A.; Bruno, J.F. (2009). Warming and resource availability shift food web structure and metabolism. *PLoS Biology* 7: e1000178

Ohkouchi, N.; Chikaraishi, Y.; Close, H.G.; Fry, B.; Larsen, T.; Madigan, D.J.; McCarthy, M.D.; McMahon, K.W.; Nagata, T.; Naito, Y.I.; Ogawa, N.O.; Popp, B.N.; Steffan, S.; Takano, Y.; Tayasu, I.; Wyatt, A.S.J.; Yamaguchi, Y.T.; Yokoyama, Y. (2017). Advances in the application of amino acid nitrogen isotopic analysis in ecological and biogeochemical studies. *Organic Geochemistry 113*: 150–174.

Pan, T.C.F.; Applebaum, S.L.; Manahan, D.T. (2015). Experimental ocean acidification alters the allocation of metabolic energy. *Proceedings of the National Academy of Sciences 112*: 4696–4701.

Paul, C.; Matthiessen, B.; Sommer, U. (2015). Warming, but not enhanced CO_2 concentration, quantitatively and qualitatively affects phytoplankton biomass. *Marine Ecology Progress Series*, *528*: 39–51.

Peter, K.H.; Sommer, U. (2013). Phytoplankton Cell Size Reduction in Response to Warming Mediated by Nutrient Limitation. *PLoS ONE 8(9)*: e71528.

Pilditch, C.A.; Grant, J. (1999). Effect of temperature fluctuations and food supply on the growth and metabolism of juvenile sea scallops (*Placopecten magellanicus*). *Marine Biology 134*: 235–248.

Pinkerton, M.H.; Sutton, P.; Wood, S. (2018). Satellite indicators of phytoplankton and ocean surface temperature for New Zealand. (Unpublished report prepared for the New Zealand Ministry for the Environment, December 2018, NIWA Client Report 2018180WN.) 87 p.

Popp, B.N.; Graham, B.S.; Olson, R.J.; Hannides, C.C.S.; Lott, M.J.; Lopez-Ibarra, G.A.; Galvan-Magana, F.; et al. (2007). Insight into the trophic ecology of yellowfin tuna, *Thunnus albacares*, from compound-specific nitrogen isotope analysis of proteinaceous amino acids. *In* Stable isotopes as indicators of ecological change. *Terrestrial Ecology Series 1*: 173–190.

Pörtner, H.O.; Langenbuch, M.; Reipschläger, A. (2004). Biological impact of elevated CO_2 concentrations: lessons from animal physiology and earth history. *Journal of Oceanography 60*: 705–718.

Ragg, N.L.; King, N.; Watts, E.; Morrish, J. (2010). Optimising the delivery of the key dietary diatom Chaetoceros calcitrans to intensively cultured Greenshell™ mussel larvae, *Perna canaliculus*. *Aquaculture 306(1-4)*: 270–280.

Ramajo, L.; Pérez-León, E.; Hendriks, I.E.; Marbà, N.; Krause-Jensen, D.; Sejr, M.K.; Blicher, M.E.; Lagos, N.A.; Olsen, Y.S.; Duarte, C.M. (2016). Food supply confers calcifiers resistance to ocean acidification. *Scientific Reports 6*: 19374.

Ren, J.; Ragg, N.L.; Cummings, V.J.; Zhang, J. (2020). Ocean acidification and dynamic energy budget models: parameterisation and simulations for the green-lipped mussel. *Ecological Modelling 426*: 109069.

Ren, J.S.; Ross, A.H. (2005). Environmental influence on mussel growth: A dynamic energy budget model and its application to the greenshell mussel *Perna canaliculus*. *Ecological Modelling 189(3-4)*: 347–362.

Ren, J.S.; Ross, A.H.; Hadfield, M.G.; Hayden, B.J. (2010). An ecosystem model for estimating potential shellfish culture production in sheltered coastal waters. *Ecological Modelling 221(3)*: 527–539.

Ren, J.S.; Schiel, D.R. (2008). A dynamic energy budget model: parameterisation and application to the Pacific oyster *Crassostrea gigas* in New Zealand waters. *Journal of Experimental Marine Biology and Ecology 361(1)*: 42–48.

Ren, J.S.; Stenton-Dozey, J.; Plew, D.R.; Fang, J.; Gall, M. 2012. An ecosystem model for optimising production in integrated multitrophic aquaculture systems. *Ecological Modelling 246*: 34–46.

Riebesell, U. 2004. Effects of CO_2 enrichment on marine phytoplankton. *Journal of Oceanography 60(4)*: 719–729.

Riebesell, U.; Schulz, K.G.; Bellerby, R.G.J.; Botros, M.; Fritsche, P.; Meyerhöfer, M.; Neill, C.; Nondal, G.; Oschlies, A.; Wohlers, J.; Zöllner, E. (2007). Enhanced biological carbon consumption in a high CO_2 ocean. *Nature 450 (7169)*: 545–548.

Rocha, G.; Katan, T.; Parrish, C.; Gamperl, A. (2017). Effects of wild zooplankton versus enriched rotifers and *Artemia* on the biochemical composition of Atlantic cod (*Gadus morhua*) larvae. *Aquaculture 479*:100–113.

Rose, N.L.; Yang, H.; Turner, S.D.; Simpson, G.L. (2012). An Assessment of the Mechanisms for the Transfer of Lead and Mercury from Atmospherically Contaminated Organic Soils to Lake Sediments with Particular Reference to Scotland, UK. *Geochimica et Cosmochimica Acta 82*: 113–135.

Rossoll, D.; Bermu´dez, R.; Hauss, H.; Schulz, K.G.; Riebesell, U.; Sommer, U.; Winder, M. (2012). Ocean Acidification-Induced Food Quality Deterioration Constrains Trophic Transfer. *PLoS ONE 7(4)*: e34737

Rossoll, D.; Sommer, U.; Winder, M. (2013). Community interactions dampen acidification effects in a coastal plankton system. *Marine Ecology Progress Series 486*: 37–46.

Rousch, J.M.; Bingham, S.E.; Sommerfeld, M.R. (2003). Change in fatty acid profiles of thermo-intolerant and thermo-tolerant marine diatoms during temperature stress. *Journal of Experimental Marine Biology and Ecology 295*: 145–156.

Sabadel, A.J.M.; Décima, M.; McComb, K.; Meyers, M.; Barr, N.; Gall, M.; Safi, K.; Law, C.S. (in press). Amino acid stable isotopes in particulates and zooplankton: potential biomarkers of climate change. Marine Ecology Progress Series.

Sabadel, A.J.M.; Woodward, E.M.S.; Van Hale, R.; Frew, R.D. (2016). Compound-specific isotope analysis of amino acids: A tool to unravel complex symbiotic trophic relationships. *Food Webs 6*: 9–18.

Safi, K.A.; Griffiths, F.B.; Hall, J.A. (2007). Microzooplankton composition, biomass and grazing rates along the WOCE SR3 line between Tasmania and Antarctica. *Deep Sea Research Part 1 Oceanographic Research Papers 54*: 1025–1041.

Saint-Macary, A.D.; Barr, N.; Armstrong. E.; Safi, K.; Marriner, A.; Gall, M.; McComb, K.; Dillingham, P.W.; Law C.S. (2021). The Influence of Ocean Acidification and Warming on DMSP & DMS in New Zealand Coastal Water. *Atmosphere 12(2)*: 181.

Sargent, J.R.; Falk-Petersen, S. (1988). The lipid biochemistry of calanoid copepods. *Hydrobiologia 167*: 101–114.

Schoo, K.L.; Malzahn, A.M.; Krause, E.; Boersma, M. (2013). Increased carbon dioxide availability alters phytoplankton stoichiometry and affects carbon cycling and growth of a marine planktonic herbivore. *Marine Biology 160(8)*: 2145–2155.

Shang, Y.; Wu, F.; Guo, W.; Chen, J.; Huang, W.; Hu, M.; Wang, Y. (2020). Specific dynamic action of mussels exposed to TiO_2 nanoparticles and seawater acidification. *Chemosphere 241*: 125104.

Shpigel, M.; Barber, B.J.; Mann, R. (1992). Effects of elevated temperature on growth, gametogenesis, physiology, and biochemical composition in diploid and triploid Pacific oyster, *Crassostrea gigas* Thunberg. *Journal of Experimental Marine Biology and Ecology 161*: 15–25.

Sommer, U.; Lengfellner, K. (2008). Climate change and the timing, magnitude, and composition of the phytoplankton spring bloom. *Global Change Biology 14*: 1199−1208.

Sommer, U.; Lewandowska, A. (2011). Climate change and the phytoplankton spring bloom: warming and overwintering zooplankton have similar effects on phytoplankton. *Global Change Biology 17*: 154−162.

Sommer, U.; Stibor, H.; Katechakis, A.; Sommer, F.; Hansen, T. (2002). Pelagic food web configurations at different levels of nutrient richness and their implications for the ratio fish production:primary production. *Hydrobiologia 484*: 11–20.

Steinberg, D.K.; Landry, M.R. (2017). Zooplankton and the Ocean Carbon Cycle. *Annual Review of Marine Science 9*: 413–444.

Styring, A.K.; Kuhl, A.; Knowles, T.D.J.; Fraser, R.A.; Bogaard, A.; Evershed, R.P. (2012). Practical considerations in the determination of compound-specific amino acid $\delta^{15}N$ values in animal and plant tissues by gas chromatography-combustion-isotope ratio mass spectrometry, following derivatisation to their N-acetylisopropyl esters. *Rapid Communications in Mass Spectrometry 26*: 2328–2334.

Styring, A.K.; Sealy, J.C.; Evershed, R.P. (2010). Resolving the bulk $\delta^{15}N$ values of ancient human and animal bone collagen via compound-specific nitrogen isotope analysis of constituent amino acids. *Geochimica et Cosmochimica Acta 74*: 241–251.

Sui, Y.; Hui, K.; Huang, X.; Dupont, S.; Hu, M.; Storch, D.; Pörtner, H.-O.; Lu, W.; Wang, Y. (2016). Combined effects of short-term exposure to elevated CO2 and decreased O2 on the physiology and energy budget of the thick shell mussel *Mytilus coruscus. Chemosphere 155*: 207–216.

Sutton, P.J.; Bowen, M. (2019). Ocean temperature change around New Zealand over the last 36 years. *New Zealand Journal of Marine and Freshwater Research 53(3)*: 305–326.

Taucher, J.; Schulz K.G.; Dittmar T.; Sommer U.; Oschlies A.; Riebesell U. (2012). Enhanced carbon overconsumption in response to increasing temperatures during a mesocosm experiment. *Biogeosciences 9*: 3531−3545.

Taylor, A.G.; Savage, C. (2006). Fatty acid composition of New Zealand green-lipped mussels, *Perna canaliculus*: Implications for harvesting for n-3 extracts. *Aquaculture* 261: 430–439.

Thor, P.; Oliva, E.O. (2015). Ocean acidification elicits different energetic responses in an Arctic and a boreal population of the copepod *Pseudocalanus acuspes. Marine Biology 162(4)*: 799–807.

Tortell, P.D.; Payne, C.D.; Li, Y.; Trimborn, S.; Rost, B.; Smith, W.O.; Riesselman, C.; Dunbar, R.B.; Sedwick, P.; DiTullio, G.R. (2008). CO_2 sensitivity of Southern Ocean phytoplankton. *Geophysical Research Letters 35(4)*: L04605.

Vance, J.M.; Currie, K.I.; Law, C.S.; Murdoch, J.; Zeldis, J. (2019). NZOA-ON: The New Zealand Ocean Acidification Observing Network. *Marine and Freshwater Research 71(3)*: 281–299.

van der Meer, J. (2006). An introduction to Dynamic Energy Budget (DEB) models with special emphasis on parameter estimation. *Journal of Sea Research 56*: 85–102.

Verity, P.G.; Robertson, C.Y.; Tronzo, C.R.; Andrews, M.G.; Nelson, J.R.; Sieracki, M.E. (1992). Relationships between cell volume and the carbon and nitrogen content of marine photosynthetic nanoplankton. *Limnology and Oceanography 37(7)*: 1434–1446.

Wang, T.; Tong, S.; Liu, N.; Li, F.; Wells, M.L.; Gao, K. (2017). The fatty acid content of plankton is changing in subtropical coastal waters as a result of OA: Results from a mesocosm study. *Marine Environmental Research 132*: 51–62.

Wu, Y.; Campbell, D.A.; Irwin, A.J.; Suggett, D.J.; Finkel Z.V. (2014). Ocean acidification enhances the growth rate of larger diatoms. *Limnology and Oceanography 59*: 1027–1034.

Wu, X.; Gao, G.; Giordano, M.; Gao. K. (2012). Growth and photosynthesis of a diatom grown under elevated CO_2 in the presence of solar UV radiation. *Fundamental and Applied Limnology/Archiv für Hydrobiologie 180(4)*: 279–290.

Yamaguchi, Y.T.; McCarthy, M.D. (2018). Sources and transformation of dissolved and particulate organic nitrogen in the North Pacific Subtropical Gyre indicated by compound-specific δ15N analysis of amino acids. *Geochimica et Cosmochimica Acta 220*: 329–347.

Zeldis, J.R.; Hadfield, M.G.; Booker, D.J. (2013). Influence of climate on Pelorus Sound mussel aquaculture yields: predictive models and underlying mechanisms. *Aquaculture Environment Interactions 4*: 1–15.

Zeldis, J.R.; Howard-Williams, C.; Carter, C.M.; Schiel, D.R. (2008). ENSO and riverine control of nutrient loading, phytoplankton biomass and mussel aquaculture yield in Pelorus Sound, New Zealand. *Marine Ecology Progress Series 371*: 131–142.

Zeldis, J.; Swales, A.; Currie, K.; Safi, K.; Nodder, S.; Depree, C.; Elliott, F.; Pritchard, M.; Gall, M.; O'Callaghan, J.; Pratt, D.; Chiswell, S.; Pinkerton, M.; Lohrer, D.; Bentley, S. (2015). Firth of Thames Water Quality and Ecosystem Health – Data Report. (Unpublished NIWA Client Report CHC2014-123 prepared for Waikato Regional Council and DairyNZ.) 177 p. http://www.waikatoregion.govt.nz/tr201523/

Zeldis, J.R.; Swaney, D.P. (2018). Balance of Catchment and Offshore Nutrient Loading and Biogeochemical Response in Four New Zealand Coastal Systems: Implications for Resource Management. *Estuaries and Coasts 41*: 2240–2259.

Other information sources

R Core Team (2019). *R: A Language and Environment for Statistical Computing*; R Foundation for Statistical Computing: Vienna, Austria, 2019. itsadug: vignettes/test.Rmd https://rdrr.io/cran/itsadug/f/vignettes/test.Rmd (accessed Jan 13, 2020).

White, C. (2017). https://www.seafoodsource.com/news/supply-trade/report-values-new-zealand-seafood-industry-at-nzd-4-billion.

Seafood New Zealand (2019). New Zealand Seafood Exports. https://www.seafoodnewzealand.org.nz/fileadmin/documents/Export_data/19.12.7.pdf.

New Zealand Government (2019). Aquaculture industry in its strategic aim to be a $3B industry, Minister for Fisheries, Stuart Nash, Sept 2019. https://www.beehive.govt.nz/release/government-delivers-plan-world-leading-aquaculture-industry.

APPENDIX 1

Fatty acid (FA) species and group. Abbreviations: Monounsaturated Fatty Acids (MUFA), Saturated Fatty Acids (SFA), Polyunsaturated Fatty Acids (PUFA)

Fatty acid species	FA group
C4:0 butyric acid	SFA
C6:0 caproic acid	SFA
C8:0 caprylic acid	SFA
C10:0 capric acid	SFA
C11:0 undecanoic acid	SFA
C12:0 lauric acid	SFA
C13:0 tridecanoic acid	SFA
C14:0 myristic acid	SFA
C14:1 myristoleic acid	MUFA
C15:0i iso pentadecanoic acid	SFA
C15:0a anteiso pentadecanoic acid	SFA
C15:0 pentadecanoic acid	SFA
C15:1 cis-10-pentadecanoic acid	MUFA
C16:0 palmitic acid	SFA
C16:1 palmitoleic acid	MUFA
C16:2n4 hexadecadienoic acid	PUFA
C17:0 heptadecanoic acid	SFA
C17:1 cis-10-heptadecanoic acid	MUFA
C18:0 stearic acid	SFA
C18:1n7 vaccenic acid	MUFA
C18:1n9c oleic acid	MUFA
C18:1t elaidic acid	MUFA
C18:2n6c linoleic acid	PUFA
C18:2t linolelaidic acid	PUFA
C18:3n3 alpha linolenic acid (ALA)	n3 PUFA
C18:3n6 gamma linolenic (GLA)	PUFA
C18:3n4 octadecatrienoic acid	PUFA
C18:4n3 stearidonic acid (SDA)	n3 PUFA
C20:0 arachidic acid	SFA
C20:1 gadoleic acid	MUFA
C20:2 eicosadienoic acid	PUFA
C20:3n3 cis-11, 14, 17-eicosatrienoic acid	n3 PUFA
C20:3n6 cis-8, 11, 14-eicosatrienoic acid	PUFA
C20:4n3 eicosatetraenoic acid	n3 PUFA
C20:4n6 arachidonic acid (AA)	PUFA
C20:5n3 eicosapentaenoic acid	n3 PUFA
C21:0 heneicosanoic acid	SFA
C22:0 behenic acid	SFA
C22:1	MUFA
C22:1n9	MUFA
C22:2 dicosadienoic acid	PUFA
C22:5n3 docosapentaenoic acid (DPA)	n3 PUFA
C22:6n3 docosahexaenoic acid (DHA)	n3 PUFA
C23:0 tricosanoic acid	SFA
C24:0 lignoceric acid	SFA
C24:1 nervonic acid	MUFA

APPENDIX 2

Total Phytoplankton Carbon in ME3 (A, B) and ME4 (C, D). A and C show the individual datapoints from each replicate bag overlain by the GAMM fits (mean and error) for the Control (green) and treatments (*2100,* orange and *2150,* red in ME3; *pH* orange and *pH/T* pink in ME4). B and D show the mean of the replicates for the Control and treatments, overlain by the mean and standard deviation for each Phase (using same colour scheme). The different phases, P1, P2 and P3 are delineated by the vertical lines.

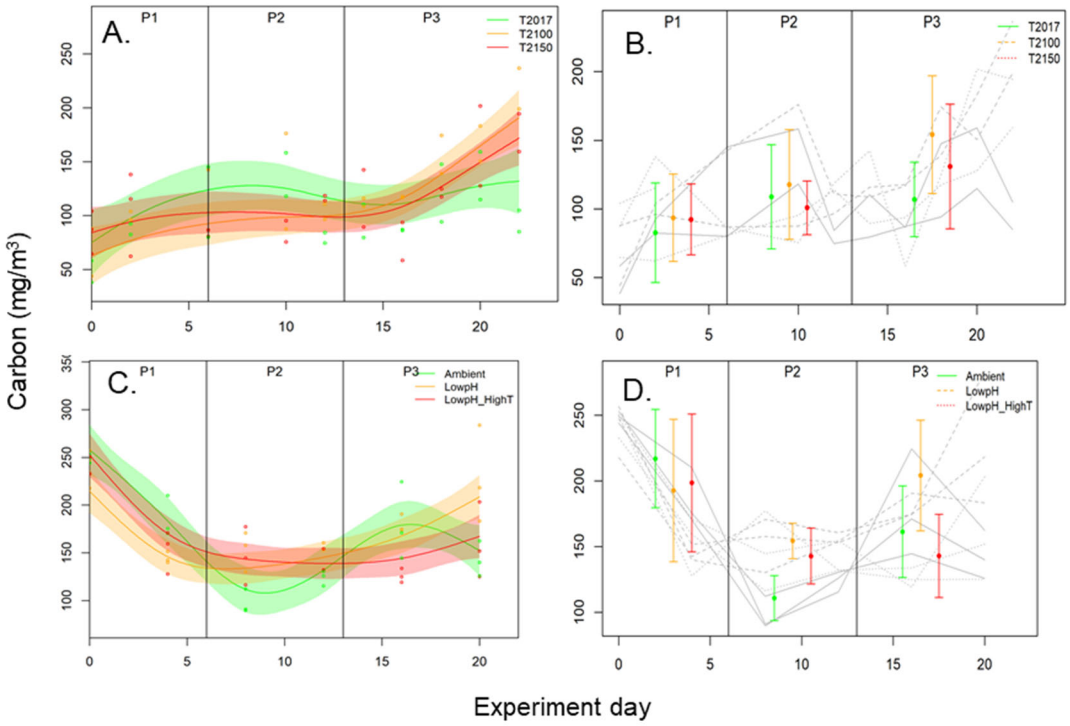

APPENDIX 3

ME1 Zooplankton species and abundance (Individuals/m^3; mean ± standard deviation).

No significant treatment effects

	pH/T	***pH***	**Control**
Bivalve Spat	37 ± 32	24 ± 35	29 ± 19
Barnacle Cyprid	0 ± 0	3 ± 5	0 ± 0
Barnacle Nauplii	874 ± 1,501	3 ± 5	5 ± 9
Hydromedusa	211 ± 220	340 ± 148	543 ± 253
Acartia sp.	5 ± 9	0 ± 0	0 ± 0
Microsetella sp.	3 ± 5	19 ± 26	11 ± 9
Oncaea sp.	0 ± 0	0 ± 0	0 ± 0
Oithona sp.	88 ± 133	21 ± 20	13 ± 23
Euterpina sp.	80 ± 89	29 ± 51	27 ± 20
Temora sp.	406 ± 358	45 ± 44	13 ± 23
Copepodite indet.	3 ± 5	0 ± 0	0 ± 0
Paracalanus sp.	5 ± 9	0 ± 0	5 ± 9
Nauplii	385 ± 653	428 ± 430	187 ± 249
Polychaete round ball	75 ± 81	115 ± 104	158 ± 55
Gastropod indet.	5 ± 9	5 ± 9	3 ± 5
Podon	0 ± 0	0 ± 0	0 ± 0
Total	**2 180 ± 1 945**	**1 032 ± 750**	**995 ± 622**

ME3 Zooplankton species and abundance (Individuals/m^3; mean ± standard deviation).

***Oithona* abundances different by treatment (ANOVA, * p<0.1).**

	2150	***2100***	**Control**
Bivalve Spat	36 ± 6	4 ± 6	16 ± 23
Hydromedusa	0 ± 0	0 ± 0	12 ± 17
Euterpina sp.	433 ± 590	353 ± 477	261 ± 119
Harpacticoid spp.	32 ± 0	4 ± 6	68 ± 96
Microsetella sp.	32 ± 11	8 ± 11	8 ± 11
Oithona* sp.	**48 ± 11**	**0 ± 0**	**12 ± 17**
Paracalanus sp.	0 ± 0	0 ± 0	0 ± 0
Temora sp.	4 ± 6	0 ± 0	0 ± 0
Oncaea sp.	0 ± 0	0 ± 0	24 ± 34
Copepodite indet.	0 ± 0	0 ± 0	4 ± 6
Nauplii	1 051 ± 1 214	666 ± 919	437 ± 221
Polychaete larva	12 ± 6	56 ± 57	20 ± 28
Gastropod indet.	0 ± 0	0 ± 0	4 ± 6
Total	**1 649 ± 630**	**1 091 ± 1 475**	**866 ± 113**

ME4 Zooplankton species and (Individuals/m^3; mean ± standard deviation).

Two groups with significant differences among treatments (ANOVA * p<0.1, **p<0.05).

	pH/T	***pH***	**Control**
Fritillaria sp.	0 ± 0	0 ± 0	0 ± 0
Bivalve Spat	67 ± 32	21 ± 20	21 ± 20
Chaetognaths	0 ± 0	8 ± 8	5 ± 9
Tintinnids	3 ± 5	3 ± 5	0 ± 0
Barnacle cyprid	13 ± 12	21 ± 12	5 ± 9
Barnacle nauplii	3 ± 5	5 ± 5	8 ± 8
Cladocerans	0 ± 0	0 ± 0	0 ± 0
Small Medusa *	**11 ± 9**	**0 ± 0**	**0 ± 0**
Acartia sp.	0 ± 0	24 ± 21	5 ± 9
Centropoges aucklandicus	5 ± 9	37 ± 58	3 ± 5
Calanus australis	0 ± 0	0 ± 0	0 ± 0
Corycaeus sp.	43 ± 36	86 ± 5	45 ± 32
Euterpina acutifrons	2 169 ± 626	2 252 ± 587	2 019 ± 538
Harpacticoid indet.	11 ± 12	8 ± 14	0 ± 0
Copepodite indet. (large)	0 ± 0	5 ± 9	0 ± 0
Copepodite indet. (small)	43 ± 46	642 ± 1,002	48 ± 83
Microsetella sp.	0 ± 0	0 ± 0	3 ± 5
Oithona sp.	361 ± 258	1 556 ± 1 279	2 819 ± 2 085
Oncaea sp.	0 ± 0	0 ± 0	5 ± 9
Paracalanus sp.	155 ± 214	666 ± 959	62 ± 56
Euterpina sp.	53 ± 25	70 ± 23	86 ± 25
Temora turbinata	104 ± 125	345 ± 521	27 ± 26
Decapoda	3 ± 5	3 ± 5	5 ± 5
Noctiluca scintillans* *	**5 ± 5**	**19 ± 26**	**75 ± 17**
Euphausiid larva	0 ± 0	0 ± 0	0 ± 0
Gastropoda indet	8 ± 8	3 ± 5	0 ± 0
Nauplii	13 262 ± 5241	11 968 ± 6 228	10 350 ± 4 667
Polychaete others	0 ± 0	0 ± 0	0 ± 0
Polychaete larva	8 ± 14	8 ± 8	24 ± 8
Ciona sp.	0 ± 0	0 ± 0	0 ± 0
Total	**16 327 ± 6 278**	**17 749 ± 4 550**	**15 615 ± 5 499**

APPENDIX 4

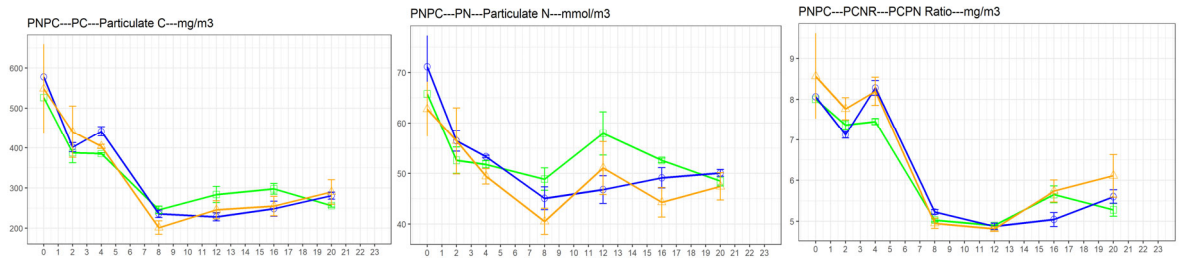

ME4 Particulate Carbon, Nitrogen, and Carbon: Nitrogen ratio means and standard deviations.

APPENDIX 5

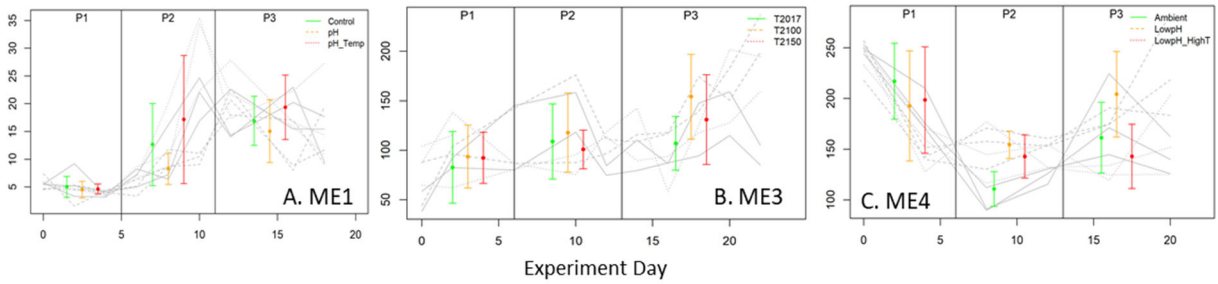

Total Phytoplankton Carbon > 5 µm for A. ME1, B. ME3 and C. ME4.

APPENDIX 6

Microzooplankton grazing

a) Phytoplankton grazing, microzooplankton growth, and net growth rates

ME1

The intrinsic growth rate of the phytoplankton community (μ_{phyto}) remained relatively constant (~0.25/day) in the first two phases of the experiment (days 5 & 12) and across treatments and the Control (Figure SF3A). In the final phase (day 18), phytoplankton growth in *pH/T* (μ_{phyto}= 0.43 ± 0.33/day, mean ± standard error of mean (sem) was higher than in *pH* (μ_{phyto}= 0.04 ± 0.010/day) and the Control (μ_{phyto}= -0.20 ± 0.16/day), although differences were not significant (One-way ANOVA, p = 0.18).

Phytoplankton growth was stimulated by nutrient addition (Figure SF3D), although this varied with phase (Two-way ANOVA, F=8.7, p=0.01), with a stronger response associated with the *Increase* phase, but no significant treatment effect (Two-way ANOVA, F=3.3, p=0.10). Nevertheless, phytoplankton growth response to nutrient addition was lower in the Control relative to the treatments, particularly during the last phase (Control: μ_{nut} = -0.01 ± 0.18/day; *pH:* μ_{nut} = 0.50 ± 0.15/day; *pH/T:* μ_{nut} = 0.49 ± 0.11/day).

Microzooplankton grazing rate (m) was less variable than phytoplankton growth (Figure SF3B), with no significant effect of treatment or time (Two-way ANOVA, p > 0.30). Grazing rate within the 2nd phase (day 12) was lower in *pH/T* (m = 0.23 ± 0.11/day) relative to both *pH* (m = 0.36 ± 0.05/day) and Control (m = 0.45 ± 0.06/day), although differences were not significant (One-way ANOVA, p = 0.21).

The net growth rate (μ_{net}) of the phytoplankton community, which is the difference between intrinsic growth and grazing rates, was overall negative or close to zero (Figure SF3C) suggesting that microzooplankton grazing kept phytoplankton growth in check. Net growth rate tended to be higher in *pH/T* (μ_{net}= 0.00 ± 0.07/day) compared to *pH* (-0.19 ± 0.06/day) and the Control (-0.32 ± 0.12/day) throughout the experiment (Two-way ANOVA, Treatment factor p = 0.08).

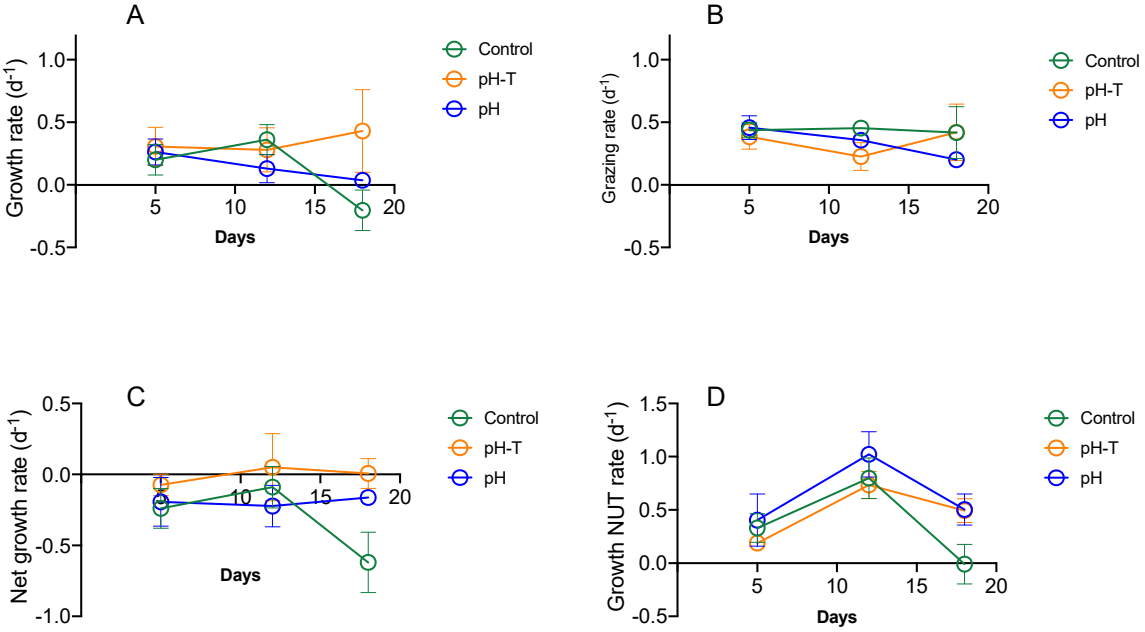

Figure SF3: A. Phytoplankton community mean (± sem, standard error of mean) in situ growth, B. microzooplankton grazing rate, C. phytoplankton net growth, and D. nutrient-amended (NUT) growth rates during ME1.

ME2

The intrinsic growth rate of phytoplankton community was only positive on the first day of ME2 and decreased rapidly to values close to zero by day 4 (Figure SF4A). From then on phytoplankton growth remained relatively constant until the last phase of the experiments when growth rate became negative. As two of the replicates of the *pH/T* treatment were lost after Day 5, only the *pH* vs Control is considered for ME2. No statistically significant difference was observed in phytoplankton growth.

Phytoplankton growth was strongly stimulated by nutrient addition (Figure SF4D) and showed a significant effect of time (two-way ANOVA, F = 10.3, p = 0.002) with values increasing from 1.0 to 2.5/day during the experiment. However, no significant effect was observed in *pH* relative to the Control (two-way ANOVA, F = 0.34, p = 0.58).

Unlike phytoplankton growth, microzooplankton grazing rate varied throughout the experiment, initially increasing with a midway plateau and decrease towards the end of the experiment (Figure SF4B). However, neither time (two-way ANOVA, F = 1.15, p = 0.36) or treatment (two-way ANOVA, F = 0.28, p = 0.62) showed a significant effect on grazing rate. Although the difference appeared greatest towards the end of the experiment, with grazing rates declining more rapidly in the Control (m = 0.35 ± 0.41/day, n = 6), relative to *pH* (m = 0.51 ± 0.27/day, n = 6), these differences were not significant (t-test, p=0.46).

Net growth rate was negative throughout the experiment (μ_{net} range = -0.25 to -1.0/day) and showed a decreasing trend with time (two-way ANOVA, F = 11.0, p = 0.008, Figure SF4C). This decrease seemed to be more pronounced in *pH*, due to the higher grazing pressure towards the end of the experiment, although differences were not significant (two-way ANOVA, F = 0.38, p = 0.57).

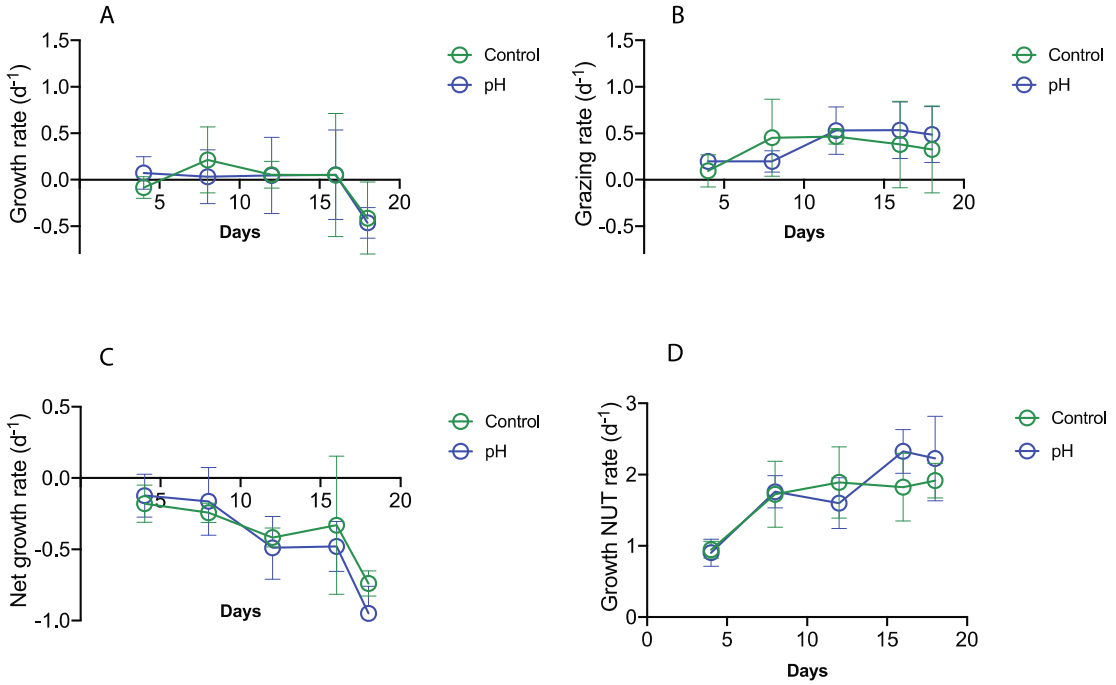

Figure SF4: A. Phytoplankton community mean (± sem, standard error of mean) in situ growth, B. microzooplankton grazing rate, C. phytoplankton net growth, and D. nutrient-amended (NUT) growth rates during ME2.

ME3

The intrinsic growth rate of the phytoplankton community increased with time (Figure SF5A), with higher values in the Control relative to the treatments, although differences were not statistically significant. Differences in growth rates were buffered by nutrient addition, which stimulated growth rates across all treatments and Controls, particularly in the initial phases when nutrient limitation were likely more severe (Figure SF5D). Grazing rates followed a similar temporal trend as intrinsic growth rates with increasing values with time (Figure SF5B). Both time and treatment had a significant effect

(two-way ANOVA, F> 4.5, $p<0.05$), on grazing response, with higher values in *2150* relative to the Control and *2100,* particularly towards the end of the experiment (One-way ANOVA, F=5.98, $p = 0.09$).

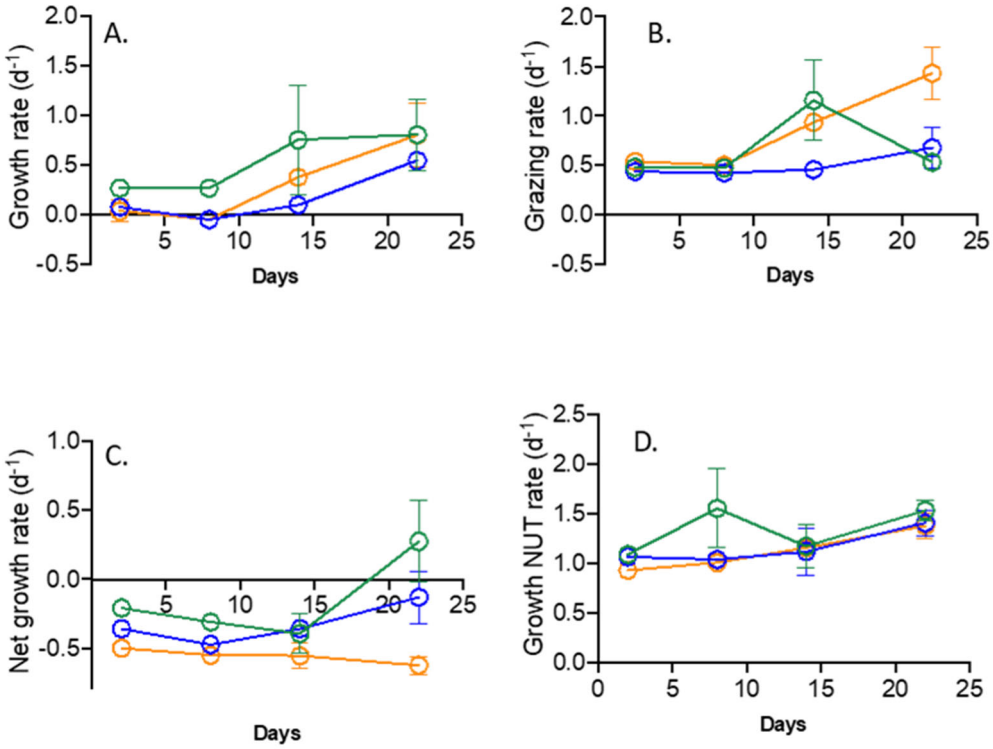

Figure SF5: A. Phytoplankton community mean (± sem, standard error of mean) in situ growth, B. microzooplankton grazing rate, C. phytoplankton net growth, and D. nutrient-amended (NUT) growth rates during ME3, showing Control (green), *2100* (blue) and *2150* (orange).

Net growth rates were negative for most of the experiment (Figure SF5C) with lower values in *2150* relative to the Control and *2100* (Two-way ANOVA, F=9.22, $p < 0.005$), particularly towards the end of the experiment, when *2100* (mean ± sem -0.13 ± 0.19), and *pH/T* (-0.62 ± 0.06) showed markedly lower net growth rates than the Control (0.27 ± 0.29).

b) Response of Phytoplankton groups

ME1

Analysis of the coupling between phytoplankton growth and microzooplankton grazing provides another approach to examine phytoplankton dynamics. In the Control and *pH* treatments in ME1, grazing rates showed a weak relationship with phytoplankton growth while both rates became significantly correlated in *pH/T* treatment (see Figure SF6). Although, the lack of significance in the former precludes a formal comparison between regression parameters, the lower intercept in *pH/T* suggests a tighter coupling between both rates than in the Control and pH.

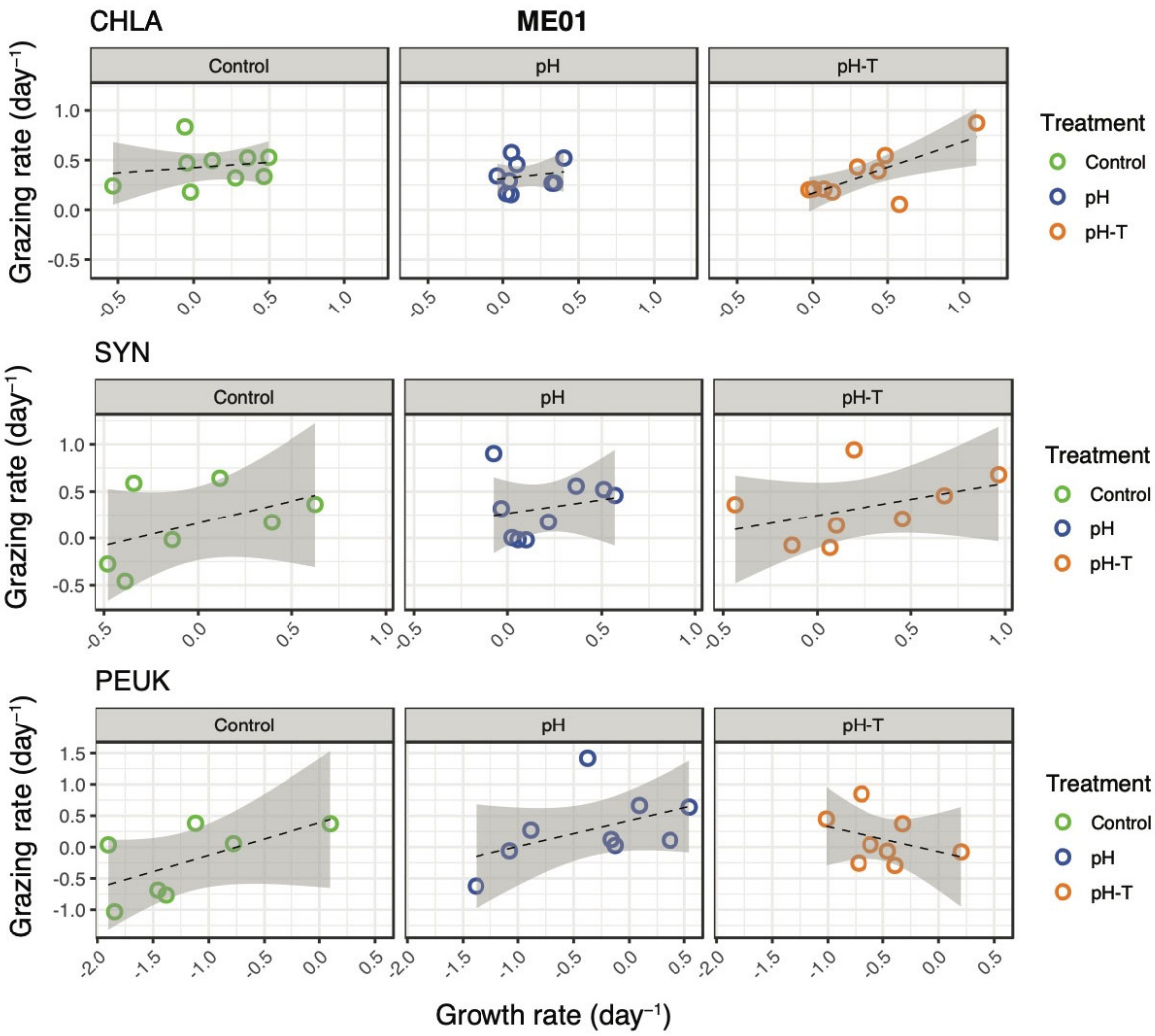

Figure SF6: Linear regression model between phytoplankton growth rate and microzooplankton grazing rates for the entire community (CHLA), Synechococcus (SYN), picoeukaryotes (PEUK), and nanophytoplankton (NANO) populations across different treatments in ME1.

The intrinsic growth rate of prokaryotic (*Synechococcus*, SYN) and eukaryotic (Picoeukaryotes, PEUK) picophytoplankton populations in ME1 showed a different pattern (see Figure SF6). SYN growth rate varied with time and peaked in the intermediate phase (2-way ANOVA, F=20.2, $p < 0.001$). Although differences between the treatments and Control were not significant across the experiment (2-way ANOVA, F=1.5, $p = 0.24$), SYN growth rate tended to be higher in *pH/T* and *pH* compared to Control treatment, particularly on the last day of the experiment when differences in mean growth rate of SYN between *pH/T* (0.01± 0.07/day), *pH* (0.06 ± 0.02/day) and Control (-0.34 ± 0.10/day) were significant (One-way ANOVA, $p = 0.018$). The growth rate of PEUK showed the same temporal pattern (Mixed-effect analysis, F=7.0, p = 0.01) and treatment effect with both *pH* and *pH/T* showing significantly higher growth rates than the Control (Mixed-effect analysis, F=6.2, $p = 0.01$). However, these results should be taken with caution due to overall negative growth rates recorded throughout the experiment across all treatments.

Grazing rates of SYN and PEUK showed a similar pattern with decreasing rates (see Figure SF6) as the experiment progressed, a trend that was statistically significant in both groups (Mixed-effects analysis, F >10, $p < 0.01$). Differences among treatments were not statistically significant for the entire experiment (Mixed-effects analysis, F < 2.5, $p > 0.15$). However, grazing tended to be higher in *pH* and *pH/T* relative to the Control, particularly in the Decline phase (Phase 3), when differences became statistically significant for PEUK (One-way ANOVA, p = 0.05).

Net growth rates of SYN and PEUK were negative throughout the experiment (see Figure SF7) and followed the same temporal trend as phytoplankton growth with highest values achieved in the *Increase* phase (Phase 2). Differences between treatments were not significant but deviated most in the *Decline* phase particularly for PEUK and between *pH/T* and Control treatments. SYN and PEUK populations showed a positive correlation between phytoplankton growth and microzooplankton grazing, although this relationship was not statistically significant for specific treatments. PEUK showed a similar pattern in the Control and *pH*, while the sign of the correlation changed in the *pH/T* treatment, but the negative intrinsic growth rates observed for this group throughout the experiment indicate that caution is required in interpretation.

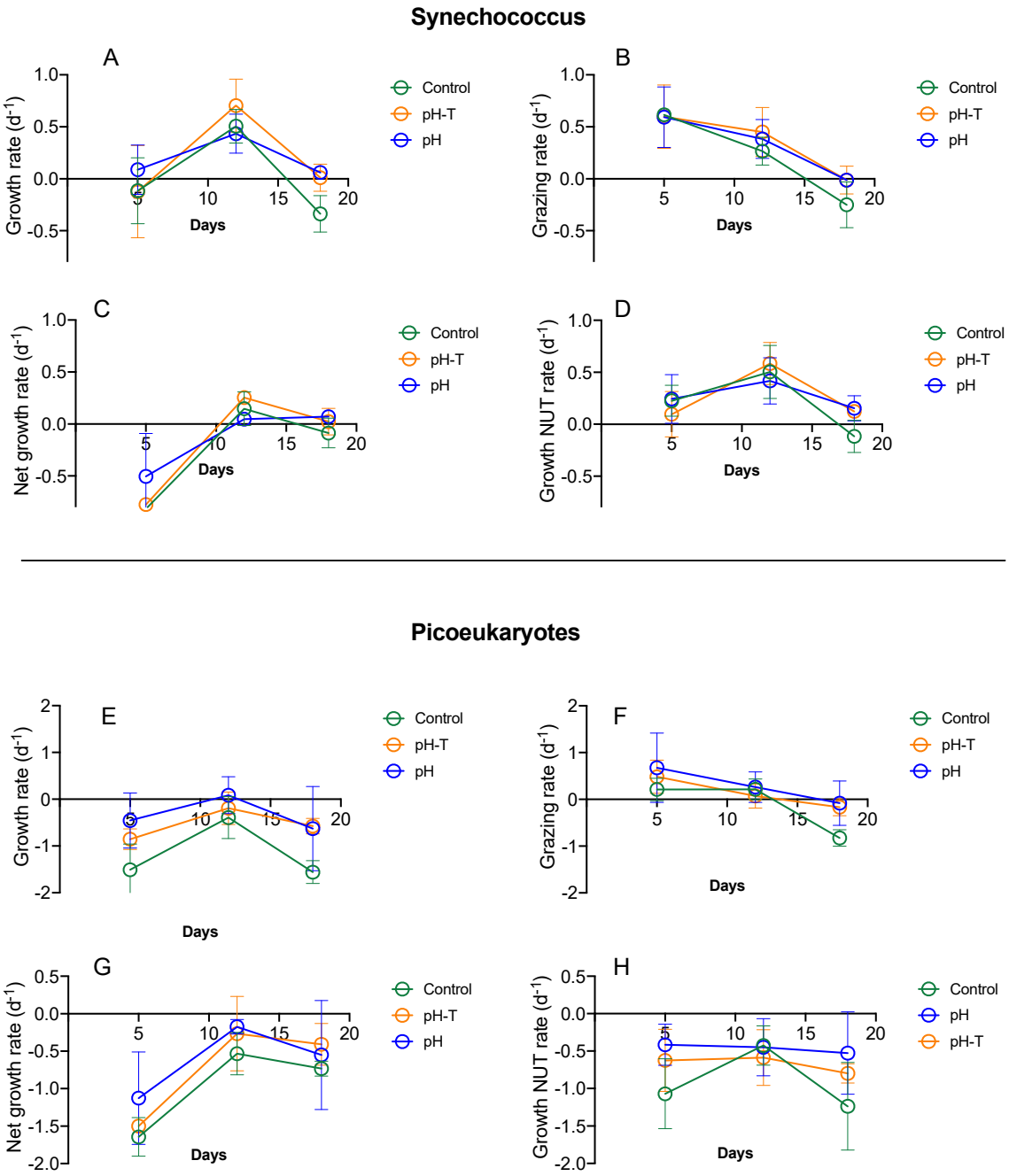

Figure SF7: In situ growth, grazing, net growth, and nutrient amended (NUT) growth rates for *Synechococcus* (A-D) and Picoeukaryotes (E-H) during ME1.

ME2

Phytoplankton growth and grazing rates were positively correlated across all treatments although a relatively small fraction of grazing variability was explained by growth (linear regression model,

F=12.0, p = 0.001, R^2 = 0.21). This relationship was only statistically significant in the control (linear regression model, F=7.8, p=0.015, R^2 = 0.35) (Figure SF8) but not in *pH*. In the case of SYN this correlation was weaker (F=5.0, p = 0.03, R^2 = 0.11), and remained significant only in *pH* (F=5.6, p = 0.03, R^2 = 0.30). This coupling was stronger for PEUK (R^2=0.64) and Nano-phytoplankton (R^2=0.32) populations, which yielded significant correlation for *pH*. In the case of PEUK, although the comparison of linear models across treatment yielded only marginally significant differences (ANCOVA, F=2.7, p = 0.061), the strength of this dynamic coupling decreased from 0.83 in the control to 0.61 in pH. In the case of Nano-phytoplankton, comparison of models across treatments yielded statistically significant differences (ANCOVA, F=6.8, p < 0.001), with a higher slope in *pH* (0.41 ± 0.13) relative to the control (0.28 ± 0.087).

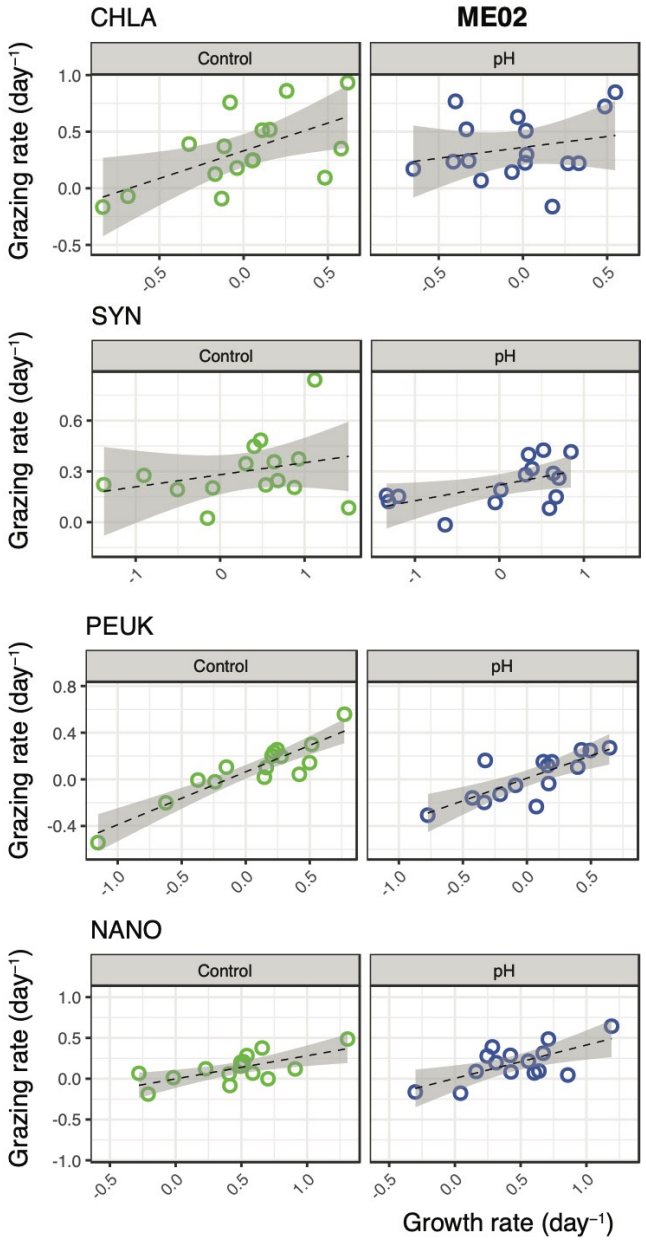

Figure SF8: Linear regression model between phytoplankton growth rate and microzooplankton grazing rates for the entire community (CHLA), *Synechococcus* (SYN), picoeukaryotes (PEUK) and nanophytoplankton (NANO) populations across different treatments during ME2.

Synechococcus and picoeukaryote intrinsic growth rate showed similar temporal trends with higher rates in the first two phases and lower values towards the end of the experiment (Figure SF9). Growth rates of nanophytoplankton followed a similar trend with maximum growth rates observed midway through the experiment. No significant differences were observed between *pH* and Control (two-way ANOVA,

p>0.5) which showed similar trends throughout the experiment. Grazing rates followed the same temporal trend as growth rates and no significant difference between treatments was observed for the Pico- or Nano-phytoplankton groups. As a result of this balance, SYN and PEUK showed slightly positive net growth rates (~0.25/day) that became negative towards the end of the experiment (Figure SF9). Net growth rate of Nano-phytoplankton populations peaked midway through the experiment but remained positive throughout the entire experiment. Overall, there were no significant differences in net growth rates between *pH* and the Control.

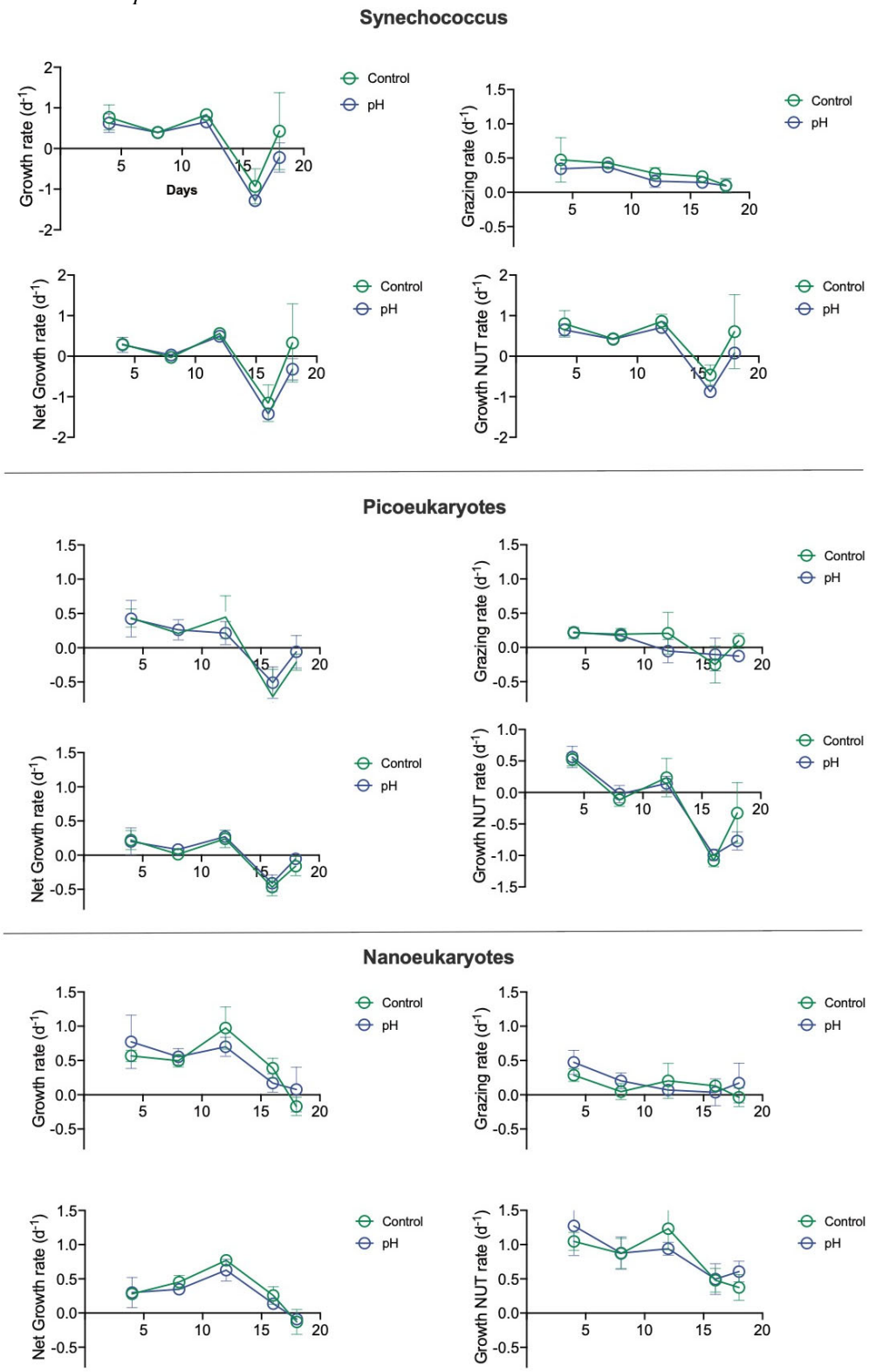

Figure SF9: In situ growth, grazing, net growth, and nutrient amended (NUT) growth rates for SYN, PEUK, and Nano-phytoplankton populations during ME2.

ME3

Growth and grazing rates were significantly correlated (linear regression model, F=14.8, p <0.001, R^2 =0.37), but the relationship differed among treatments (ANCOVA, F = 9.5, *p* <0.001) (See Figure SF10). Coupling tended to be tighter in the *pH/T* treatment, relative to the Control and *pH*, as indicated by the increasing significance of the correlation, higher slope and intercept of the regression in the *pH/T* treatment.

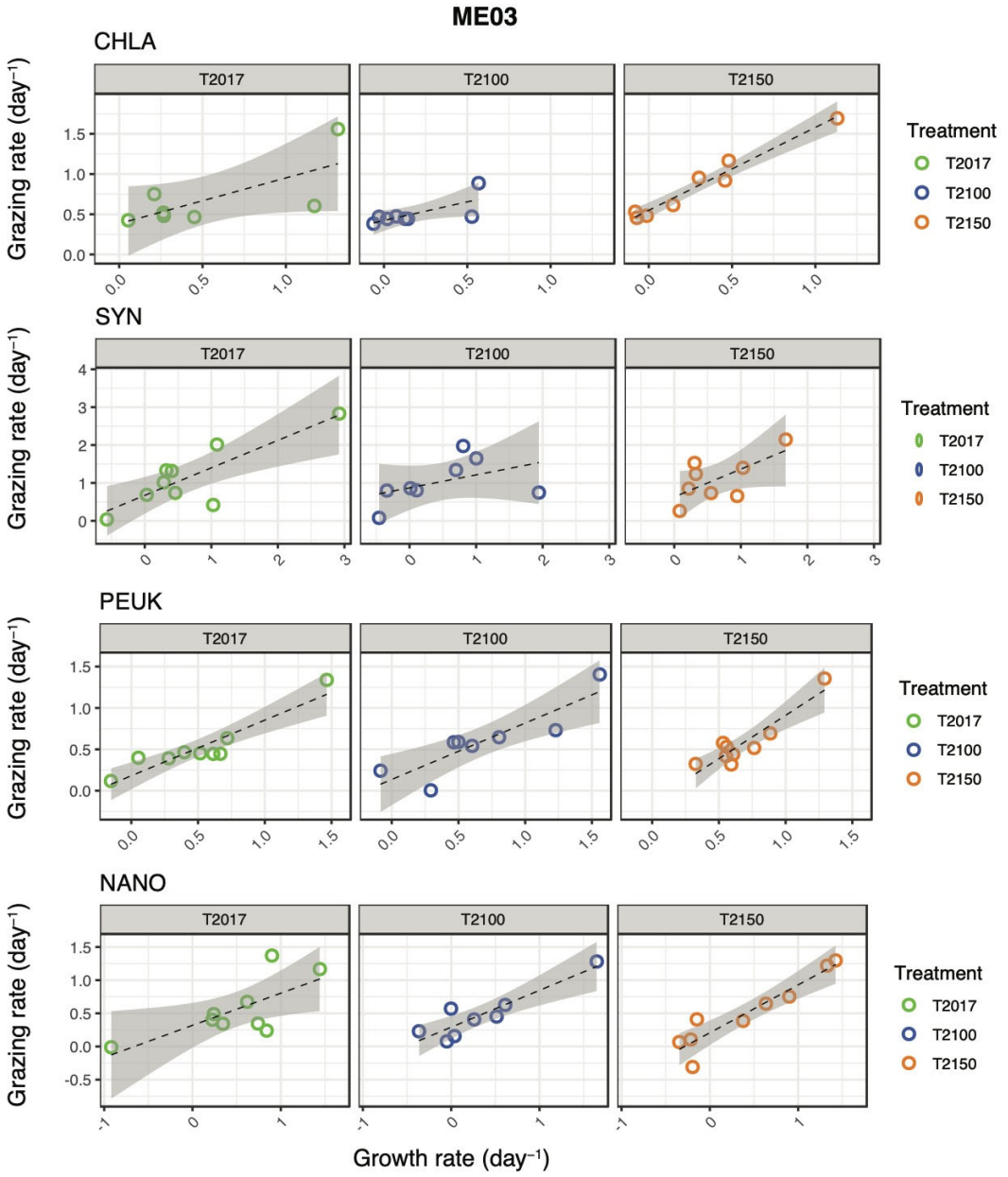

Figure SF10: Linear regression model between phytoplankton growth rate and microzooplankton grazing rates for the entire community (CHLA), Synechococcus (SYN), picoeukaryotes (PEUK) and nanophytoplankton (NANO) populations across different treatments during ME3.

Growth and grazing rates were closely coupled for all groups (Figure SF10 and SF11). In the case of SYN the strength of this coupling was greater in *pH* and *pH/T*, as indicated by the higher slope (pH = 1.05 ± 0.21, *pH/T* = 1.40 ± 0.29) and R2 (pH = 0.78 *pH/T* =0.77) than in the Control (slope = 0.72 ± 0.18, R^2 = 0.70), although differences among treatments were only marginally significant (ANCOVA, F= 2.7, p = 0.09). In the case of PEUK, the grazing to growth relationship was strongly correlated across treatments (Figure SF11), with a higher slope in *pH/T* (1.05 ± 0.17) relative to *pH* (0.70 ± 0.13) and

Control (0.67 ± 0.10), although the observed relationship did not statistically differ among treatments ((ANCOVA, F= 0.25, p = 0.86). In the case of Nano-eukaryotes, the correlation between both rates was significant across treatments. Differences in the linear regression models among treatments was not significant (ANCOVA, F=0.07, p=0.97), although the higher slope and R^2 values in *pH/T* (slope = 0.72 ± 0.11, R^2 = 0.88) relative to *pH* (slope = 0.56 ± 0.11, R^2 = 0.79) and the Control (slope = 0.48 ± 0.18, R^2 = 0.50) suggests a strengthening of the dynamic coupling between grazing and growth rates in the nano-eukaryotes under future conditions.

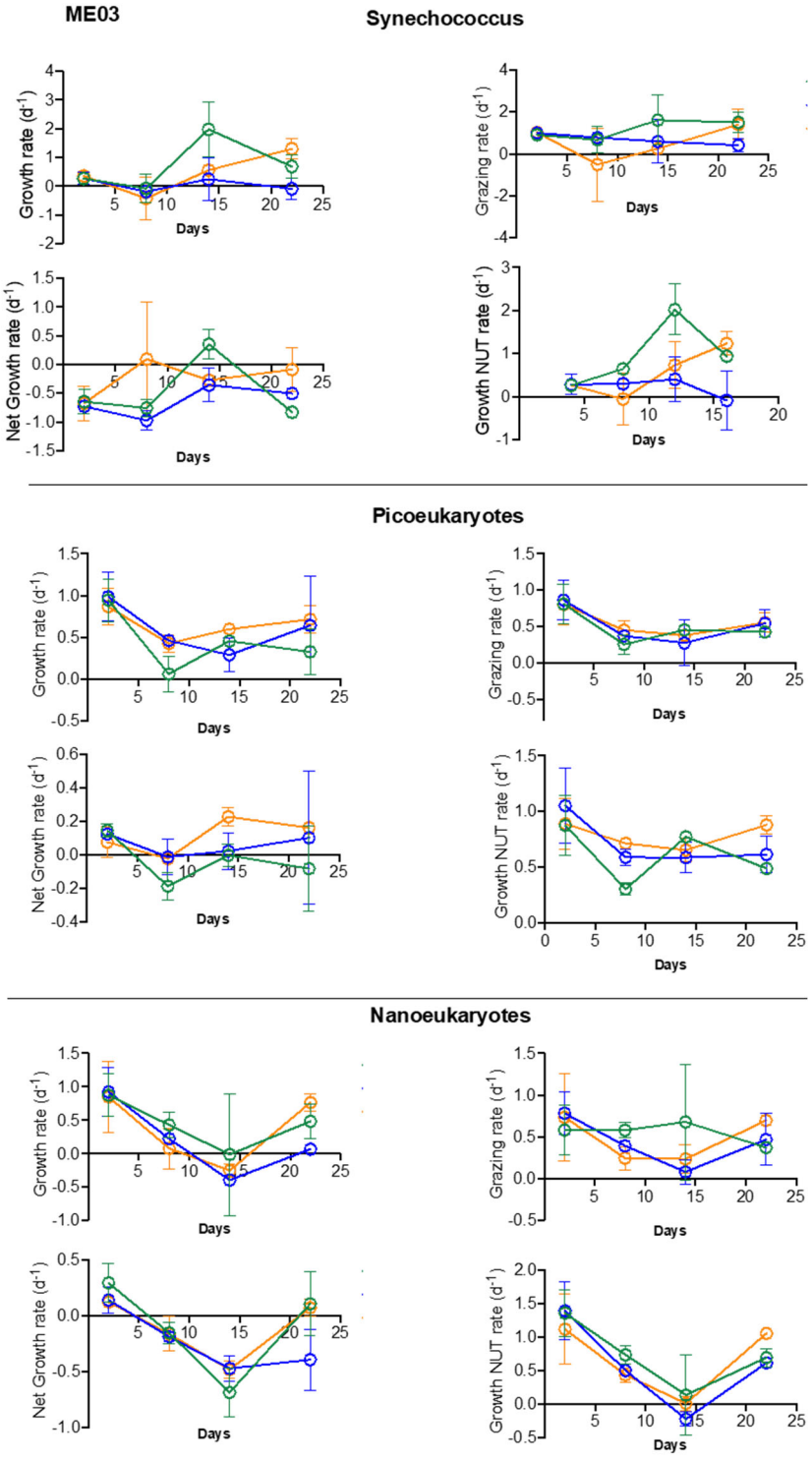

Figure SF11: In situ growth, grazing, net growth, and nutrient amended (NUT) growth rates for SYN, PEUK, and Nano-phytoplankton populations during ME3, showing Control (green), *2100* (blue) and *2150* (orange).

OUTPUTS

1. Law, C.S. Effects of rising ocean acidification on fisheries in spotlight http://www.stuff.co.nz/business/farming/aquaculture/83102158/effects-of-rising-ocean-acidification-on-fisheries-in-spotlight
2. Law C.S and the CARIM Team, 2016. The CARIM Project, 9th NZ Ocean Acidification workshop, Victoria University of Wellington.
3. Law C.S.; and the CARIM Team, 2017. The CARIM Project Overview. 10th NZ Ocean Acidification workshop, University of Otago.
4. Law C.S, Barr N, Northcote, L.; Gutierrez-Rodriguez, A.; Decima, M.; Marriner A.; Graham B.; Fang, Z.; Deans F.; Allen, R.; Hoffmann, L.; Baltar, F.; Gall, M. 2017. How will coastal plankton respond to increasing CO2? Preliminary results from the first two CARIM mesocosm experiments. 10th NZ Ocean Acidification workshop, University of Otago.
5. Law C.S.; 2017. Ocean acidification in New Zealand waters. Forest & Bird Climate conservation science symposium, Wellington Zoo.
6. Law, C.S. 2017. ZBD2017-06 Progress Report. The impact of acidification and warming on food quality in coastal plankton, MPI BRAG Planning meeting, NIWA Wellington.
7. Law, C.S. and the CARIM Team. 2017. The CARIM Project. Invited Talk, Ocean Acidification-Nutrients and Productivity workshop, School of Science, University of Waikato
8. V. Meduna 2017, Acid Seas, *New Zealand Geographic*, Sept-Oct 2017 Issue 147 https://www.nzgeo.com/stories/acid-seas/
9. Law C.S. and the CARIM Team. 2017. Coastal Acidification, Invited presentation, MfE Coastal Hub, Environment House, Wellington.
10. Law C.S, Zeldis J, Bostock H.; Cummings V.; Currie K.; Frontin-Rollet G.; MacDonald H.; Mikaloff-Fletcher S.; Parsons D.; Ragg N.; Sewell M. 2019. A synthesis of New Zealand ocean acidification research, with relevance to the Hauraki Gulf. NIWA Client Report*:* 2019165WN
11. V. J. Cummings, C. J. Lundquist, M. R. Dunn, M. Francis, P. Horn**,** C. Law, M. H. Pinkerton, P. Sutton, D. Tracey, L. Hansen, and E. Mielbrecht. 2021. Assessment of biological impact of climate-related changes in coastal and offshore waters on New Zealand's seafood sector. *New Zealand Aquatic Environment and Biodiversity Report No. 261* ISBN 978-1-99-100390-4
12. Law C.S and the CARIM Team, 2019. Ocean Acidification, Presentation to Level 3 Science Class, St Patricks School, Wellington.
13. *Ocean Acidification: Implications for New Zealand.* Forest and Bird Report, 52 p.
14. *Ocean Acidification*, Sunday Morning with Wallace Chapman on RNZ National, 28/9/18, https://www.radionz.co.nz/national/programmes/sunday/audio/2018664725/growing-concern-over-rising-acidity-levels-in-seawater
15. Howard, M. *The pH problem*, Resilient Magazine, Otago Daily Times, 9/4/19 https://www.odt.co.nz/lifestyle/resilient
16. *Ocean acidification: What is it?* Online video, https://www.niwa.co.nz/videos/ocean-acidification%E2%80%94what-is-it
17. Law C.S et al. 2019. Coastal phytoplankton response to acidification & warming, NZ Ocean Acidification Workshop, Dunedin, February 2019.
18. Barr, N. et al. 2019. The trials, tribulations and successes in controlling pH and temperature in 9 giant test-tubes. NZ Ocean Acidification Workshop, Dunedin, February 2019.
19. Saint-Macary, A. et al. 2019. Will Ocean Acidification and warming alter DMS emissions from coastal waters? NZ Ocean Acidification Workshop, Dunedin, February 2019.
20. Sabadel A.; et al. 2019. Climate change impact on coastal particulate organic matter cycling and nutritional value, using amino acid concentrations and C and N stable isotopes. NZ Ocean Acidification Workshop, Dunedin, February 2019.
21. Meyers, M.; et al. 2019. Grazing of calanoid copepod *Temora turbinata* on natural prey communities during the CARIM Mesocosm 4 experiment. NZ Ocean Acidification Workshop, Dunedin, February 2019.
22. Deans, F. et al. 2019. Bacterial communities show resilience to climate change in New Zealand's coastal waters. NZ Ocean Acidification Workshop, Dunedin, 20-21 February 2019, February 2019.

23. Saint-Macary, A.; Luan, Q.; Meyers, M.; Gall, M.; Barr, N.; Law, C.S. 2019. Will ocean acidification and warming alter DMS emissions from coastal waters? SOLAS OSC, Sapporo, Japan, 22/4/19. Poster.
24. Sabadel, A.J.M.; Luan Q.; Northcote L.; Law, C.S. 2019. Climate change impact on coastal particulate organic matter cycling and nutritional value, using amino acid concentrations and stable isotopes. Goldschmidt Conference, 20/8/19.
25. Law C.S. and the CARIM Team. 2018. Ocean Acidification - A potential issue for New Zealand Seafood, Seafood Industry Conference Technical Day, Te Papa, Wellington, 1/8/18
26. Law C.S.; Currie, K. 2018 Ocean acidification research networks – New Zealand. Reinvigorating Ocean Acidification research in Australia, Canberra.
27. Ministry for the Environment & Stats NZ, 2019. *New Zealands Environmental Reporting Series: Our Marine Environment 2019. pp 70.*
28. Law C.S. and the CARIM Team. 2019. CARIM & the CRACZ Project. Department of Conservation Head Office, Wellington, 27/11/2019
29. Law C.S.; 2019. A Sea Change, Public lecture, Dunedin Museum, 18/9/2019
30. Deans, F.; Law, C.S.; Morales, S.E.; Baltar, F. 2020. Coastal bacterioplankton communities show resilience to climate change under varying nutrient regimes. AGU Ocean Sciences, San Diego. Poster.
31. Law, C.S.; Cummings, V.; Currie, K.; Ragg, N.; MacDonald, H.; Bostock, H.; Murdoch, J.; Parsons, D.; Barr, N.; Gall, M.; Zeldis, J.; LaMare, M. 2019. Coastal Acidification: Rate, Impacts & Management. Keynote Presentation, New Zealand Coastal Society. Annual Conference 2019: "Life on the Edge - Mataora kei runga i te Tapātai". Invercargill, 14/11/19.
32. Law, C.S.; Cummings, V. 2019. Progress on the CARIM Project. CARIM Steering & Technical Advisory Group Meeting, NIWA Wellington.
33. Law, C.S. et al. 2020. Impacts on primary producers and ecosystem interactions. Final CARIM Stakeholder Workshop, Victoria University of Wellington, February 2020
34. Law, C.S. Coastal Acidification: Rate, Impacts & Management, Dept Marine Sciences Seminar, 22/9/20
35. Sellegri, K.; Nicosia, A.; Freney, E.; Uitz, J.; Thyssen, M.; Grégori, G.; Engel, A.; Zäncker, B.; Haëntjens, N.; Mas, S.; Picard, D.; Saint-Macary, A.; Peltola, M.; Rose, C.; Trueblood, J.; Lefevre, D.; D'Anna, B.; Desboeuf, K.; Meskhidze, N.; Guieu, C.; Law, C.S. (2021) Surface ocean microbiota determine cloud precursors. *Scientific Reports*, *11*(1), 1-11.
36. Saint-Macary, A.D.; Barr, N.; Armstrong, E.; Safi, K.; Marriner, A.; Gall, M.; McComb, K.; Dillingham, P.W.; Law, C.S. (2021) The Influence of Ocean Acidification and Warming on DMSP & DMS in New Zealand Coastal Water. *Atmosphere* 2021 Feb 12(2):181.
37. Sabadel, A.J.M.; Décima, M.; McComb.; K, Meyers.; M.; Barr, N.; Gall, M.; Safi, K.; Law, C.S. Amino acid stable isotopes in particulates and zooplankton: potential biomarkers of climate change. *Marine Ecology Progress Series, submitted*
38. Meyers, M.; Décima, M.; Law, C.; Gall, M.; Barr, N.; Miller, M.; Safi, K.; Sabadel, A.; Wing, S.; Hoffmann, L. No evidence of altered relationship between diet and consumer fatty acid composition in a natural plankton community under combined climate drivers. *Journal of Experimental Marine Biology and Ecology submitted*
39. Law, C.S. Retrospective 4: Ocean Acidification, Media interview, Our Changing World, 22/4/21.